Alexandru-Spiridon MILCA

Physical modelling of mass oscillations
in Roskrepp Hydropower Plant

August 2020

Master's thesis

Master's thesis

2020

Alexandru-Spiridon MILCA

NTNU
Norwegian University of
Science and Technology
Faculty of Engineering
Department of Civil and Environmental Engineering

NTNU
Norwegian University of
Science and Technology

NTNU
Norwegian University of
Science and Technology

NTNU

Norwegian University of
Science and Technology

Physical modelling of mass oscillations in Roskrepp Hydropower Plant

Alexandru-Spiridon MILCA

◼ NTNU

M.Sc. THESIS IN HYDRAULIC ENGINEERING

Candidate: Alexandru-Spiridon Milca

Title: Physical modeling of mass oscillations in Roskrepp hydropower plant

1. Background

During the past decade, the installation of unregulated power sources such as wind, solar and small hydro has been significantly increasing, yielding a higher need of energy storage options. Pump storage plants (PSPs) have represented the most relevant energy storage alternative for large scale storage so far, both in terms of stored energy volume and power capacity. A PSP may be used for several purposes:
- Storing of energy
- Generation of peak power
- Balancing of the power production and the electric grids

The power company Sira-Kvina showed an interest into PSPs, currently studying the possibility of upgrading the existing Roskrepp hydropower plant (HPP). Roskrepp HPP was commissioned in 1979, has a single 50 MW Francis unit with nominal head 83 m and nominal discharge of approximately 70 m^3/s.

One of the main problems with upgrading to PSPs is the uncertainty whether the tunnel system is capable of dealing with the changed hydraulic conditions (flow and pressure). The headrace tunnel in Roskrepp HPP is 3.5 km and includes one surge tank and one brook intake. The tunnel is in general unlined with asphalt invert. A new reversible pump turbine unit along with numerous start-stop operations will result into more frequent and more adverse transient phenomena. In this regard, the effect on the mass oscillations in the tunnel system is to be evaluated.

2. Main content for the thesis

The thesis shall cover, though not necessarily be limited to the main content listed below.

2.1   Literature and desk study

The candidate shall carry out a literature study of the dynamic flow design of pump storage plants and the relevant hydraulic laboratory techniques.
1   Analysis of Roskrepp HPP tunnel system drawings
2   Desk study of hydraulic transients in Roskrepp HPP tunnel system
3   Desk study of measurement techniques in hydraulic laboratories

2.2   Main tasks

The candidate must collect available background material such as reports, papers and books about previous studies and operational strategy of PSP in the future power market. Related to the thesis, the following must be carried out:
1   Calibration and validation of Roskrepp physical model
2   Development of test program
    a.   Experimental study of hydraulic transients in Roskrepp HPP
    b.   Experimental study of hydraulic transients in Roskrepp PSP
3   Identify weak points and propose countermeasures to allow the upgrade
4   Conclusions

NTNU

3 Supervision and data input

Professor Leif Lia and PhD Candidate Livia Pitorac will supervise and assist the candidate and make relevant information available.

Discussion with and input from colleagues and other research or engineering staff at Norwegian University of Science and Technology (NTNU) and Politehnica University of Bucharest (UPB), Bucharest, is recommended. Significant inputs from other shall be referenced in a appropriate manner.

The research and engineering work carried out by the candidate in connection with this thesis shall remain within an educational context. The Roskrepp power plant is selected as a study object. The candidate and the supervisors are therefore free to introduce assumptions and limitations which may be considered unrealistic or inappropriate in a contract research or a professional context.
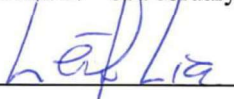
4 Report format and reference statement

The report should be written with a text editing software, with figures, tables, photos, etc. of good quality. The report should contain an executive summary, a table of content, a list of figures and tables, a list of references and information about other relevant sources. The report should be submitted electronically in B5-format .pdf-file in INSPERA and the system required at UPB.

The executive summary should not exceed 450 words and should be suitable for electronic reporting.

The Master's thesis should be submitted within 16th of July 2020.

Trondheim 27th of February 2020

Leif Lia
Professor
Department of Hydraulic and Environmental Engineering
NTNU

Abstract

The purpose of the present study is mass oscillations analysis in Roskrepp Pumped Storage Project located in south of Norway. The power plant is presently a conventional hydropower plant desired to be redesigned to a pump storage capacity, due to the most recent tendencies in terms of power system stability. The owner of the power plant, Sira-Kvina company, showed a high interest into pumped storage plants commenced with the study of upgrading Roskrepp into one of these.

Roskrepp Hydropower Plant is a hydropower plant commissioned in 1979 which processes an 83 m head between Roskreppfjorden and Øyarvatn lakes using one 50 MW Francis turbine. Considering the tunnel system, mostly consisted of unlined tunnels and reinforced pipes, can withstand the pumping conditions, the new configuration will result into a much more adverse transient phenomena due to numerous start-stop operations. Therefore, mass oscillations behavior for the new plant configuration is to be evaluated.

The study relies on a set of data collected from the field during plant operating, used for the calibration and validation of a 1:70 scale physical model built in Hydraulic Laboratory (Vassdragslaboratoriet) in NTNU. Afterwards, the model is used for the simulation of the new operating conditions characteristic to a pumped storage plant. The experiments are performed in the hypothesis of a new reversible pump turbine unit installed instead of the current turbine.

The experiments considered the implementation of a reversible pump-turbine unit, with respect to the maximum discharge that can be economically transported by the tunnel system. The results showed that the highest issues in what regards mass oscillations are related to the downstream surge tank. Upstream surge tank also registered some slight exceeding of its upper boundary, however, solvable with some small operating restrictions. Thus, its redesigning is not mandatory. Downstream surge tank, on the other hand requires immediate redesigning and reconstruction for the pump storage configuration to be operative.

Following the data analysis, a numerical model will be used for the evaluation of the possible improvement options and the optimal solutions will be highlighted. The solutions proposed by the study must be subsequently analyzed by physical modelling to ensure their relevance.

Sammendrag

Hensikten med den nåværende studien er massesvingningsanalyse i Roskrepp Pumped Storage Project lokalisert i Sør-Norge. Kraftverket er i dag et konvensjonelt vannkraftverk som ønskes ominnredet til pumpens lagringskapasitet, på grunn av de nyeste tendenser med hensyn til kraftsystemstabilitet. Eieren av kraftverket, Sira-Kvina-selskapet, viste stor interesse for pumpede lagringsanlegg startet med studien om å oppgradere Roskrepp til et av disse.

Roskrepp vannkraftverk er et vannkraftverk som ble satt i gang i 1979, og behandler et 83 m hode mellom Roskreppfjorden og Øyarvatn innsjøer ved hjelp av en 50 MW Francis turbin. Tatt i betraktning at tunnelsystemet, som for det meste besto av uforede tunneler og forsterkede rør, tåler pumpeforholdene, vil den nye konfigurasjonen føre til et mye mer ugunstige forbigående fenomener på grunn av mange start-stop-operasjoner. Derfor skal massesvingningsatferd for den nye anleggskonfigurasjonen evalueres.

Studien er avhengig av et sett med data samlet inn fra feltet under drift av anlegg, brukt til kalibrering og validering av en 1:70 skala fysisk modell bygget i Hydraulic Laboratory (Vassdragslaboratoriet) i NTNU. Etterpå blir modellen brukt til simulering av de nye driftsforholdene som er karakteristiske for et pumpet lagringsanlegg. Eksperimentene blir utført i hypotesen om en ny reversibel pumpeturbinenhet installert i stedet for den nåværende turbinen.

Eksperimentene vurderte implementering av en reversibel pumpeturbinenhet, med hensyn til maksimal utslipp som kan transporteres økonomisk av tunnelsystemet. Resultatene viste at de høyeste problemene med hensyn til massesvingninger er relatert til nedstrøms overspenningstank. Oppstrøms overspenningstank registrerte også noe svakt overskridelse av sin øvre grense, men løselig med noen små driftsbegrensninger. Dermed er omdesign ikke obligatorisk. Nedstrøms overspenningstank krever derimot øyeblikkelig omdesign og rekonstruksjon for at pumpelagerkonfigurasjonen skal være i drift.

Etter dataanalysen vil en numerisk modell bli brukt for evaluering av mulige forbedringsalternativer og de optimale løsningene vil bli fremhevet. Løsningene foreslått av studien må deretter analyseres ved fysisk modellering for å sikre deres relevans.

Preface

This study has been written as a final assignment on a six months student exchange at NTNU Trondheim, Faculty of Engineering, in the Department of Civil and Environmental Engineering. The exchange was a part of a two years master's degree in "Politehnica" University of Bucharest, Romania and it was possible thanks to my supervisor, Professor Bogdan POPA. The thesis is evaluated with a total of 30 ETCS and represents the final assessment of the master programme.

The study has been developed under the supervision of Professor Leif LIA and PhD candidate Livia PITORAC which I would like to sincerely thank for all the kindness and warmth they have shown. The exchange would not have been possible without the support from Professor LIA, to whom I will be forever grateful.

Lastly, I would like to thank to all Hydraulic Laboratory staff for their co-operation, hospitality and kindness. It truly has been a pleasure to work here surrounded by such lovely people, which I will always remember of.

During my stay in Norway, in addition to the academic activity, I discovered a culture with wonderful people and a high level of civilization. I rediscovered the passion for cycling, which is an ideal way of commuting in Trondheim. Besides cycling, Trondheim is surrounded by numerous places ideal for hiking on mountains or on the edge of the fjord with breathtaking views, thus, the city will be amongst first recommendations for travelling I will make.

Trondheim, 14 July 2020

Alexandru Spiridon MILCĂ

Table of contents

List of figures

List of tables

List of symbols

Symbol	Unit	Description
HPP	**-**	**Hydropower Plant**
PSP	**-**	**Pump Storage Plant**
UST	**-**	**Upstream Surge Tank**
DST	**-**	**Downstream Surge Tank**
UT	**-**	**Upstream Turbine**
DT	**-**	**Downstream Turbine**
UR	**-**	**Upper Reservoir**
LR	**-**	**Lower Reservoir**
GV	**-**	**Globe Valve**
BfV	**-**	**Butterfly Valve**
g	m/s^2	*Gravitational acceleration*
ρ	kg/m^3	*Water density*
t	s	*Time*
A	m^2	*Cross section area*
L	m	*Length*
D	m	*Diameter*
D_h	m	*Hydraulic diameter*
R_h	m	*Hydraulic radius*
M	$s/m^{1/3}$	*Manning's number*
Q	m^3/s	*Discharge*
Q_P	m^3/s	*Pump discharge*
Q_T	m^3/s	*Turbine discharge*
v	m/s	*Velocity*
p	Pa	*Pressure*
H	$masl$	*Pressure height (meters above sea level)*
α	*-*	*Head loss coefficient in stepwise integration*
λ	*-*	*Friction head loss coefficient*
k	*-*	*Friction head loss coefficient (script)*
h_f	m	*Friction head loss*
ζ	*-*	*Singular head loss coefficient*
ks	*-*	*Singular head loss coefficient (script)*
h_s	m	*Singular head loss*
τ	N/m^2	*Wall shear stress*

1 Introduction

1.1. Background

In the recent years, renewable energy sources such as solar and wind undergone a continuous spread bringing new matters regarding power systems stability. These environmental-friendly energy sources are prioritized over classic energy sources due to their smaller impact on the environment. They are known as renewable energy sources. Unlike hydro power plants, also considered renewable energy sources with some exemptions, solar and wind power sources do not have an easy predicted operating schedule as this is mostly related to weather conditions. Thus, these types of energy sources have a specific volatility and so, they can be very challenging in terms of power systems stability. Therefore, comes the requirement of storing the energy produced by these sources during low demand periods and supplement the production when required.

There are several ways of energy storage known so far, but when referring to a power system, the amount of energy required to be stored is considerable. Therefore, water pumping technology is the most sustainable energy storage option from this point of view. Most of the hydropower plants built in Norway before 1980 were constructed as base load power plants (Pitorac, Vereide, & Lia, 2020), namely designed for continuous operating, nowadays they became peaking plants with frequent start-stops due to new power grid stability issues. Among these power plants, those equipped with reservoirs can be redesigned as pump storage plants. One major advantage of converting these conventional hydropower plants in pump storage plants is reducing this way the environmental impact caused by the construction of new large pump storage capacities.

1.2. Basic literature in the topic

Previous work in this field has been found and reviewed and the most relevant that can be mentioned is the project developed for upgrading the 960 MW Tonstad HPP in Norway with additional 2 units each of 480 MW reversible pump turbine units. Even though the licensing application was delivered and the project was ready to be implemented, the application was withdrawn in the end, due to high uncertainty regarding the future power market. (Pitorac, Vereide, & Lia, 2020)

Another similar project is found in Austria, where (Nakler2012) presents the conversion of 50 MW Koralpe hydro power plant into a pump storage plant constructing a pumping station in

parallel with the existing plant and using the same tunnel system. (Peran et al 2019) evaluated the possible methods of upgrading an existing Cortes II power plant into a pump storage plant analyzing different options for implementation costs cutting. (Gimeno-Gutierrez and Lacal-Arantegui2013) evaluate pump storage plant potential in Europe, while (Lia et al2016) evaluates this potential in Norway, including the upgrading of existing hydro power plants. (Pitorac, Vereide, & Lia, 2020).

1.3. Roskrepp Power Plant

Roskrepp Hydropower Plant located in south Norway produces annually around 105 GWh by processing 83 m of gross water pressure head throughout a 50 MW Francis turbine. It consists of a water storage hydropower system commissioned in 1980.

The hydraulic system of this power plant is as following: water is provided to the plant from the dam intake installed on Roskreppfjorden, watercourse dammed to an elevation between 890 and 929 masl. Afterwards it flows through an unlined headrace tunnel drilled and blast, paved with asphalt. The tunnel has a 38 m^2 cross section area and a length of 3513 m between the water intake and the surge tank. Headrace tunnel is equipped with a two chambers surge tank, open in the atmosphere. Its lower chamber cross section area is 435 m^2, while its upper one is 510 m^2. The shaft between the two chambers has a 60 m^2 cross section area. Penstock, located downstream the surge tank, is a 70 m long and 4 m diameter steel conduit which concentrates the pressure head towards the turbine. The powerhouse is underground cavern, located in the mountainside by Heiestøl, in Sirdal municipality, Vest-Agder county. It can be reached through an access tunnel. Water is evacuated out of the turbine through a draft tube continued with a tailrace tunnel similar with the headrace, 38 m^2 cross section area and 300 m length into the lower reservoir, namely Øyarvatn lake. Minimum and maximum water levels of this lake are 825 masl, 837 masl respectively. Downstream surge tank is provided right at the end of the draft tube. It has a 90 m^2 cross section area and it is open to the atmosphere. An unplugged adit starts a few meters downstream the surge tank and it connects to the Øyarvatn lake, namely lower reservoir of the development. (Pitorac, Vereide, & Lia, 2020)

Roskrepp Power Plant represents the case study for the present work. The purpose is the upgrade of the plant into a pumped storage plant using the same hydraulic system for the pumping process. Table 1.1 provides a centralized overview for Roskrepp Hydropower Plant characteristics.

Table 1.1 Roskrepp HPP main parameters

Roskrepp Hydropower Plant		
Turbine	Type	Francis
	Elevation [masl]	822
	Rated power [MW]	51.7
	Rated head [m]	83
	Rated discharge [m³/s]	67
	Efficiency [-]	0.947
Headrace tunnel	Type	drilled and blast paved with asphalt
	Cross section area [m²]	38
	Length [m]	3513
	Diameter [m]	6.96
	Head loss [m]	6.42
	Water velocity [m/s]	1.58
Upstream surge tank	Type	2 chamber surge tank
	Shaft cross section area [m²]	60
	Lower chamber's cross section area [m²]	435
	Lower chamber's upper limit elevation [masl]	885
	Upper chamber's cross section area [m²]	510
	Upper chamber's lower limit elevation [masl]	935
Penstock	Type	Steel pipe
	Cross section area [m²]	12.57
	Length [m]	70
	Diameter [m]	4
	Head loss [m]	0.8
	Water velocity [m/s]	4.77
Draft tube	Type	Concrete draft tube
	Length [m]	24
	Diameter [m]	4.54
	Head loss [m]	0.4
	Water velocity [m/s]	3.71
Downstream surge tank	Type	Simple surge tank
	Shaft cross section area [m²]	110
	Lower limit elevation [masl]	813.5
	Upper limit elevation [masl]	845
Tailrace tunnel	Type	drilled and blast paved with asphalt
	Cross section area [m²]	38
	Length [m]	320
	Diameter [m]	6.96
	Head loss [m]	0.7
	Water velocity [m/s]	1.58

A simplified sketch of Roskrepp Hydropower Development is presented in Figure 1.1:
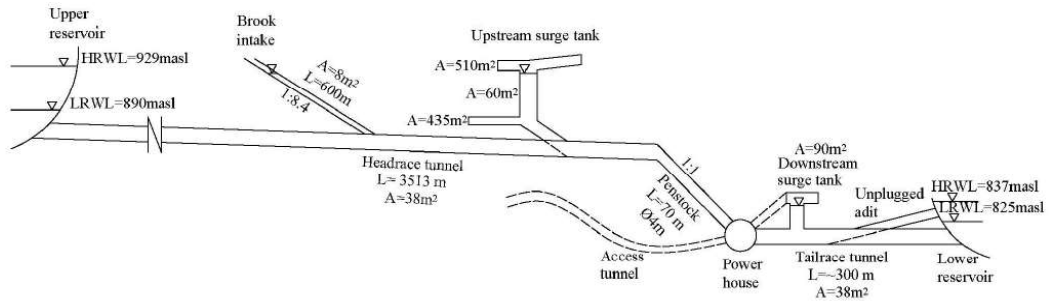
Figure 1.1 Roskrepp Hydropower Plant tunnel system (Pitorac, Vereide, & Lia, 2020)

1.4. Upgrading hydropower plants to pump storage plants

The conversion of an existing hydropower plant into a pumped storage plant is a very complex and challenging task. Even though the simplest method for the upgrade is the design and construction of a new hydraulic system, this process might be not always feasible due to very high costs. Also, such a large-scale work is sometimes not possible due to numerous issues in the field. Thus, the most favorable method in what regards the costs is to use as much as possible the existing constructions and tunnel system.

Power plants in general have tunnel consisting of underground galleries and reinforced pipes which could, with some improvements with take the conditions imposed by a pumping process. In the end, an optimal solution for such a conversion is being achieved for the redesign of the plant, with smaller costs and faster implementing time. However, the problem appearing in the event of pumping water using the same hydraulic system is the mass oscillations. The surge tanks of the existing power plants were not designed for pumping, thus, in most cases the redesign of the surge tanks is required.

This thesis is a case study of upgrading an existing hydropower plant to a pump storage plant, process desirable for several other existing hydropower developments in Norway or abroad. The main point of interest for this thesis is redesign and reconstruction of the tunnels and pressure shafts required to comply the new operating conditions. Roskrepp Hydropower Plant is being used as a case study, reproduced at a scale of 1:70 in the Hydraulic Laboratory (Vassdragslaboratoriet) at NTNU in Trondheim (Pitorac, Vereide, & Lia, 2020).

The opportunity of upgrading Roskrepp Power Plant to a pumped storage plant came due to the configuration of the reservoirs used by the plant. The distance between them is small and the water level difference is significant. Another aspect to be considered for a pump storage plant

is the reservoirs volumes since they give the capacity of energy storage for the plant. Therefore, Table 1.2 presents the main characteristics for Roskrepp upper and lower reservoirs.

Table 1.2 Roskrepp reservoirs main characteristics (retrieved from nve.no)

	Roskreppfjorden	Øyarvatn
Year of commissioning	1968	1981
Lowest reservoir water level (LRWL) **[masl]**	890	825
Highest reservoir water level (HRWL) **[masl]**	929	837
Water surface area at HRWL **[km²]**	29,75	8,08
Reservoir capacity **[mil.m³]**	695	104

2 Theory

2.1 Pressure shafts in hydropower plants

A hydroelectric power plant uses the hydraulic energy of water which, with the help of a set of machines and equipment, transforms it into electricity. Therefore, the operation of such a plant requires the existence of a hydrotechnical system that takes water from a water source, transports it to the place of production, and then returns it into the watercourse. This translates into a long-distance water flow, often significant.

Hydropower plants usually provide the energy needed for peak periods of consumption, which requires their intermittent operation, meaning that the hydrotechnical system is subject to a discontinuous and non-uniform operation. This causes the appearance of transient phenomena encountered in the form of hydraulic shock known as water hammer. In order to reduce the effects caused by these transient phenomena and to prevent the possible damages they can bring to the system, the installation of some outlets at the extremities in the vicinity of the power plant of these systems is required. These outlets are called water surge tanks. Figure 1 shows the schematic diagram of a hydraulic system equipped with a surge tank.

A surge tank can be seen, in its simplest form, as a vertical pipe connected to the main water conduit, in this case the headrace of a hydropower plant. Positioning of this vertical pipe in the system aims to maintain the values of water hammer that occurs when discharge conveyed in the penstock changes into reasonable limits.
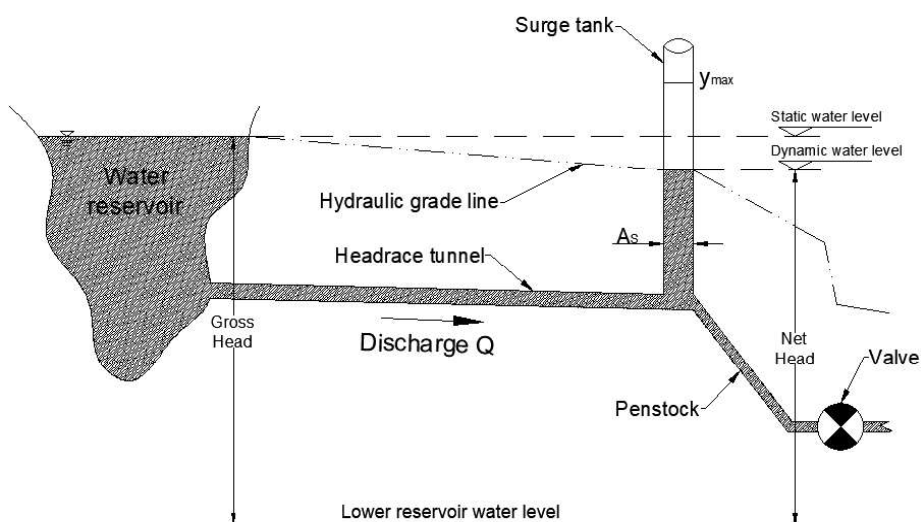
Figure 2.1 Main scheme of a hydraulic system with a surge tank (ST)

2.2 Mass oscillations

Water hammer is a hydraulic transient consisting in the appearance of overpressure or under pressure waves, usually lasting for a short period of time, which travel along the hydraulic system with velocities higher than 1000 m/s. This transient is mostly caused by power plant's operating maneuvers which reflects in the change of the discharge flowing in the system. Usually, extreme maneuvers such as sudden stopping of the power plant or starting from rest are the most challenging in terms of flow regime change in the hydraulic system. Significant highly masses of water in the tunnels must be either dragged or accelerated in order to comply with the new operating conditions. Due to the high inertia of these water masses, the change of the operating regime is not gradually varied, but in an oscillating regime. (Stefan, n.d.)

Surge tanks are various types and forms constructions, with role of reducing the effects of hydraulic transients that can occur during hydropower plant's operation. Even though surge tanks are being used for reducing water hammer's effects, the usage of these shafts returns another phenomenon in the hydraulic system, namely oscillations of the water surfaces inside known as water mass oscillations. The operating principle of a surge tank is as following:

• In case of power plant's shut down, the overpressure occurred in the hydraulic system results in water level rising in the surge tank reaching a maximum value, thereafter this level decreases reaching a minimum value and these oscillations repeat until they are damped due to hydraulic losses;

• In case of power plant's start up, the under pressure occurred in the hydraulic system results in water level decreasing in the surge tank, reaching a minimum value, thereafter the level increases reaching a maximum value and the oscillations repeat until they are damped due to hydraulic losses.

For surge tanks positioned downstream of the power plant, among the tailrace, the behavior of these shafts is opposite from what is stated above, which describes the headrace surge tanks behavior.

In case of partial variations of the power plant's load, i.e. for decreases or increases of the power required by the system, the phenomena are similar and the behavior of the water surface in the surge tank is identical. In these situations, the values which the water level oscillates in between are lower than those occurred in total variation of the load, but the frequency of the oscillations is higher and sometimes, their damping over time is a problem. (Stefan, n.d.)

The two cases of total plant load variation stated above are graphically presented in the figures below, power plant shut down in Figure 2.2, respectively power plant start up in Figure 2.3.
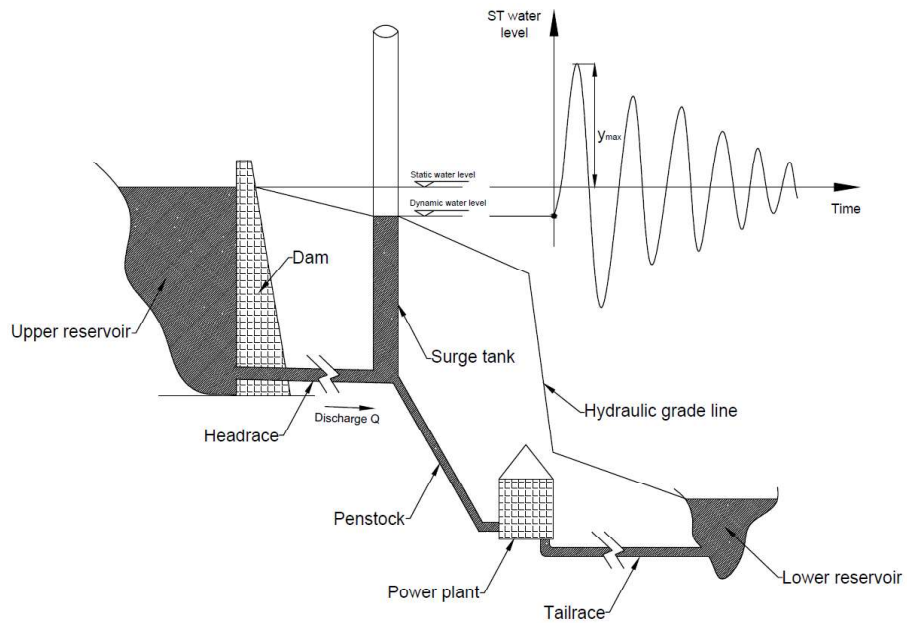
Figure 2.2 Surge tank water level oscillations in case of HPP shut down
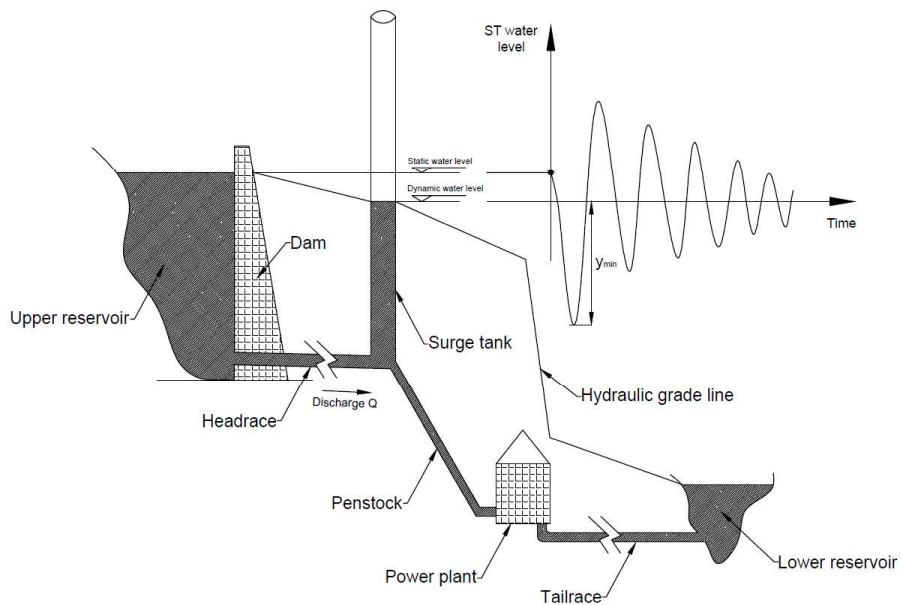
Figure 2.3 Surge tank water level oscillations in case of HPP start up

2.3 Governing equations

Roskrepp Power Plant type consistd of an upper water reservoir, a pressurized headrace tunnel, upstream surge tank, penstock, turbine, downstream surge tank, pressurized tailrace tunnel and lower water reservoir. In case of valve maneuvers in the system, namely discharge variations, the waterhammer appears in the penstock and in the draft tube, while in the pressurized tunnels and in the surge tanks the water discharge is slowly varied. (Popescu, Arsenie, & Vlase, 2003)
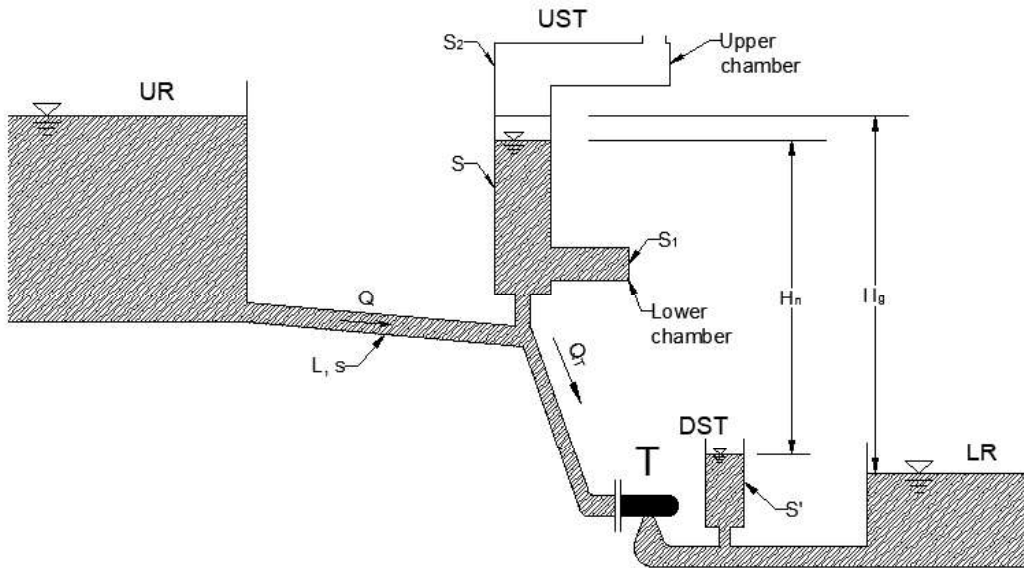
Figure 2.4 Simplified scheme of Roskrepp hydraulic system

The water motion in the hydraulic system is described by the following system of equations:

$$\begin{cases} \dfrac{L}{g}\dfrac{dV}{dt} + z \pm h_{f0}\left(\dfrac{sV}{Q_0}\right)^2 = 0 \\ \pm sV = SU + Q_T \end{cases} \qquad (2.1)$$

where L is the pressurized tunnel length, V is the water velocity in the tunnel, z — the water surface level in the surge tank, hf0 — the friction head losses in the tunnel, s — tunnel cross section area, Q0 — the nominal discharge in the tunnel, S — surge tank cross section area, QT — penstock discharge. For simplification, a constant cross section area surge tank was considered.

The mathematical model that conducts to the system presented above is based on two fundamental equations, the energy equation, known also as Bernoulli's equation in hydraulics field and the continuity equation, respectively. The mathematical model applied for the upstream part of the system will be presented below.

2.3.1 Energy equation on headrace (Bernoulli)
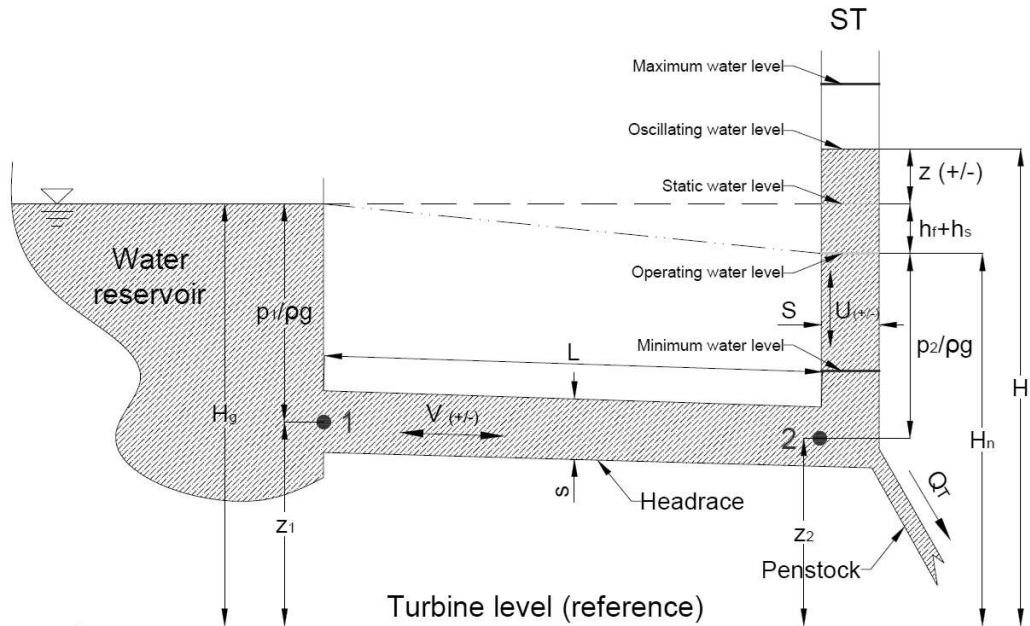
Figure 2.5 Bernoulli's equation applied between 1 − 2

Assuming headrace flow a semi-permanent motion, namely constant acceleration on each element of headrace length *dx*, Bernoulli's equation can be applied between 1 and 2:

$$\frac{p_1}{\rho g} + z_1 + \frac{\alpha V_1^2}{2g} = \frac{p_2}{\rho g} + z_2 + \frac{\alpha V_2^2}{2g} + \frac{1}{g}\int_1^2 \frac{\partial V}{\partial t}\,dx + h_{f1-2} \qquad (2.2)$$

where:

- $z = -\frac{p_1}{\rho g} - z_1 + \left(\frac{p_2}{\rho g} + z_2\right)$ − pressure head between headrace extremities;

- $\frac{\partial V}{\partial t}$ − local acceleration, constant on each headrace elementary length sector dx ($\frac{\partial V}{\partial t} = ct$);

Thus, $\frac{\partial}{\partial t} \to \frac{d}{dt}$ and so inertial acceleration (local acceleration modification between $1 - 2$ resulting factor becomes:

$$\frac{1}{g}\int_1^2 \frac{\partial V}{\partial t}\,dx = \frac{L}{g}\frac{dV}{dt} \qquad (2.3)$$

The variation between kinetic term in the two headrace extremities is very small, therefore, it can be assumed as negligible compared with the rest of the equation terms ($V_1=V_2=V$).

$$\Rightarrow z + \frac{L}{g}\frac{dV}{dt} + h_f = 0 \Rightarrow \frac{L}{g}\frac{dV}{dt} + z + h_f = 0 \tag{2.4}$$

where:

$$h_f = \pm\lambda\frac{L}{d}\frac{V^2}{2g} = \pm kV^2 \tag{2.5}$$

The nominal flow unfolds in constant motion ($V = V0 = ct \; and \; \frac{dV}{dt} = 0$) thus, Bernoulli's equation for constant flow:

$$z_0 + h_{f0} = 0 \qquad \Rightarrow z_0 = -h_{f0} = -kV_0^2 \qquad \Rightarrow k = \frac{h_{f0}}{V_0^2} \tag{2.6}$$

knowing $V_0 = \frac{Q_0}{s}$ (water velocity on headrace in constant motion) constant k can be expressed as $k = \frac{h_{f0}}{V_0^2} = h_{f0}\frac{s^2}{Q_0^2}$, resulting $h_f = \pm\frac{h_{f0}}{V_0}V^2 = \pm h_{f0}\left(\frac{sV}{Q_0}\right)^2$ therefore, Bernoulli's equation (2.7) can also be written as following:

$$\frac{L}{g}\frac{dV}{dt} + z \pm h_{f0}\left(\frac{sV}{Q_0}\right)^2 = 0 \tag{2.8}$$

2.3.2 Continuity equation applied in the junction spot between headrace – surge tank – penstock

The equation assumes that the flow coming on headrace distributes to the penstock and to the surge tank as following:

$$\pm sV = SU + Q_T \tag{2.9}$$

In the equation (2.9), water velocity in the surge tank U depends by water surface level which varies in the surge tank *z(t)*

$$U = \pm\frac{dz}{dt} \tag{2.10}$$

and it can be positive($+$) or negative($-$) depending on its direction ($+$ for rising or $-$ for decreasing) and the flow variation over time is caused by turbine valve operating, opening or closing of this valve as well as by the adjustment of the power amount produced by the plant:

$$Q_T = Q_T(t) \quad or \quad Q_T = \frac{P}{\rho g(H_n \pm z)\eta_{HPP}} \qquad (2.11)$$

where hydropower plant's efficiency depends on the efficiencies of turbine, generator and transformer: $\eta_{HPP} = \eta_T \cdot \eta_G \cdot \eta_{tr}$.

Junction between headrace and surge tank usually generates a singular head loss $h_{sST} = h_s$. The form of this singular head loss is:

$$h_s = \pm \xi \frac{V^2}{2g} = \pm k'V^2,$$

$$where \; k' = \frac{h_{s0}}{V_0^2} = h_{s0}\frac{S^2}{S^2 V_0^2} = \frac{h_{s0}}{Q_0^2}S^2 \qquad (2.12)$$

$$\Rightarrow h_s = h_{s0}\left(\frac{SV}{Q_0}\right)^2$$

Thus, Bernoulli's equation among headrace written in form (2.4) becomes:

$$\frac{L}{g}\frac{dU}{dt} + z + h_f + h_s = 0 \qquad (2.13)$$

and the one written in form (2.8) becomes:

$$\frac{L}{g}\frac{dV}{dt} + z \pm h_{f0}\left(\frac{sV}{Q_0}\right)^2 \pm h_{s0}\left(\frac{SV}{Q_0}\right)^2 = 0 \qquad (2.14)$$

Bernoulli's equations (2.8), (2.14) and continuity equation (2.9), with explanations (2.10) and (2.11) form a system of 4 differential equations of order 2 including 4 unknowns: z, V, U, Q_T (Nistoran Gogoase, 2017-2018). This system can be solved:

- analytically – only in full valve closing and without head losses;
- numerically – finite differences, finite element, method of characteristics, using specialized software and computers;
- graphically – based on numerical methods (e.g.: Schoklitsch method in finite differences).

In case of stable differential equations system solution, are obtained as results sinusoidal damped oscillations (due to head losses), z(t) and system states graph ("snail") which tend to a point. These results shape can be seen in Figure 2.6:
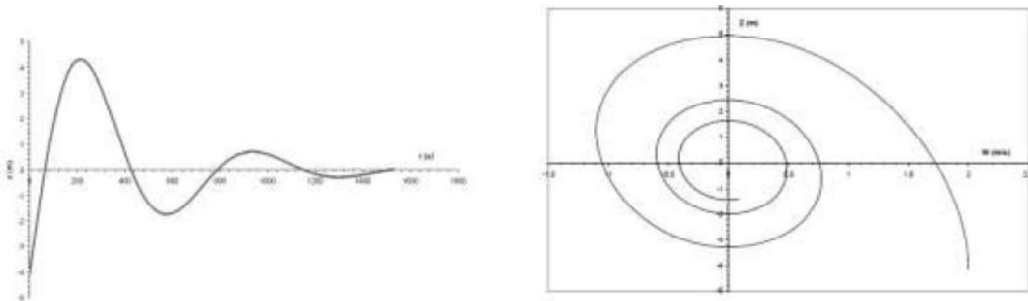
Figure 2.6 Sinusoidal damped oscillations and system states graph (Nistoran, Moatar, Manoliu, & Ionescu, 2007)

2.4 Hydraulic losses

Water motion involves inevitably energy losses caused either by friction due to the roughness of the materials water gets in contact to or by the turbulences created in certain elements such as bending, cross section enlargements or restraints and so on. In order to simplify their computation, they have been divided in two categories based on their nature, namely friction losses attributed to a water duct length and singular losses attributed to a structural modification the water duct.

2.4.1 Friction losses

Water friction against the water duct generates head losses distributed all along the duct's length. In order to calculate these head losses, Manning's equation can be used. This equation introduces a Manning's coefficient depending on the wall's roughness.

$$h_f = \frac{L \cdot v^2}{M^2 \cdot R_h^{4/3}} \qquad (2.15)$$

One other way to calculate the friction losses in Darcy-Weisbach equation. Here, instead of Manning's coefficient, a head loss coefficient f is being used. Similar to Manning's coefficient, it is related to wall's roughness.

$$h_f = f \cdot \frac{L}{D} \cdot \frac{v^2}{2g} \qquad (2.16)$$

Head loss coefficient f also depends by the flow regime, namely by Reynold's number $Re = vD/v$, where v is the kinematic viscosity of the fluid. For a laminar flow in a circular pipe it can be simple determined as following:

$$f = \frac{64}{Re} \tag{2.17}$$

If the flow regime is turbulent, there are several ways to calculate the friction coefficient f. One way is by using a formula such as Colebrook formula which is one of the most common used for turbulent flow in circular pipes and depends by k_s which is the pipe's walls roughness and pipe's radius R. Other way is by using diagrams based on experimental data. One example of such diagram is Moody's diagram presented below.

$$\frac{1}{\sqrt{f}} = -0{,}91\ln\left(0{,}27 \cdot \frac{k_s}{2 \cdot R} + \frac{2{,}51}{\sqrt{f} \cdot Re}\right) \tag{2.18}$$
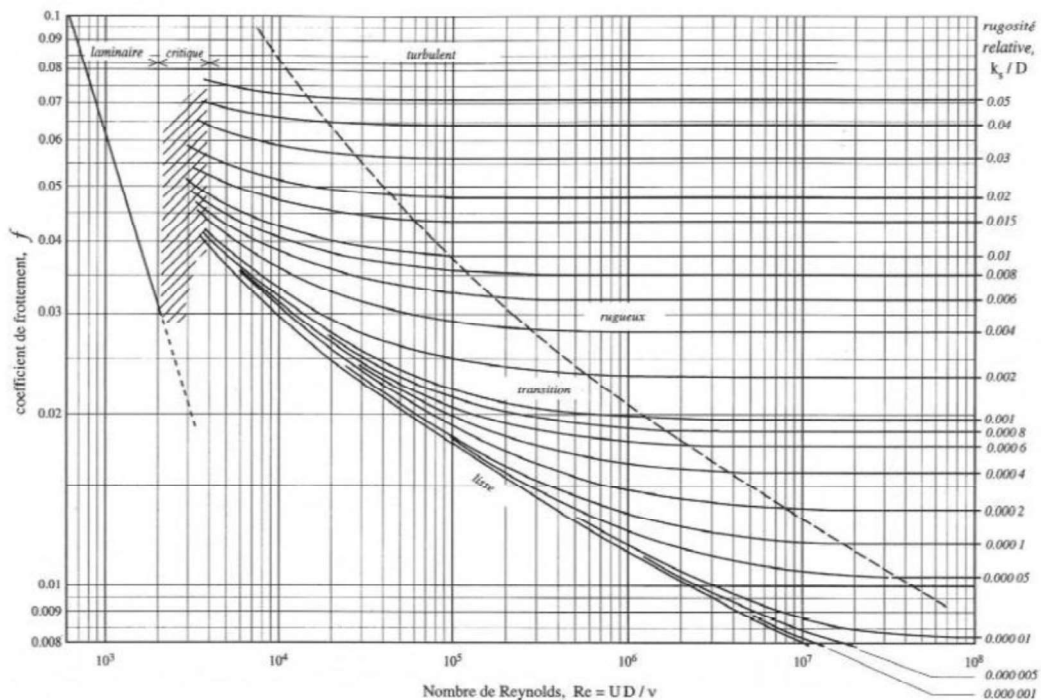
Figure 2.7 Moody's diagram (Ancey, 2014)

2.4.2 Singular losses

Singular losses appear wherever a structural modification of the pipe or water duct takes apart. Such modifications can be represented for example, by a bend, a cross section enlargement or

restraint, a valve installed and everything similar. To calculate these singular losses, a general form equation can be used:

$$h_s = \zeta \cdot \frac{v^2}{2g} \tag{2.19}$$

where ζ is the singular head loss coefficient and it depends on the nature of the pipe or water duct modification.

For an expansion of the cross section area in the pipe system (Figure 2.8), determining the value for singular head loss will be done using the upstream velocity v_1, and the coefficient of this singular loss will differ depending on the flow regime, namely for laminar flow it will be determined using equations (2.20) or (2.21) for turbulent flow respectively. In case of an entry in a reservoir, $A_2 \rightarrow \infty$ will be considered.
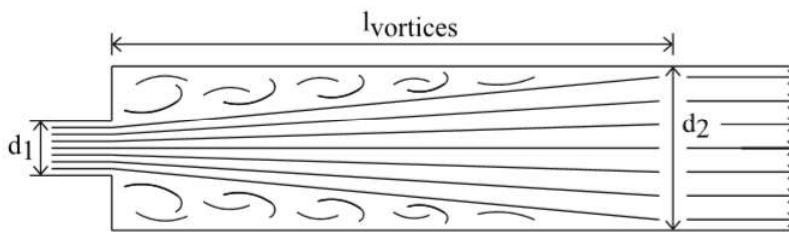
Figure 2.8 Schematic diagram of flow at a sudden expansion (Idelchik, 1986)

$$\zeta = 2 - \frac{8}{3}\frac{A_1}{A_2} + \frac{2}{3}\frac{A_1^2}{A_2^2} - for\ laminar\ flow \tag{2.20}$$

$$\zeta = \left(1 - \frac{A_1}{A_2}\right)^2 - for\ turbulent\ flow \tag{2.21}$$

A cross section expansion can also be smooth, rather than sudden, to diminish the local head loss. In case of a smooth expansion, a converging angle appears, thus, for values below 40º, (Idelchik, 1986) gives the equation (2.22) for calculating the local loss coefficient, while for values above 40º, the local loss coefficient can be found in diagram 5-2 in (Idelchik, 1986).

$$\zeta = 3,2 - \tan\left(\frac{\alpha}{2}\right)\left(tan\frac{\alpha}{2}\right)^{1/4}\left(1 - \frac{1}{n_1}\right)^2 \tag{2.22}$$

where:

$$n_1 = \frac{A_{pipe}}{A_{throttle}} \tag{2.23}$$

Converging angle values between 40 and 50 degrees retrieve a smaller local loss coefficient than in case of sudden expansion, while for values between 50 and 90 degrees, it will be larger than a sudden expansion (Landskaug, 2015). This is desired when the local loss is desired to be different depending on the flow direction.

For a cross-section area constriction of the hydraulic system, the downstream value for the velocity v_2 will be used in determining the singular loss for this structural modification. In case of turbulent flow, the singular head loss coefficient will be determined as stated below. In the situation of water exiting into a reservoir, the singular head loss coefficient will be $\zeta = 0.5$.
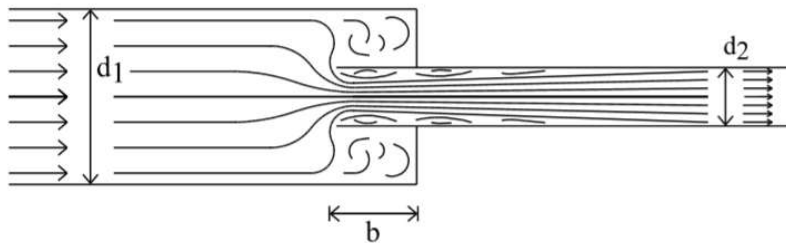
Figure 2.9 Schematic diagram of flow with a sudden contraction (Idelchik, 1986)

$$h_s = \zeta \cdot \frac{v_2^2}{2g} \tag{2.24}$$

$$\zeta = \left(1 - \frac{1}{0.59 + 0.41\left(\frac{A_2}{A_1}\right)^3}\right)^2 \tag{2.25}$$

As well as the expansion, the contraction of the cross section area can be smooth. This way, a converging nozzle connects the two different cross sections introducing a local head loss depending on the angle and the area ratio (Landskaug, 2015). For an angle above 10 degrees, the water begins separating from the walls leading to a local head loss. This head loss increases with the converging angle until this angle reaches 180 degrees, practically becoming a sudden expansion. (Idelchik, 1986) gives the equation (2.26) for the calculation of the loss coefficient in a converging nozzle.

$$\zeta = (-0,0125 \cdot n_0^4 + 0,0224 \cdot n_0^3 - 0,00723 \cdot n_0^2 + 0,00444 \cdot n_0$$
$$- 0,00745) \cdot (\alpha_p^3 - 2 \cdot \pi \cdot \alpha_p^2 - 10\alpha_p) \tag{2.26}$$

where:

$$n_0 = \frac{A_{throttle}}{A_{pipe}} \tag{2.27}$$

$$\alpha_p = 0,01745 \cdot \alpha[°] \qquad [rad] \tag{2.28}$$

If α is situated between 10 and 40 degrees, head loss coefficient reaches a minimum, nearly constant value of $\zeta = 0,05$ (Idelchik, 1986).

For a flow direction change in the pipe system, the head loss coefficient will be determined using Weissbach formula (2.29), where θ represents the direction change expressed in degrees [°] and R_c represents the radius of curvature.

$$\zeta = \frac{\theta}{90}\left(0.13 + 1.85\left(\frac{R}{R_c}\right)^{\frac{7}{2}}\right) \tag{2.29}$$

For sudden direction changes without radius of curvature, the singular head loss coefficient will depend on the direction change angle θ as following:

$$\zeta = sin^2\frac{\theta}{2} + sin^4\frac{\theta}{2} \tag{2.30}$$

2.5   Method of finite differences

The evolution of the surge tank water surface oscillation can be computed by using several numerical methods. Out of these, the finite differences method is one of the simplest methods, thus, it will be used for developing a numerical model which shall describe the physical evolution of the water surface oscillation in the surge tank. This method, as its name says, relies on the finite differences transcription of the equations of motion (Popescu, Arsenie, & Vlase, 2003). (Chaudhry, 2014) also presents the method in his work. Starting from the general expression of the equations in finite differences, in the situation of a constant cross section area surge tank:

$$
\begin{cases}
\dfrac{L}{g}\dfrac{dV}{dt} + z \pm h_{f0}\left(\dfrac{sV}{Q_0}\right)^2 = 0 \\
\pm sV = SU + Q_T
\end{cases}
\tag{2.31}
$$

which can be written also:

$$
\begin{cases}
\Delta V = -\left(z \pm h_{f0}\left(\dfrac{sV}{Q_0}\right)^2\right)\dfrac{g \cdot \Delta t}{L} = 0 \\
\Delta z = \dfrac{s\Delta t}{S}V - \dfrac{\Delta t}{S}Q_T
\end{cases}
\tag{2.32}
$$

Thus, solving the finite differences system of equations (2.32) consists in direct calculation of the intermediate values ΔV and Δz considering the values of V and z the values at the beginning of a specific time interval $\Delta t = t_i - t_{i-1}$, resulting:

$$
\begin{cases}
\Delta V_i = -\left(z_{i-1} \pm h_{f0}\left(\dfrac{sV_{i-1}}{Q_0}\right)^2\right)\dfrac{g \cdot \Delta t}{L} = 0 \\
\Delta z_i = \dfrac{s\Delta t}{S}V_{i-1} - \dfrac{\Delta t}{S}Q_T
\end{cases}
\tag{2.33}
$$

For a better accuracy, the time interval Δt is desired to be as small as possible. Researchers using this method of computation improved it (Popescu, Arsenie, & Vlase, 2003) in the form written below:

$$
\begin{cases}
\Delta V_i = -\left(z_i \pm h_{f0}\left(\dfrac{sV_{i-1}}{Q_0}\right)^2\right)\dfrac{g \cdot \Delta t}{L} = 0 \\
\Delta z_i = \dfrac{s\Delta t}{S}V_{i-1} - \dfrac{\Delta t}{S}Q_T
\end{cases}
\tag{2.34}
$$

As a conclusion, the system of equations written in the finite differences form, can be also computed using numerical integration or any other improved iterative method. In this case, the system can be rewritten in the following form:

$$
\begin{cases}
\Delta V_j = -\left(z_i \pm h_{f0}\left(\dfrac{sV_i}{Q_0}\right)^2\right)\dfrac{g \cdot \Delta t}{L} = 0 \\
\Delta z_j = \dfrac{s\Delta t}{S}V_i - \dfrac{\Delta t}{S}Q_T
\end{cases}
\tag{2.35}
$$

This computation method, in the hypothesis of just one surge tank can be extended to the case of a variable surge tank, case in which it is recommended a higher attention when choosing the

Δz_i step. This will follow to ensure a better convergence for the solution of the system. The method can also be extended to multiple surge tanks hypothesis with the required adapts.

2.6 Types of surge tanks

This chapter presents the most usual types of surge tanks as presented in the literature (Chaudhry, 2014). The simplest surge tank can be represented by a vertical shaft connected to a pipeline, with its top usually open to the atmosphere (Bulu, n.d.). This equipment will reduce the effect of the overpressure caused by a closing valve or it will reduce the negative pressure caused by a suddenly opening valve. This type of surge tank is shown in Figure 2.10.
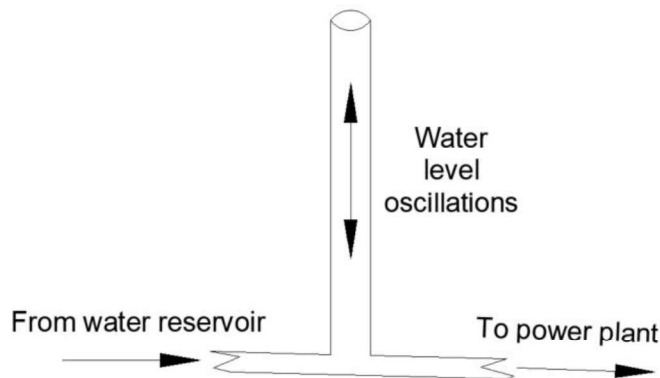
Figure 2.10 Simple surge tank (ST)

However, the simple shape of a surge tank creates constructive problems when the range of oscillations is significant, in the sense that its dimensions in terms of height are very difficult to achieve in practice. Therefore, it is necessary to adapt it in terms of shape and area cross section. Thus, in practice there are a multitude of constructive typologies of this shaft. In the followings some of the most common types will be reviewed.

An option to increase the damping action and reduce surges amplitude is a widening of the water tank cross section area. This cross-section area increase results in a considerable hydraulic singular head loss which increases the hydraulic energy dissipation and so, the damping of the oscillations will be faster. One other advantage brought by this configuration is the fact that the amplitude of the surges will be smaller due to higher cross section area of the tank. This increased cross section area surge tank is presented in Figure 2.11.
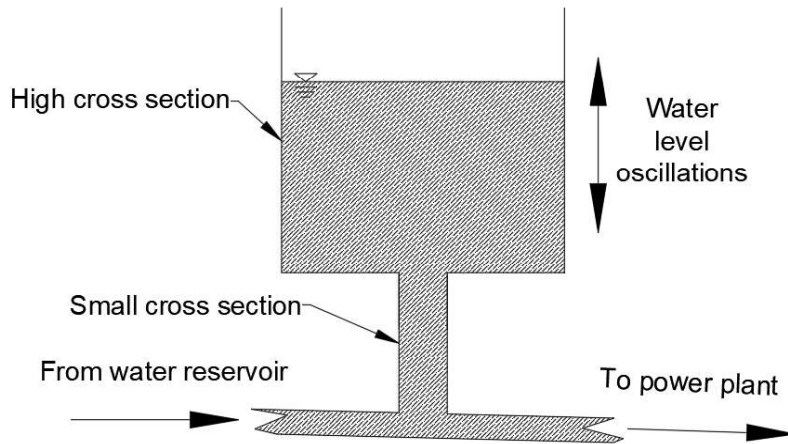
Figure 2.11 Increased cross section area surge tank (ST)

By adding a constraint at the entrance in the larger cross section of the tank, such as a restricted orifice, the singular head loss in this area in highly increased. This will result in a higher amount of hydraulic energy dissipation, namely higher damping and smaller amplitude of surges. The configuration of this type of surge tank is shown in Figure 2.12.
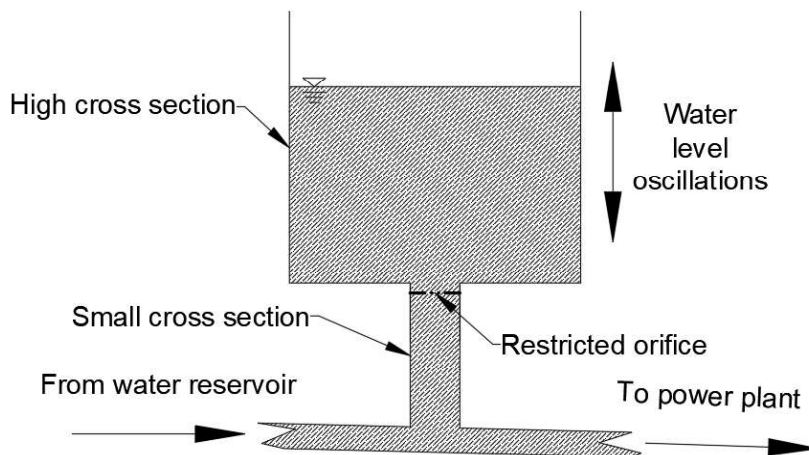
Figure 2.12 Restricted orifice surge tank (ST)

This type of surge tank can be improved in terms of dimensions by closing its top, which leads to another type of surge tank, namely pressurized surge tank. This way, the air cushion created above the water surface will absorb a part of the water hammer energy. Another advantage given by this type of surge tank is the fact that the amplitude of mass oscillations is significantly reduced meaning that the dimensions of the tank will be smaller comparing with a breathing surge tank. Its configuration can be seen in Figure 2.13.
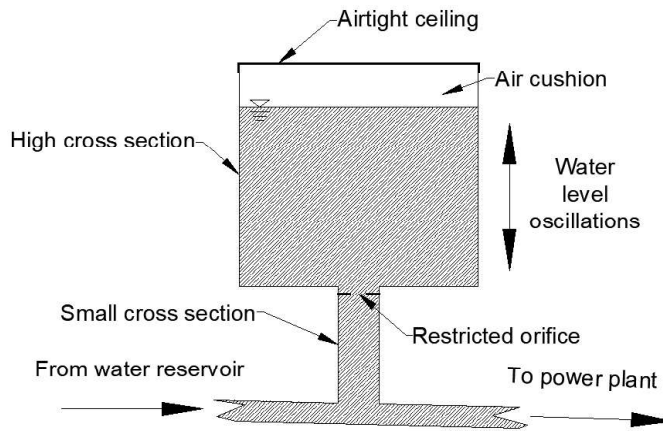
Figure 2.13 Pressurized surge tank (ST).

There are also possibilities to reduce the surge tank diameter when this is required. By adding a vertical riser in the center of the surge tank with orifices in it. The vertical riser diameter is usually around the same diameter as the pipe which surge tank is connected to. The water flow in the main surge tank is limited by the capacity of these openings in the vertical riser. Thus, the oscillations in the riser are not in phase with the oscillations in the main tank and so the hydraulic energy loss leads to a quicker damping of the oscillations in the riser. Using this type of surge tank returns in a diameter decrease up to 70% comparing with using a restricted orifice surge tank in the same conditions. This type of surge tank is known as differential surge tank and its main scheme is presented in Figure 2.14.
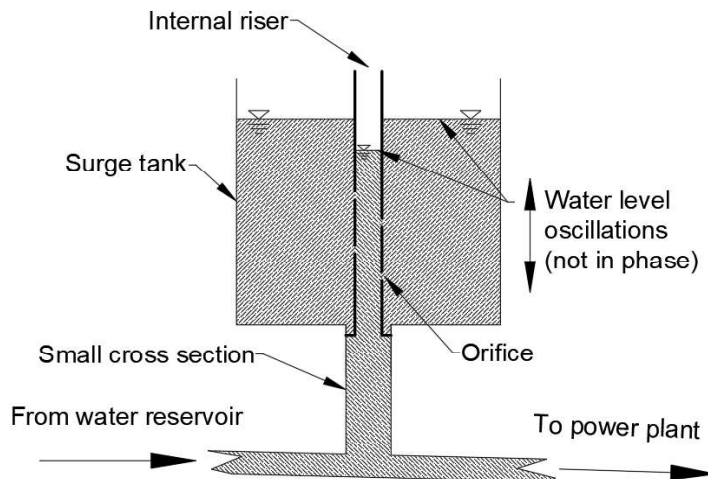
Figure 2.14 Differential surge tank (ST).

For high pressure head hydraulic systems, the surge tank's height increases significantly, therefore, using one of the surge tanks presented above would result in a very high volume of excavation, which in not always feasible. This led to the improvement of a simple surge tank with a reasonable diameter by adding some cavities located on its both ends, known as chambers. This way, the higher chamber can take the required water volume when the water surface oscillation reaches its elevation, during a sudden valve closure and the lower chamber provides the required water volume needed to compensate the low pressure caused by a suddenly opening valve. The chambers are also named galleries therefore, this surge tank configuration is known as gallery surge tank. Having both galleries is not mandatory, there can be only one of the galleries either the higher or the lower one, depending on the hydraulic system requirements. Gallery surge tank main configuration is presented in Figure 2.15.
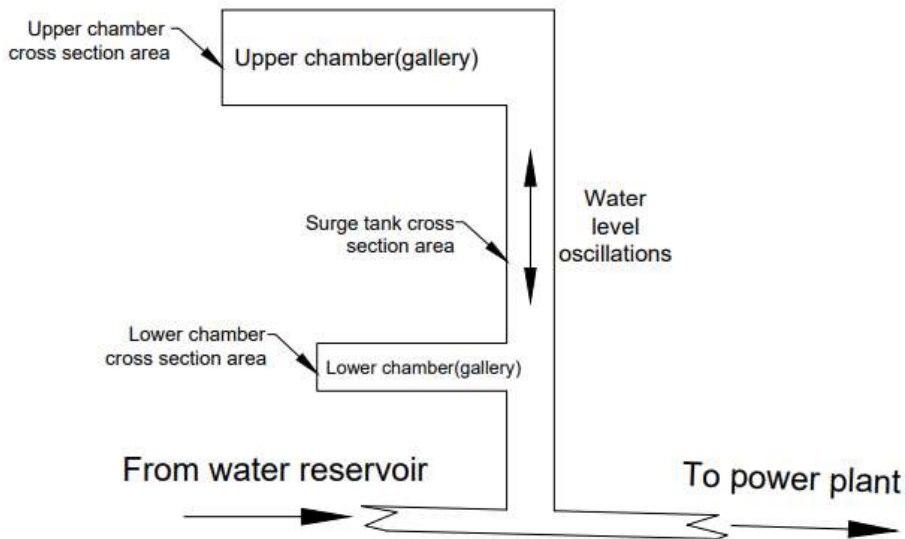
Figure 2.15 Gallery surge tank (ST).

In some cases, a surge tank construction can deal with height constraints that make no possible the implementation of any of the surge tank configurations presented above. The solution in this case is to incline the surge tank in order to comply with the reachable height. This results in another surge tank configuration known as inclined surge tank, presented in Figure 2.16. This configuration of surge tank also brings the advantage of a larger water surface area which reduces the amplitude of surges.
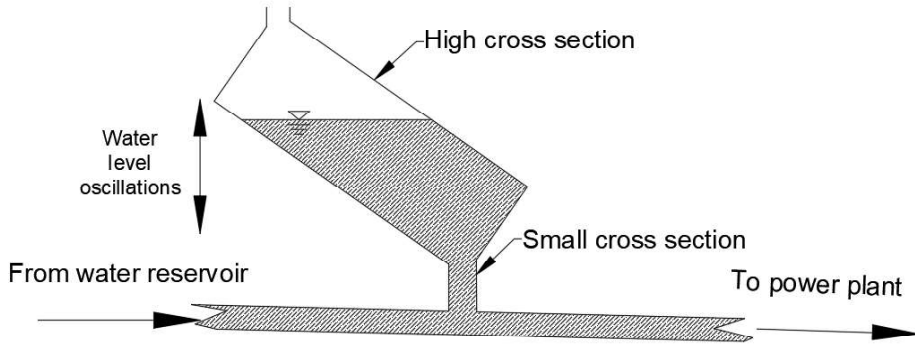
Figure 2.16 Inclined surge tank (ST).

The configurations of surge tanks presented until this point cover most of the situations usually met in the field. However, there are situations when none of the types presented can deal with in terms of height or even if they do, their construction may not be feasible. This issue conducted to one more configuration of surge tank which involves the evacuation of water when the water level surface in the tank exceeds a certain elevation. A spillway is then required to be installed inside the surge tank. This type of surge tank is known as spillway surge tank. It is presented in Figure 2.17.
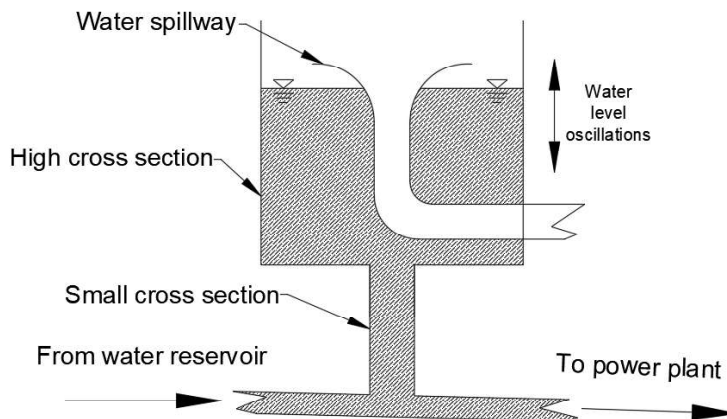
Figure 2.17 Spillway surge tank (ST).

2.7 Surge tank main tasks

Based on what presented until this point, a few conclusions regarding the main tasks a surge tank can fulfil can be withdrawn. These tasks can be structured with respect to each phenomenon occurred in the surge tank. Thus, there are 3 major points of view when referring

to a surge tank, such as pressure transients consisting of water hammer and mass oscillations, water masses or volumes circulated in the hydraulic system and the water surface level.

In what regards pressure transients, a surge tank (Bulu, n.d.):

•   diminishes the effect of the pressure wave caused by the intermittent operating of the power plant. Due to water moving water masses inertia, high overpressures occur at the end of the penstock during flow changes into the system. This is made possible by dividing this pressure wave in two different waves: one wave of damped water surface oscillations occurred in the surge tank and one pressure wave spread into the headrace;

•   diminishes the overpressure or under pressure appeared in the penstock or in the draft tube during intermittent operation by shortening the propagation length. The magnitude of so-called water hammer appeared in case of a sudden valve closure, depends on the dimensions and the elastic properties of the pipe. This pressure wave propagates along the pipe and will be relieved when it reaches a free water surface;

In the field of water masses or volumes circulated in the hydraulic system of a hydropower plant a surge tank (Bulu, n.d.):

•   provides the necessary water volume for the power plant's start up. The water volume demanded by the plant when start is supplied by the surge tank until the masses of water in the headrace reach the required velocity. However, the surge tank shall prevent air intake into the penstock even in the worst downsurge that can occur;

•   takes over the exceeding water volume in case of power plant's shut down;

Last point of view for characterizing surge tanks tasks is water surface level, where a surge tank can provide the possibility of monitoring the water level in the reservoir in a steady state, when oscillations damped completely.

3   Research methodology

3.1   Measurement techniques in hydraulic laboratories

3.1.1   Background

This study consists of experimental work in Hydraulic Laboratory (Vassdragslaboratoriet) at NTNU Trondheim, thus, the acknowledgement and the familiarization with laboratory equipment and procedures applied in experimental work is mandatory. In order to make this easier, a desk study of (Bureau Of Reclamation, 1980) has been done. The book mentioned represents 50 years of research and testing performed by United States Department of the Interior, Bureau of Reclamation. This institution responsibility consists of studies for development and conservation of US water sources.

Another desk study was performed based on (Nielsen, 1990), book presenting the main dimensioning requirements regarding hydropower plants with accent on dynamic properties involved in the processes. This reference also dedicates an entire chapter to the surge phenomena in hydropower plants which is exactly the focusing direction of the present study.

(Chaudhry, 2014) and (Popescu, Arsenie, & Vlase, 2003) present applied hydraulic transients in hydropower plants and pump stations along with plenty of case studies. These papers also made the object of the desk study that the present study is based on.

3.1.2   Dimensional analysis

It is well known that mathematical analysis, even though it is the cheapest, most of the time does not provide enough information or, the information provided by a mathematical model is rather not satisfactory and this leads to the requirement of an experimental analysis of the phenomena in addition to the theoretical results. However, when about large-scale applications such as power plants, it is not possible to reproduce the system analyzed at a real scale. Thus, the necessity of reproducing the analyzed system at a smaller scale emerges. This can be achieved using analysis methods such as Buckingham π theorem in order to reduce the physical equations parameters involved in nondimensional numbers (Bureau Of Reclamation, 1980). This way, the time required for computation is improved and the number of necessary variables is diminished. In the present study, following the implementation of the theorem mentioned, several parameters resulted as being relevant for the analysis of Roskrepp Power Plant. These parameters have been structured in Table 3.1.

Table 3.1 Roskrepp HPP characteristic parameters

Parameter	Symbol	Unit
Gravitational acceleration	g	m/s^2
Water density	ρ	kg/m^3
Pressure head	H	m/s2
Tunnel diameter	D	m
Tunnel length	L	m
Tunnel slope	s	‰
Tunnel friction	f	-
Water discharge	Q	m^3/s
Water velocity	v	m/s
Wave celerity (speed of sound in water)	a	m/s
Dynamic viscosity of water	μ	Pa·s
Time	t	s
Pressure	p	Pa

In what regards dimensional analysis, for simplifying the procedures, in some cases the hydraulic diameter is often considered same as diameter D (Pitorac, Vereide, & Lia, 2020). Out of the parameters shown in Table 3.1, water density, water velocity and tunnel diameter are the ones defining the π terms used in Buckingham theorem dimensional analysis. (Pitorac, Vereide, & Lia, 2020) mention 10 characteristic π terms for the analysis of the hydraulic systems as shown in Table 3.2.

Table 3.2 Hydraulic systems π terms (Pitorac, Vereide, & Lia, 2020)

	Name	Expression
π_1	Froude number	$\dfrac{v}{\sqrt{g \cdot D}}$
π_2	Head factor	$\dfrac{H}{D}$
π_3	Length factor	$\dfrac{L}{D}$
π_4	Tunnel slope	s
π_5	Friction factor	f
π_6	Discharge factor	$\dfrac{Q}{D^2 \cdot v}$
π_7	Mach number	$\dfrac{v}{a}$
π_8	Reynolds number	$\dfrac{\rho \cdot v \cdot D}{\mu}$
π_9	Keulegan-Karpenter number	$\dfrac{v \cdot t}{D}$
π_{10}	Euler number	$\dfrac{p}{\rho \cdot v^2}$

Out of the π terms presented in Table 3.2, π_1, π_7, π_8, π_9 and π_{10} are the ones characterizing the system, however, not all of them are relevant in the present study. Knowing that the focus of

the study is mass oscillations in a pressurized system, the adequate term in this field will be π_{10}, namely Euler number. By adding the assumption of incompressibility for the flow agent, namely water, π_9 and π_{10} terms become equal. π_7 and π_8 cannot be scaled correctly, however this will not affect the analysis significantly as their influence in the phenomena is known to be limited. For example, Reynolds number, after the turbulence has been reached, does not influences significantly the flow furthermore and, Mach number, which characterizes the water hammer in a hydraulic system, is also not very important since water hammer does not influence mass oscillations significantly (Pitorac, Vereide, & Lia, 2020).

Table 3.3 Similarity characteristic forces

Symbol	Description
F_i	*Inertial forces*
F_v	*Viscosity forces*
F_g	*Gravity forces*
F_p	*Pressure forces*
F_s	*Surface tension forces*
F_e	*Elastic forces*

Similarity laws have been used in verifying the dimensional analysis with respect to the forces that occur in the flow. These forces are presented in Table 3.3. Knowing that mass oscillations phenomena is basically represented by the transformation of kinetic energy into potential energy, results that only three out of six presented predominate. Inertial forces, gravitational forces and pressure forces are relevant in the presented study. Froude and Euler numbers consist of these three mentioned forces (Pitorac, Vereide, & Lia, 2020).

3.2   Roskrepp HPP tunnel system

In the summer of 2018, Roskrepp HPP was dewatered and a team of engineers performed a 3D scan for the headrace tunnel, upstream surge tank and powerhouse complex and georeferenced the scan by leveling from the surface and into the tunnels (Pitorac, Vereide, & Lia, 2020). It is important to mention that this operation of tunnels scan was vital since there have been 40 years now from Roskrepp Hydropower Plant commissioning. Even though construction drawings have been found, these can be sometimes inaccurate and as-build drawing do not exist (Leroquais, 2018). Considering the nature of the tunnels, namely drilled and blast, with no lining applied, the analysis of roughness and structure is mandatory in the present study, especially when comes about the physical laboratory reproduction of these tunnels. Figure 3.1 shows the allure of the upstream surge tank among with a portion of the headrace tunnel.
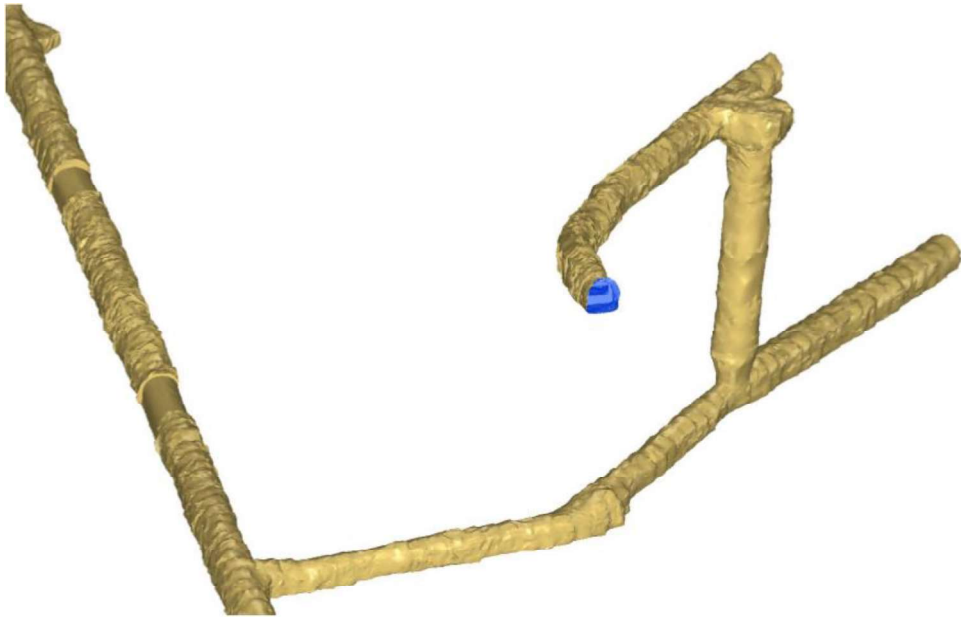
Figure 3.1.The 3D scan for the upstream surge tank (Pitorac, Vereide, & Lia, 2020)

(Leroquais, 2018) presents data related to the Roskrepp Hydropower Plant tunnel and surge tanks geometry. As presented, the plant has two surge tanks installed upstream the penstock and respectively downstream the turbine.

The headrace tunnels consist of D-shape tunnels paved with asphalt, at least they were paved with asphalt at the construction. During time, some sections of the headrace and respectively the tailrace remained without the asphalt pavement due to mass oscillations. The profiles of the tunnels are presented in Figure 3.2.
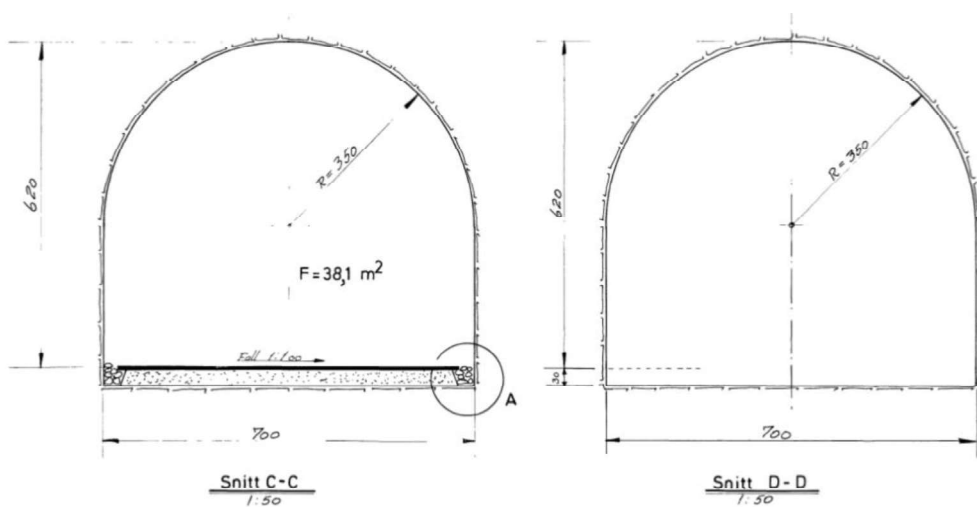
Figure 3.2 Roskrepp tunnels profiles (Leroquais, 2018)

The upstream surge tank is a variable surge tank composed by two chambers connected in between by a vertical circular cross section shaft. Both chambers consist of D-shape tunnels similar to the headrace tunnel. The configuration of the surge tank is presented in Table 3.4.

Table 3.4 Upstream surge tank configuration

	Lower limit [masl]	*Cross section [m²]*	*Upper limit [masl]*
Lower chamber	865	450	885
Transition cone	885	28÷60	890
Shaft	890	60	936
Upper chamber	936	667	940

The surge tank has been presented in a simplified form in Figure 3.3.
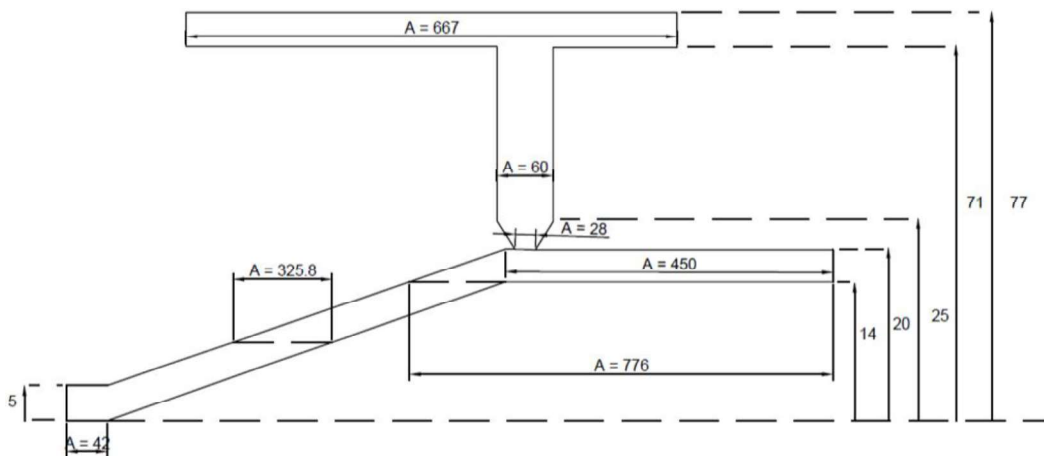
Figure 3.3 Simplified sketch of the upstream surge tank (Leroquais, 2018)

The downstream surge tank has a rectangular configuration with a constant cross section area of 110 m². It is installed in line with the tailrace tunnel and can be reached from the Power House. Downstream surge tank lower limit is situated at 817.1 masl and its upper limit is at 840 masl.

3.3 Roskrepp prototype data

3.3.1 Commissioning data from the owner

In the year of 1980, the owner of Roskrepp power plant contracted the Norges Hydrodynamiske Laboratorier for a set of pressure measurement on site (Leroquais, 2018). The purpose was determining the total head loss in Roskrepp power plant tunnel system. In order for this, two pressure sensors were installed on the turbine inlet and outlet. Measurements have been performed for two different values of load, 40MW and 50MW, respectively. During the measurements, the water level in the two reservoirs were monitored, generally there were slight differences only for the lower reservoir. As expected, headrace losses prevail in both cases, while for the tailrace in the first case they are almost nil. Table 3.5 shows the result report of the measurements performed.

Table 3.5 1980 Roskrepp field measurements (Leroquais, 2018)

P	Q	Water level Upper reservoir	$H_{upstream}$	$\Delta H_{upstream}$	Water level Lower reservoir	$H_{downstream}$	$\Delta H_{downstream}$
[MW]	[m3/s]	[masl]	[masl]	[mWC]	[masl]	[masl]	[mWC]
40	46.5	928.2	925.5	2.7	828.22	828.3	0.08
50	58.3	928.2	924.1	4.1	828.3	828.5	0.2

The fact that both cases involve estimated values for the discharge. Another thing required to be considered is the fact that since the commissioning, some things might be changed, thus, nowadays different head losses might occur.

3.3.2 Roskrepp field measurements

On 19th of September 2017, a team of engineers and researchers from NTNU and Sira-Kvina power company performed a set of measurements in the Roskrepp power plant. In order for this to be possible, the plant was disposed for this purpose for several hours. The measurement setup consisted of two pressure sensors on the turbines inlet and outlet, another two sensors monitoring the two hydraulic actuators responsible for the wicket gate opening and closing, while the power produced, the speed of rotation and water levels in both reservoirs were monitored by the power plants hardware. It is required to specify that the discharge, respectively the speed of the water in the hydraulic system was not known during the measurements. The tests proceeded around 9 am, after a complete closeup of the plant for several hours before. It consisted of several load variations and ended with an emergency shut down at noon. It is very important for the further computation of the experimental results a precise acknowledgement

about the exact location for the two pressure sensors used. As seen in Figure 3.5, these sensors are located as following: the inlet one is just after the butterfly valve in front of the turbine, while the outlet one is at the very beginning of the draft tube.
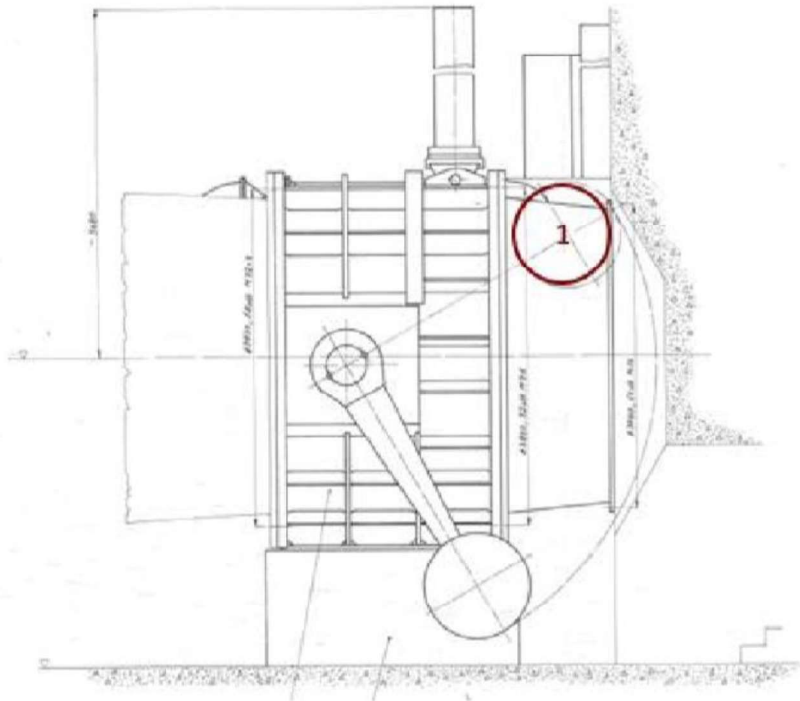
Figure 3.4 Butterfly valve and inlet pressure sensor location (Leroquais, 2018)

Figure 3.4 presents the butterfly valve responsible for water admission in the turbine. Red number 1 shows the positioning of the first pressure sensor used for measuring the pressure at the turbine inlet. It is necessary to be mentioned that normally pressure sensors location in a power plant is constraint by a series of field conditions therefore, for Roskrepp power plant, pressure sensors locations are as shown in Figure 3.5.
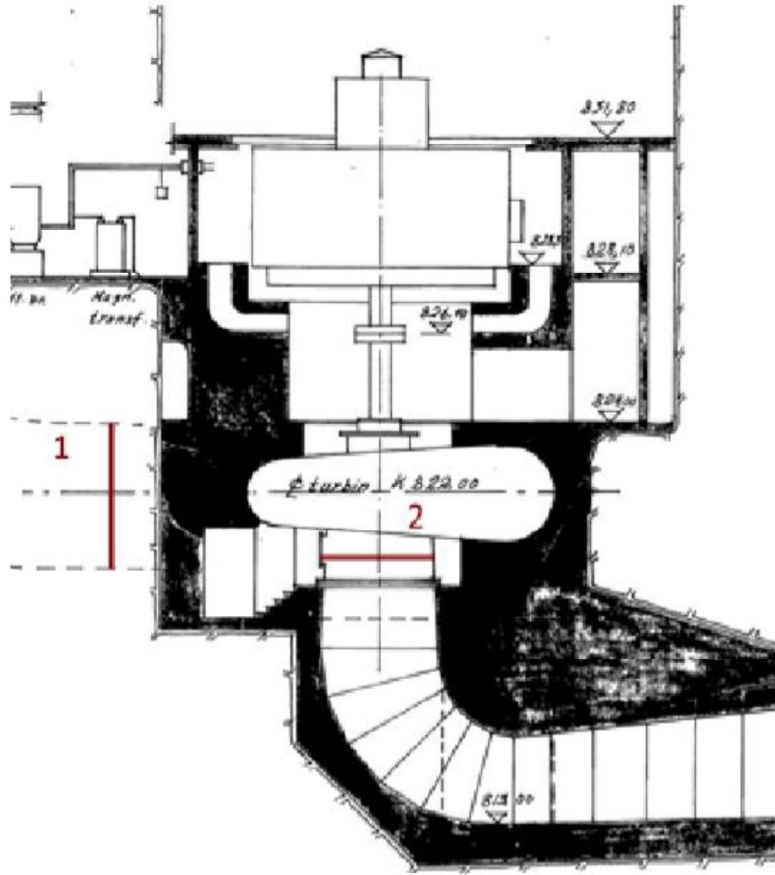
Figure 3.5 Pressure sensors locations in Roskrepp power plant (Leroquais, 2018)

Using the location of the sensors, measured pressure values can be either related to the turbine elevation or reported to the sea level in order to make their interpretation easier. For the easiest understanding of the pressure variation, the measured values will be converted into head values reported to the sea level as seen below:

$$h_{sensor} = \frac{p_{sensor}}{\rho g} + z_{sensor} \qquad (3.1)$$

where h_{sensor} is the pressure head measured using the sensor and expressed in meters water column [mWC]; p_{sensor} is the value measured by the sensor expressed in Pascals [Pa] and z_{sensor} is the sensor elevation above the sea level [m].
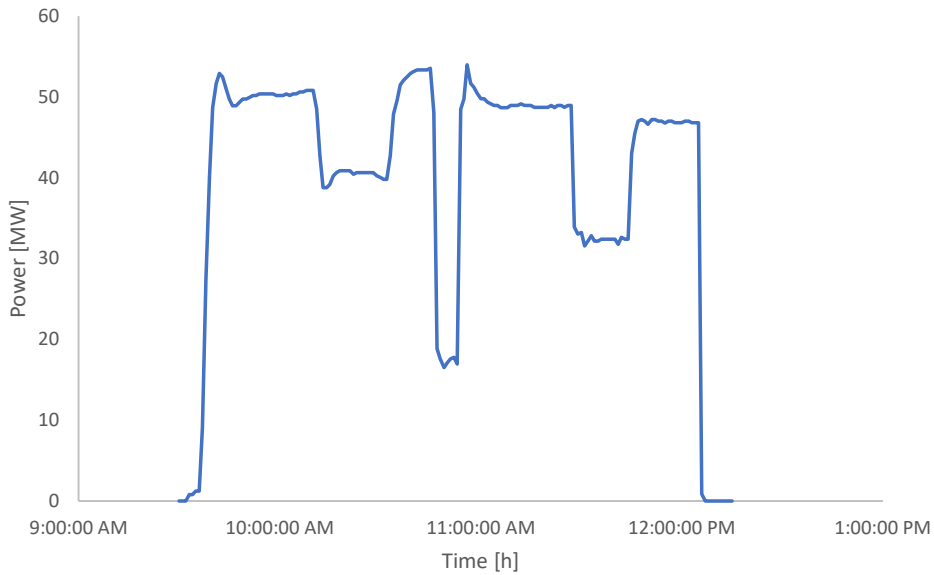
Figure 3.6 Roskrepp HPP load variation during tests

During the measurements, as can be seed in Figure 3.6, several operations have been performed. Out of these, two representative extractions have been made and will be used for the calibration and respectively validation of the physical model. The sets extracted are the emergency shut down from the end of the measurements set. The emergency shut down (ESD) maneuver will be used for the calibration of the physical model. The other set of data extracted is a load rejection, namely the one performed between 11 and 12 o'clock. This one will be used for the verification of the physical model. Therefore, these representative prototype data will be presented forward.

3.3.2.1 Emergency shut down

Verification of the laboratory physical model requires set of prototype data characterizing a transient maneuver in the power plant operation. The set of data collected is too large to be computed easily, thus, the very last part of it, consisting of an emergency power plant shut down, has been extracted. Figure 3.7 shows pressure head variation measured upstream turbine, while Figure 3.8 shows the variation downstream the turbine.
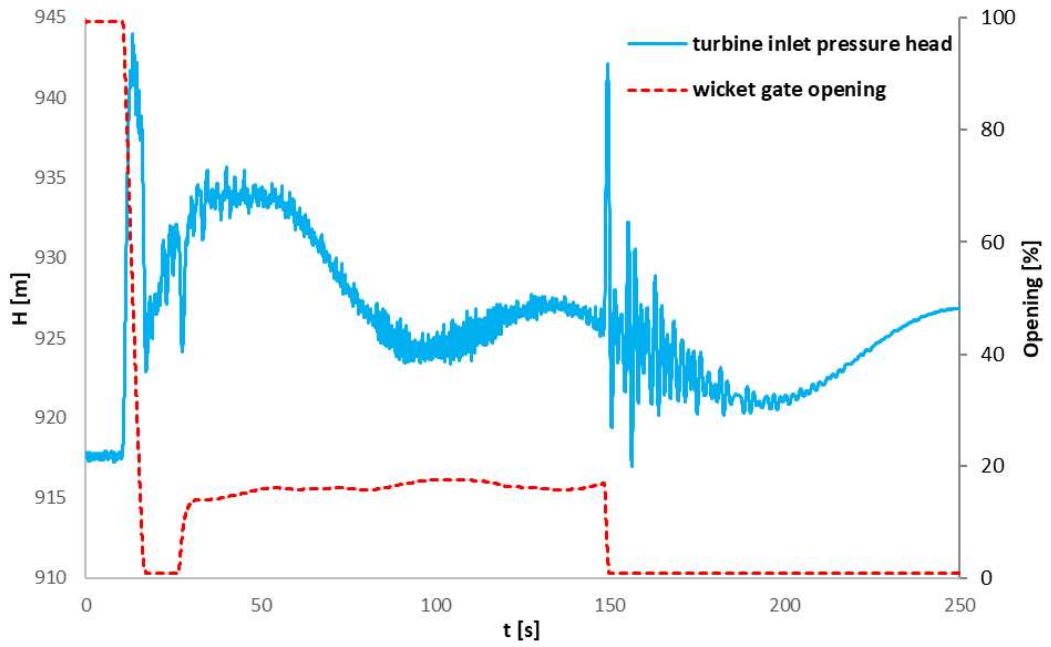
Figure 3.7 Prototype upstream turbine emergency shut down
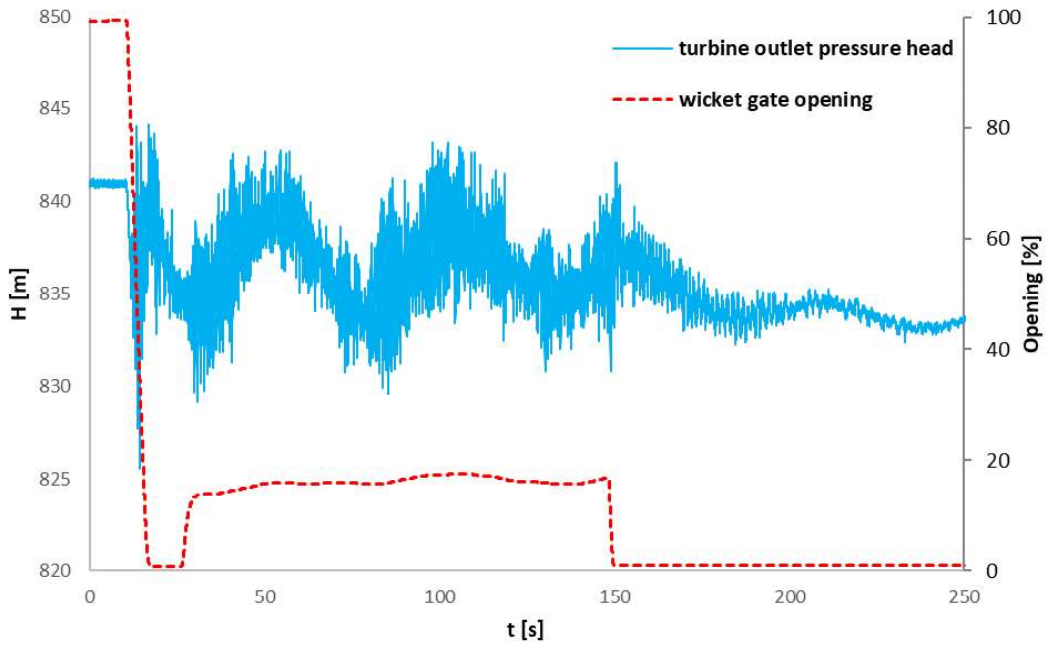
Figure 3.8 Prototype downstream turbine emergency shut down

3.3.2.2 Load rejection

Validation of the physical model requires, as well, a transient maneuver in the power plant operation. Since during the tests, several load rejections have been proceeded, another smaller set of data, containing a load rejection, has been extracted from the prototype measurements. On a completely random basis, the load rejection performed at 11:27AM has been chosen. This maneuver is characterized by the parameters shown in Table 3.6.

Table 3.6 Prototype load rejection parameters

	time	Power [MW]	Discharge [m³/s]	Wicket gate [%]	H_{UT} [masl]	H_{DT} [masl]
initial	11:27:00 AM	48.90	62	99.90	916.76	829.66
final	12:30:20 PM	32.39	40	65.65	921.23	833.48

For the time interval specific to the load rejection presented in Table 3.6, graphical evolution of the pressure head both upstream and downstream the turbine has been extracted from the data set available. Thus, this new set of data will be used for the validation of the physical model. Figure 3.9 and Figure 3.10 show the evolution of the pressure head measured both upstream and downstream the turbine together with the wicket gate closure during the load rejection of the power plant.
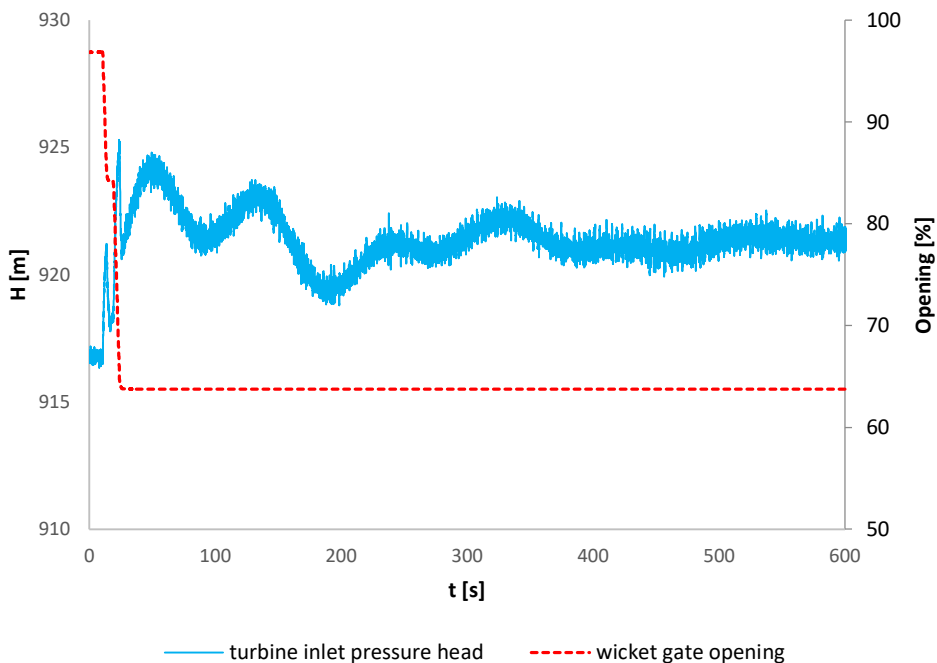
Figure 3.9 Prototype upstream turbine load rejection
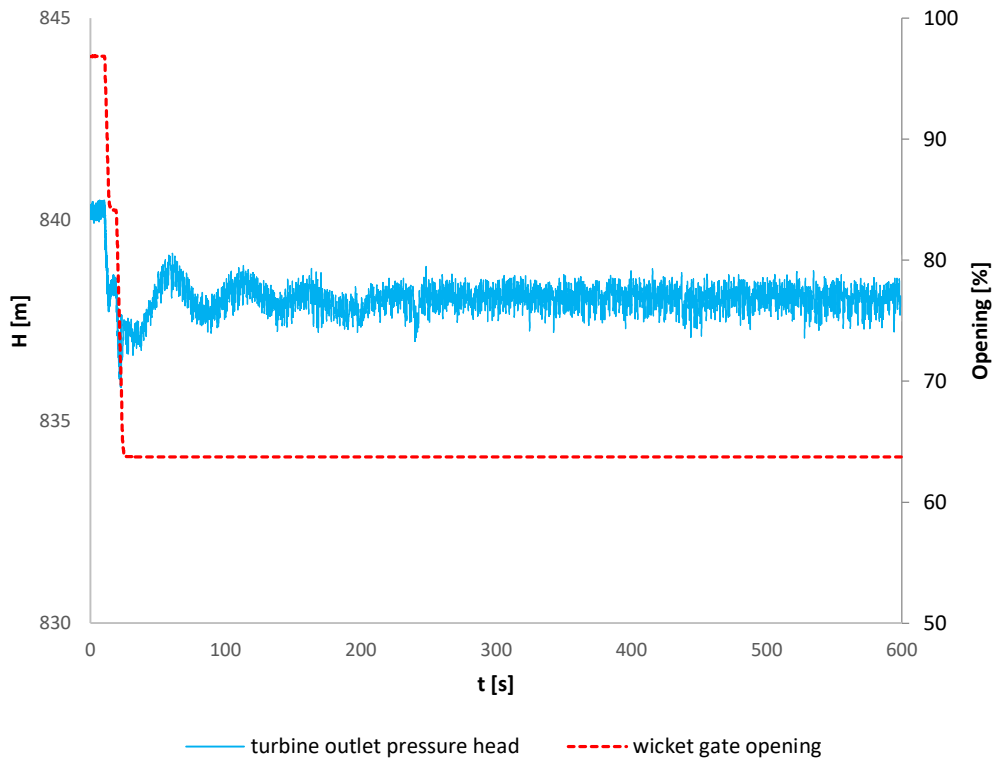
Figure 3.10 Prototype downstream turbine load rejection

3.4 Physical model

3.4.1 Physical model overview

Using the collected data, a physical model on a 1:70 scale was built in the NTNU Hydropower Laboratory. The scale was determined based on the available space in the laboratory and the availability of the equipment and materials required for the model construction. Even though all the dimensions measured in the prototype have been scaled accordingly, tunnel roughness could not be scaled as linear roughness, thus, the entire headrace head loss was scaled using 4 valves installed on each relevant pipe stretch. Another parameter not implemented in the physical model is the tunnel slope, neglected due to its limited influence in what regards mass oscillations. The two water sources consisting of upper and lower reservoir were built as variable levels water tanks, while the two surge tanks and the adit follow the existing design in prototype. The brook intake initially built as a vertical shaft has been adapted to an inclined pipe in order to satisfy the water surface cross section area required.

A parallel between the model built in the laboratory parameters and the parameters of the prototype is presented in Table 3.7. All the elevation values are relative to the turbine elevation. Figure 3.11 presents the configuration of the physical model.

Table 3.7 Prototype model analysis (Pitorac, Vereide, & Lia, 2020)

Parameter	Prototype	Model
Scale [-]	1:1	1:70
Turbine elevation [m]	0	0
Pump elevation [m]	-6.6	-0.095
Upper reservoir elevation [m]	107 ÷ 68	1.5 ÷ 1.0
Lower reservoir elevation [m]	15 ÷ 3	0.2 ÷ 0.04
Tunnel diameter [m]	7	0.1
Total waterway length [m]	3886	56
Turbine closing time [s]	10	1.2
Mead discharge [m^3/s]	60	$1.5 \cdot 10^{-3}$
Froude number [-]	0.19	0.19
Reynolds number [-]	10^7	$2 \cdot 10^4$
Mach number [-]	0.001	0.000
Euler number [-]	494	494
Strouhal number [-]	337	3521
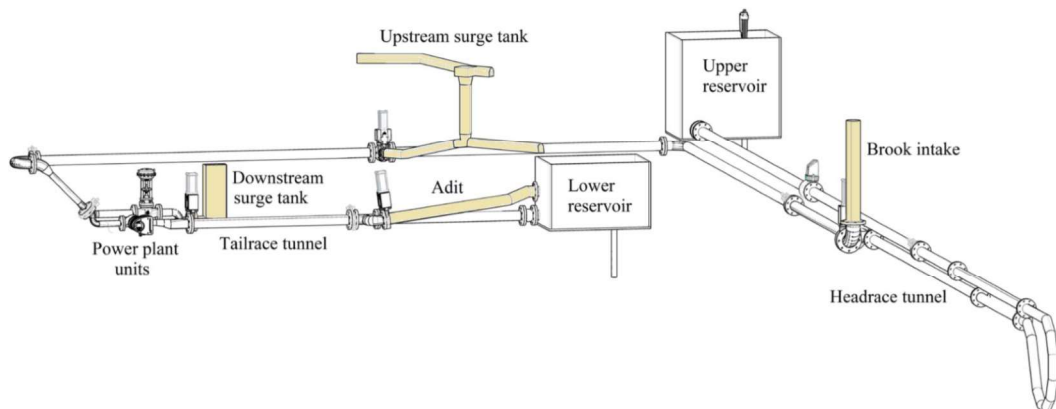
Figure 3.11 Hydraulic scale model of Roskrep hydropower plant (Pitorac, Vereide, & Lia, 2020)

3.4.2 Model construction and instrumentation

The tunnel system in the physical model consists of welded AISI304, 100mm diameter stainless steel pipes with 3mm thickness, while the penstock consists in a 56mm diameter stainless steel pipe, 2mm thickness. The four shafts represented by the brook intake, upstream surge tank, downstream surge tank and adit were constructed using acrylic pipes or plates. In what regards

the upstream surge tank, these plates were modelled into D-shape cross section to comply with the real shape in the prototype. Each of this shaft is equipped with a pneumatic controlled knife gate valve right at the junction with the system and so is can be easily disconnected from the main tunnel system. The two water reservoirs consist of wooden boxes sealed with fiberglass, the upper one having 0.8 m^3 volume and the lower one 0.45 m^3. The water level inside these two reservoirs can be adjusted with the help of a 2.8m length weir installed in each of them and which can be adjusted using 2 linear actuators. The model operates in an open loop in what regards water supply, meaning that it takes water from the laboratory water supply and returns it into the main drainage. In order to simulate the turbine in the system and control the flow, a pneumatic controlled globe valve is being used, while for the fast shut down a pneumatic controlled butterfly valve is installed at the lower end of the penstock (Pitorac, Vereide, & Lia, 2020). The main equipment used in the physical model construction is presented in the figures:

Figure 3.12 Pneumatic controlled knife gate valve

Figure 3.14 Electromagnetic flow meter

Figure 3.13 Pressure sensor

Figure 3.15 Butterfly valve

Figure 3.16 Pump

Figure 3.18 Pneumatic controlled globe valve

Figure 3.17 Pneumatic controlled burretfly valve

Figure 3.19 Electrical actuated ball valve

All the pictures shown in the figures 3.12 - 2.19 have been retrieved from www.alibaba.com.

3.4.3 Model sensors calibration

Pressure sensors used in the physical model are pressure transducers retrieving an electrical current signal depending on the pressure in the system. Therefore, first step in the model calibration was the calibration of the sensors. This was done by using a calibration pump, proceeding increasingly from 0 to the maximum pressure value of the sensor calibrated and backwards. Further, a linear evolution of the current signal depending on the pressure measure was determined. The operation was repeated for all the sensors in the physical model and the equations describing each sensor was used further to convert the signal measured in amps to bar.

$$p_{sensor} = a * I_{sensor} + b \qquad\qquad (3.2)$$

where p_{sensor} is the value for the pressure measured, converted to bar, I_{sensor} is the current retrieved by the sensor, a and b are 2 constants determined experimentally using the calibration pump in the way described above. As an example, below is the calibration for the sensor used for measuring the pressure downstream turbine. The sensor has a range up to 300 mbar and a response frequency of 3.5 kHz. It can measure within this range with an accuracy of $\pm 1\%$.

Table 3.8 Calibration of a pressure sensor used in the physical model

I [mA]	4	8.4	12.8	16.9	21.3	17	12.7	8.4	4
p [mbar]	1	80	160	240	322	240	159	80	0

The sensor output current dependence on the pressure measured is shown in Figure 3.20. As can be seen, it is a linear dependence which can easily be computed knowing the line graph slope, namely the 2 constants contained in the equation (3.2).

y = 18689x - 76.986
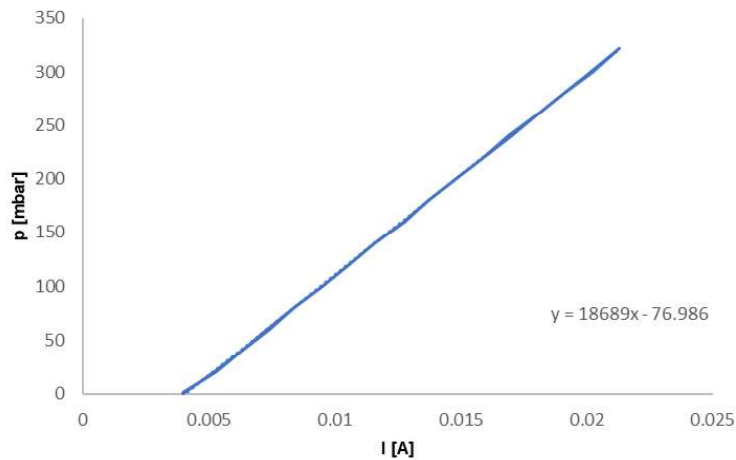
Figure 3.20 Pressure sensor calibration

Once all pressure sensors in the model have been calibrated, their signal is computed in the computer software used for data acquisition, with the help of both (3.1) and (3.2) equations and multiplied with the scale factor as in the end the software will retrieve prototype scale values for the pressures measured in the physical model. The same thing has been done for the two discharge measurement units installed on model's headrace resulting porotype scale values for the discharge flowing in the model. Time is also scaled to prototype values and so, in the end real scale evolutions of phenomena will be retrieved.

Based on the prototype data available, a calibration for the laboratory model was performed, seeking to obtain the same values of pressure head after computing them with the scale factor

in a shutdown model state. This results in determining the water levels required in the model to fulfil ones existing in the prototype at the time when measurements were performed. After proceeding this operation, the model scale head pressure values related to the prototype ones resulted as seen in Table 3.9. Both cases are reported to the turbine level for the prototype, to the globe valve for the physical model.

Table 3.9 Physical model water levels

	Prototype [mWC]	Model [mWC]
Upper reservoir water level	103.53	1.513
Lower reservoir water level	11.39	0.216

After ensuring the levels in the model required to satisfy the conditions in the prototype and checking correctitude of sensors calibration, the next step is the adjustment of the scaled prototype hydraulic linear losses in the physical model using the butterfly valves installed in the model as following: one between upper reservoir and the brook intake; one between brook intake and upstream surge tank; one between the upstream surge tank and penstock. These three valves mentioned are being used for headrace tunnel calibration, while for the tailrace tunnel calibration, a similar valve has been installed between downstream surge tank and adit. The procedure followed involved scaling the pressure head losses calculated for the prototype on each length section as shown in Table 3.10. The values for the prototype head loss have been determined for the nominal operating point, namely 50MW load for the power plant.

Table 3.10 Length sections head losses

Section	Prototype		Physical model	
	Length [m]	Head loss [m]	Length [m]	Head loss [m]
Upper reservoir - brook intake	2201.3	5.1	31.6	0.07
Brook intake - upstream surge tank	970.2	1	13.9	0.01
Upstream surge tank - penstock	341	0.32	4.9	0.005
Penstock	50	0.8	0.72	0.01
Inlet pipe	7.3	0.8	0.1	0.01
Draft tube	24	0.4	0.34	0.01
Downstream surge tank - adit	155	0.35	2.2	0.01
Adit - lower reservoir	145	0.35	2.1	0.01

Considering the fact that there were no discharge measurements during tests, the discharge was estimated based on the available data at a value of approximately 60 m^3/s which corresponds to a physical model scale value of 0.00145 m^3/s, 1.45 l/s respectively. Further, with this discharge flowing into the system, each of the four butterfly valves used for head loss calibration has been adjusted. The procedure consisted of maintaining the water level values specified in Table 3.9

in the two water reservoirs, adjusting the globe valve closure in order to have 1.45 l/s discharge in the system. Then, starting from the first valve installed between upper reservoir and brook intake forward, each of these valves has been adjusted until the head loss value for each length section has been reached. Once this has been achieved, the model is considered calibrated and the verification step shall be pursued.

3.4.4 Physical model calibration

Verification of the physical model is a mandatory step in the process. This action require the simulation of a transient operation for the power plant such as a startup or an emergency shut down. In this study, the verification of the model has been done for an emergency shut down, which was extracted from the data set available. The setting for the simulation of an emergency shut down is presented in Table 3.11.

Table 3.11 Emergency shut down simulation parameters

	Upper reservoir water level [m]	Lower reservoir water level [m]	Discharge [m³/s]	Valve closing time [s]
Prototype	103.53	11.39	60	9.5
Model	1.513	0.216	0.00145	1.14

After ensuring the correct setting for the model, the simulation proceeded and the results obtained were represented scaled at prototype values among with the prototype data presented above in Figure 3.7 and Figure 3.8. Thus, Figure 3.21 and respectively Figure 3.22 will result as shown.
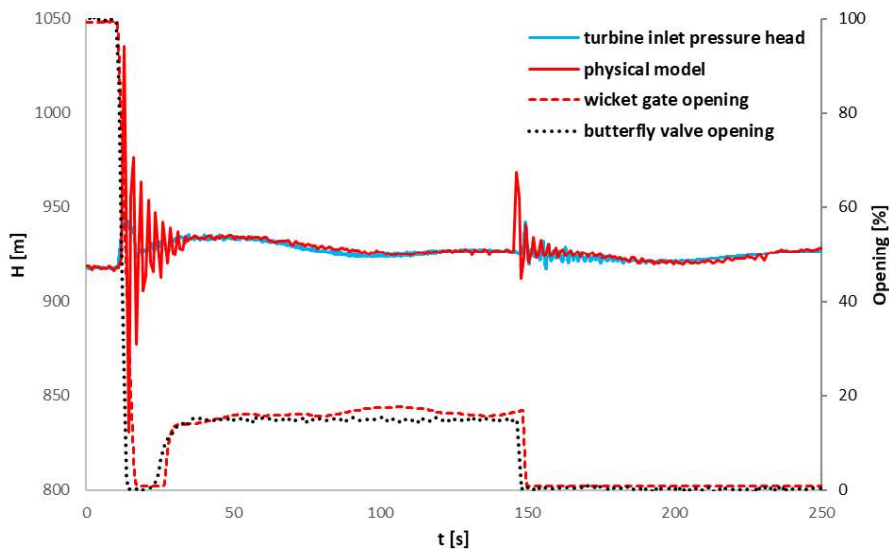
Figure 3.21 Upstream turbine model verification
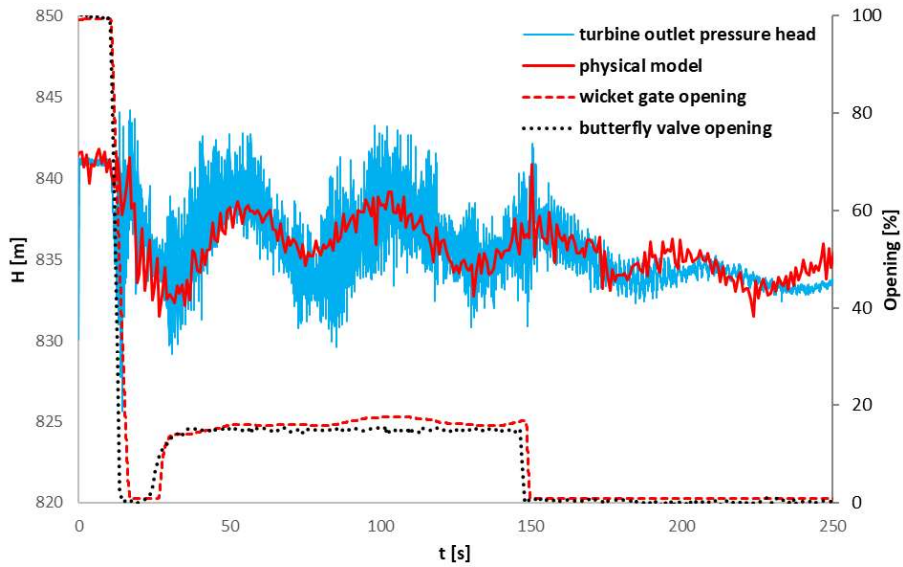
Figure 3.22 Downstream turbine model verification

3.4.5 Physical model validation

Validation of the physical model is the last step required before admitting the correctitude of the model behavior. Similar with the verification, this step requires prototype data for a transient maneuver performed in the power plant operation. Thus, the load rejection set of data will be used for the validation. The setting for the model has been made as shown in Table 3.12.

Table 3.12 Load rejection simulation parameters

	Upper reservoir water level	Lower reservoir water level	Discharge		Valve opening		Valve closing time
			initial	final	initial	final	
	[m]	[m]	[m^3/s]	[m^3/s]	[%]	[%]	[s]
Prototype	103.53	11.39	58	38	96	100	8.5
Model	1.513	0.216	0.00145	0.00095	64	40	1.08

Once the simulation parameters have been ensured, the simulation proceeded and the results have been represented at prototype scale values and represented together with the prototype data shown previously in Figure 3.9 and Figure 3.10. Therefore, the pressure head variations for both prototype and physical model upstream and downstream the turbine have been represented in Figure 3.23 and Figure 3.24 respectively.
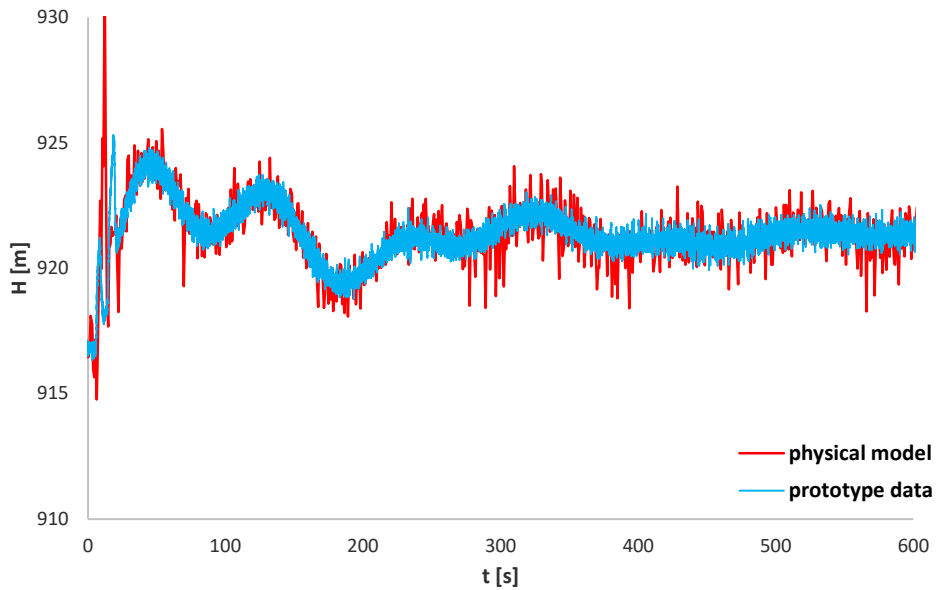
Figure 3.23 Upstream turbine model validation
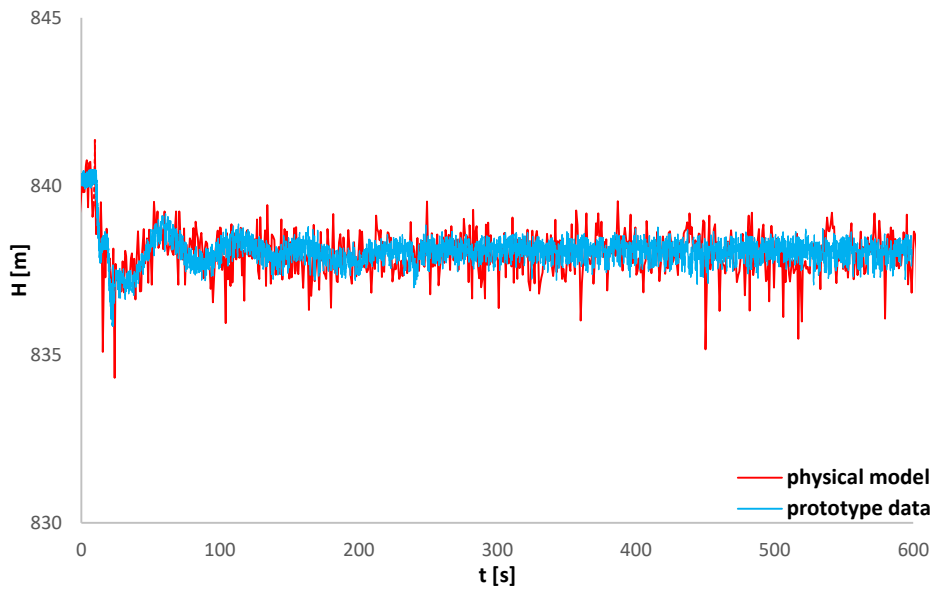
Figure 3.24 Downstream turbine model validation

3.5 Numerical model

Based on the theory presented in chapter 2.5, a numerical model has been developed. The model has the same geometrical inputs as the prototype, namely Roskrepp Power Plant. However, due to the complexity of the hydraulic system and the restrictions in what regards the lack of experience in numerical modelling, the numerical model does not take account of the brook

intake for the headrace tunnel and of the adit for the tailrace respectively. The numerical model consists of a MatLAB script based on the finite differences method of solving the system of equations that describes the water surface oscillations in the surge tank.

For a discharge Q flowing in a steady state in the hydraulic system, between the water level in the reservoir and the water level in the surge tank will be a difference z_0 corresponding to the frictional losses in the tunnels. If the discharge value changes, the equilibrium state in the system ceases, thus the water level in the surge tank no longer corresponds to the friction head losses and mass oscillations begin.

The driving force in the velocity direction v at all times will be:

$$F = \rho \cdot g \cdot a \cdot z \qquad (3.3)$$

where:

ρ = water density;

g = gravitational acceleration;

a = tunnel cross section area;

z = water level difference between the surge tank and the reservoir;

The friction in the tunnels gives a head loss that is proportional with the water velocity for turbulent flow:

$$R = \rho \cdot g \cdot a \cdot h_f = \rho \cdot g \cdot a \cdot \alpha \cdot v \cdot |v| \qquad (3.4)$$

where:

$\alpha = \dfrac{L}{M^2 R_h^{4/3}}$ = friction head loss coefficient;

v = water velocity in the tunnel;

L = tunnel length;

M = Manning number;

R_h = hydraulic radius.

The force caused by friction is acting against the velocity direction v, thus it gives the sign for the numerical value of R. The result in combining the two forces will then be:

$$F = \rho \cdot g \cdot a \cdot z - \rho \cdot g \cdot a \cdot \alpha \cdot v \cdot |v| = \rho \cdot g \cdot a \cdot (z - \alpha \cdot v \cdot |v|) \tag{3.5}$$

This force acts on behalf of the water mass existing in the tunnel system $m = \rho \cdot g \cdot L$, where L is the tunnel length. Therefore, it will result:

$$\rho \cdot g \cdot a \cdot (z - \alpha \cdot v \cdot |v|) = \rho \cdot g \cdot a \cdot L \frac{dv}{dt} \tag{3.6}$$

which can also be written in the form:

$$\frac{dv}{dt} = \frac{g}{L} \cdot (z - \alpha \cdot v \cdot |v|) \tag{3.7}$$

Mass oscillations in a hydraulic system are significantly slow, thus, the water can be considered inelastic. As a result, the usual continuity equation can be applied:

$$Q = v \cdot a + \frac{dz}{dt} \cdot A \tag{3.8}$$

where:

A = surge tank cross section area;

$\frac{dz}{dt}$ = instantaneous velocity of the water surface in the surge tank.

The continuity equation can also be written as:

$$\frac{dz}{dt} = \frac{Q}{A} - \frac{a}{A} \cdot v \tag{3.9}$$

or:

$$v = \frac{Q}{a} - \frac{A}{a} \cdot \frac{dz}{dt} \tag{3.10}$$

The equations (3.7) and (3.8) can be combined by introducing:

$$\frac{dv}{dt} = -\frac{A}{a} \cdot \frac{d^2z}{dt^2} \tag{3.11}$$

Therefore, it results into:

$$\frac{d^2z}{dt^2} + \left(\frac{g}{L} \cdot \frac{a}{A} \cdot z\right) - \left(\frac{g}{L} \cdot \frac{a}{A} \cdot (\alpha \cdot v \cdot |v|)\right) = 0 \tag{3.12}$$

The equation (3.12) has got a link with the friction as well, thus, it cannot be solved using ordinary integration. It is therefore advisable to solve the problem numerically using stepwise integration. The equations (3.7) and (3.9) can be written as following:

$$\Delta v = \frac{g}{L} \cdot (z - \alpha \cdot v \cdot |v|) \cdot \Delta t \tag{3.13}$$

$$\Delta z = \left(\frac{Q}{A} - \frac{a}{A}\right) \cdot \Delta t \tag{3.14}$$

The numerical model solves the equations (3.13) and (3.14) starting from the initial solution described by the steady state before the transient to occur.

For the present study, the numerical model was first verified with the data measured in the experiments performed. Thereafter, the model has been adapted for the simulation of two improvement methods proposed in the study. Even though the numerical model results seem promising, there must be taken into account that there is a significant uncertainty among with these results, mostly due to the simplicity of the numerical model and also due to the fact that the model does not take into account the secondary shafts represented by the brook intake in the headrace tunnel and the adit in downstream tunnel.

3.5.1 Numerical model calibration

Numerical model developed must be calibrated before being used in modelling. Considering there is no data available from the prototype regarding the oscillations in the surge tank, after the physical model has been validated and verified, this one will be used for the calibration and respectively validation of the numerical model. Also, considering that the simplicity of the numerical model does not take into account the secondary shafts, namely the brook intake and the adit, the physical model data used for this step has been obtained running the experiments with the brook intake, respectively the adit closed.

The calibration of the numerical model will be done for an emergency shut down. In what regards water levels, for the downstream surge tank, running the experiment for different water levels in the reservoirs is not relevant as the surge tank has a constant cross section area, while for the upstream surge tank, it is important to verify the correctitude of the calibration for both boundaries. Thus, Figure 3.25 shows the calibration of the numerical model for both extremities of the upstream surge tank and Figure 3.26 shows the calibration for the numerical model on the downstream surge tank.

a) lower chamber   b)upper chamber

Figure 3.25 Numerical model calibration - upstream surge tank
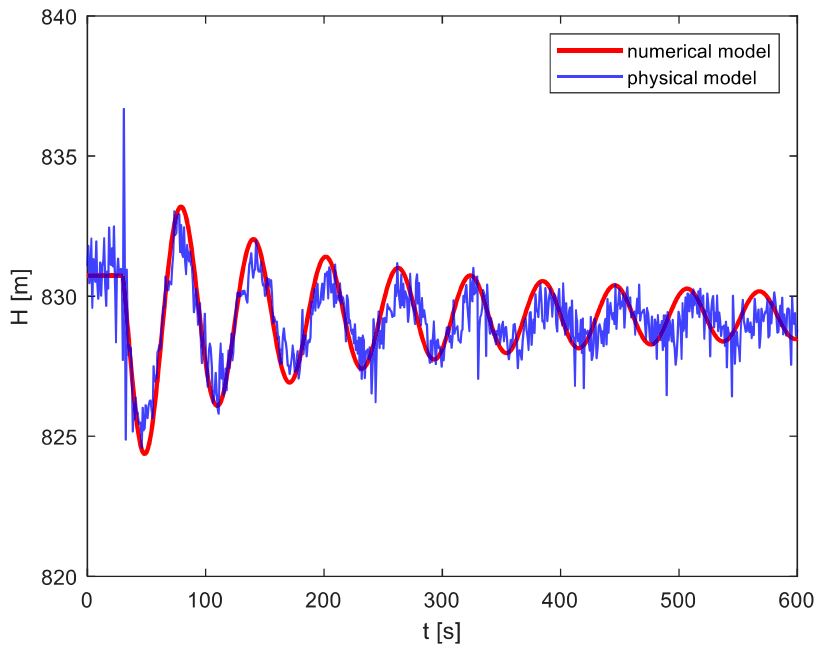
Figure 3.26 Numerical model calibration - downstream surge tank

3.5.2 Numerical model validation

The validation of the numerical model has been done based on a startup maneuver. As stated in the calibration chapted, the downstream surge tank validation does not require experiments for different water levels due to the constant cross section area. However, the upstream surge tank has to be verified in both extremities in order to check the correctitude of the model in the two chambers. Therefore, the validation data of the numerical model is presented in Figure 3.27 for

both water level extremities in upstream surge tank and respectively in Figure 3.28 for the downstream surge tank.

The discharge setup for running the validation experiments has been considered the nominal discharge required by the power plant, 60 m^3/s and the water levels in the reservoirs have been set at the minimum (929 masl for the upper, 837 masl for the lower reservoir), respectively maximum (890 masl for the upper reservoir, 825 masl for the lower reservoir).

a) lower chamber   *b)upper chamber*

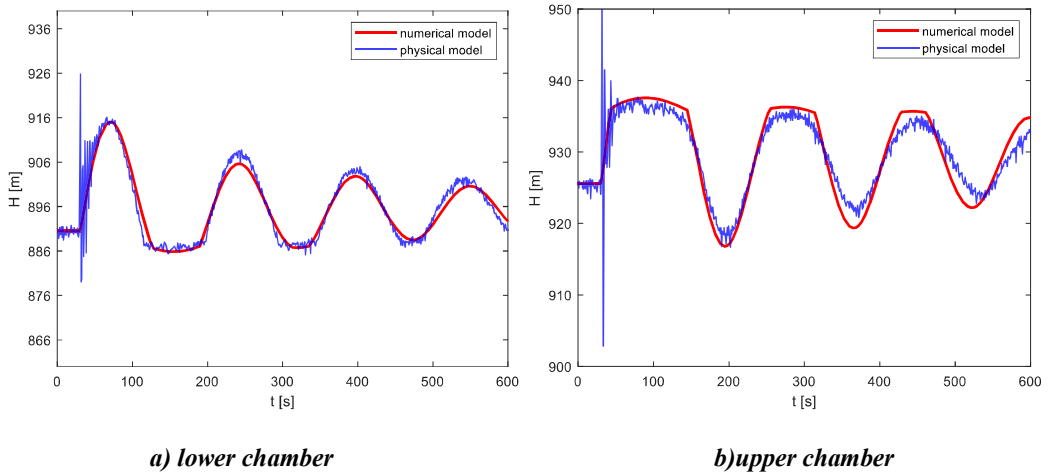*Figure 3.27 Numerical model validation - upstream surge tank*

Figure 3.28 Numerical model validation - downstream surge tank

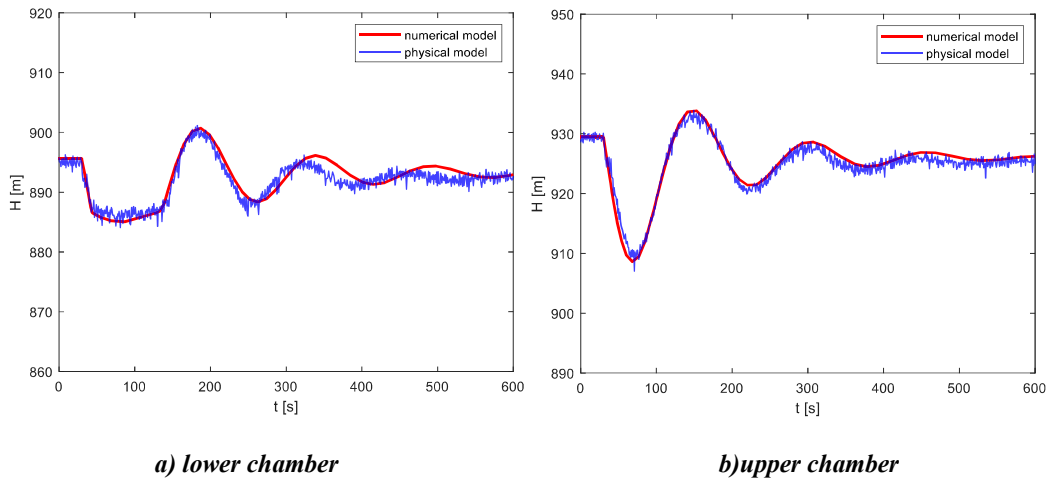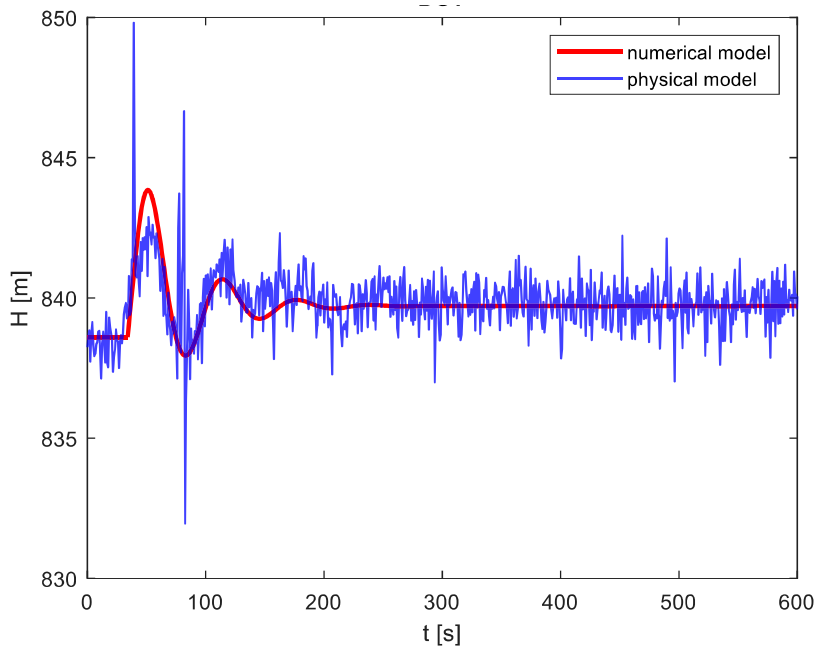## 3.6 Improvement methods for the surge tanks

In this chapter several methods of surge tanks improvement will be presented. As the study focuses on mass oscillations, respectively the evolution of the water surface oscillations in these shafts, it will resume in the end at redesigning of the surge tanks.

3.6.1 Surge tank enlargement

The first option to be considered in the matter of a surge tank improvement is the cross section area increase. Knowing that the amplitude of the surges depends directly on the surge tank cross section area, when a lower amplitude of the surges in desired, the simplest method to reduce this amplitude within the required limits is to enlarge the shaft at the new cross section area.

In a simple surge tank configuration, the surges consist basically in water volumes that enter and exit the shaft. Thus, the enlargement of the surge tank has to be done until the volume of water spilling in an upsurge or not enough in a downsurge is satisfied. The enlargement will be studied using the numerical model in order to find the optimal value for the new cross section area of the shaft.

The numerical model used for simulating the enlargement of the surge tank is basically the same as the model used for the actual surge tank with the only mention that the input for the cross section are of the surge tank in the system of equations that the model is based on with the enlarged value for the cross section area.

$$\Delta v = \frac{g}{L} \cdot (z - \alpha \cdot v \cdot |v|) \cdot \Delta t \qquad (3.15)$$

$$\Delta z = \left(\frac{Q}{A_{enlarged}} - \frac{a}{A_{enlarged}} \right) \cdot \Delta t \qquad (3.16)$$

Even though the surge tank enlargement is the simplest method of reducing the amplitude of the surges, it comes with high costs due to high volumes of excavation. Also, sometimes available space and positioning might be a problem when about very high values for the cross section area.

3.6.2 Variable surge tank

Transforming the simple surge tank into a variable surge tank option follows the similar principle as the enlargement method, however the cross section area of the shaft is increased only at the extremities. Thus, a less volume of excavation, namely less costs comparing to the enlargement method, is characteristic for the transformation into a variable surge tank.

However, this method is also restricted by available space and positioning issues as the enlargement of the tank.

The behavior of a two chambers surge tank will be studied using the numerical model developed in order to determine the optimal configurations of the chambers that will be able to withstand the new operating conditions. The conditioning of the system used in the numerical model will be as following:

- for $z \leq z_{LC}$

$$\Delta v = \frac{g}{L} \cdot (z - \alpha \cdot v \cdot |v|) \cdot \Delta t \tag{3.17}$$

$$\Delta z = \left(\frac{Q}{A_{LC}} - \frac{a}{A_{LC}} \right) \cdot \Delta t \tag{3.18}$$

- for $z_{LC} < z \leq z_{UC}$

$$\Delta v = \frac{g}{L} \cdot (z - \alpha \cdot v \cdot |v|) \cdot \Delta t \tag{3.19}$$

$$\Delta z = \left(\frac{Q}{A} - \frac{a}{A} \right) \cdot \Delta t \tag{3.20}$$

- for $z > z_{UC}$

$$\Delta v = \frac{g}{L} \cdot (z - \alpha \cdot v \cdot |v|) \cdot \Delta t \tag{3.21}$$

$$\Delta z = \left(\frac{Q}{A_{UC}} - \frac{a}{A_{UC}} \right) \cdot \Delta t \tag{3.22}$$

where:

z_{LC} = lower chamber upper boundary;

z_{UC} = upper chamber lower boundary;

A_{LC} = lower chamber cross section area;

A_{UC} = upper chamber cross section area;

A = existing surge tank cross section area.

3.6.3 Throttled surge tank

The throttling method of improvement consists of implementing a significant head loss at the entrance in the shaft. This way, the amplitude of the surges will be damped proportionally with the hydraulic head loss coefficient introduced by the throttle.

Implementing a throttle in the current configuration of the surge tank is the most favorable when about space available and positioning. The throttle requires significantly less space than the enlargement or the chambers, practically the surge tank dimensions will remain the same.

The numerical model simulates the throttle by introducing a hydraulic head loss characteristic to the flow entering and exiting the surge tank during the oscillations. The throttle introduces a singular head loss which depends on the flow in the surge tank. The singular loss is proportional with the water velocity in the surge tank and with the singular loss coefficient of the throttle. This singular head loss is calculated using the equation (3.23) (Idelchik, 1986):

$$\Delta h_{throttle} = \zeta_{throttle} \cdot \frac{v^2}{2 \cdot g} \tag{3.23}$$

Introducing the head loss in the system of equations for the numerical model has to made as a dependence of the flow entering and exiting the surge tank and independent on the flow in the tunnels. Also, the direction is important because it gives the sign for the value of the head loss. The discharge flowing in the surge tank is the difference between the tunnel discharge and the surge tank discharge. It will be determined as following:

$$\Delta Q_{surge\ tank} = v \cdot A - Q \tag{3.24}$$

where:

A = surge tank cross section area;

v = water velocity in the tunnels;

Q = discharge coming in the tunnel.

Therefore, the equation describing the velocity in the stepwise integration system will become:

$$\Delta v = \frac{g}{L} \cdot \left(z - \alpha \cdot v \cdot |v| - \zeta_{throttle} \cdot \frac{v_{surge\ tank}^2}{2 \cdot g} \right) \cdot \Delta t \tag{3.25}$$

where:

$$v_{surge\ tank}^2 = \frac{(v \cdot A - Q) \cdot (|v \cdot A - Q|)}{A^2}$$

The system of equations modelling the throttled surge tank will then be as following:

$$\Delta v = \frac{g}{L} \cdot \left(z - \alpha \cdot v \cdot |v| - \frac{\zeta_{throttle}}{2 \cdot g} \cdot \frac{(v \cdot A - Q) \cdot (|v \cdot A - Q|)}{A^2} \right) \cdot \Delta t \qquad (3.26)$$

$$\Delta z = \left(\frac{Q}{A} - \frac{a}{A} \right) \cdot \Delta t \qquad\qquad (3.27)$$

The throttle considered will be a simple thick edged orifice installed in the current surge tank. (Idelchik, 1986) presents the method for calculating the singular loss coefficient introduced by the orifice.
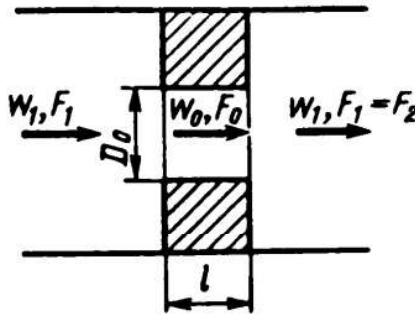
Figure 3.29 Flow through a thick edged orifice (Idelchik, 1986)

For $Re > 10^5$, the singular loss coefficient is given by (Idelchik, 1986) as following:

$$\zeta = \frac{\Delta H}{\frac{\gamma \cdot w_1^2}{2 \cdot g}} \cong \left[\left(0,5 + \tau \sqrt{1 - \frac{F_0}{F_1}} \right) \left(1 - \frac{F_0}{F_1} \right) + \left(1 - \frac{F_0}{F_1} \right)^2 + \lambda \frac{l}{D_h} \right] \left(\frac{F_1}{F_0} \right)^2$$

$$= \left(\zeta_0 + \lambda \frac{l}{D_h} \right) \left(\frac{F_1}{F_0} \right)^2 \qquad (3.28)$$

where:

$\tau = f\left(\frac{l}{D_h} \right);$

$D_h = \frac{4 \cdot F_0}{\Pi_0};$

Π_0 = orifice perimeter

Table 3.13 presents calculated values for ζ at specific $\frac{l}{D_h}$ and respectively $\frac{F_0}{F_1}$ rates (Idelchik, 1986):

Table 3.13 Orifice singular loss coefficient ζ (Idelchik, 1986)

$\frac{l}{D_h}$	τ	F_0/F_1															
		0.02	0.04	0.06	0.08	0.10	0.15	0.20	0.25	0.30	0.40	0.50	0.60	0.70	0.80	0.90	1.0
0	1.35	7 000	1 670	730	400	245	96.0	51.5	30.0	18.2	8.25	4.00	2.00	0.97	0.42	0.13	0
0.2	1.22	6 600	1 600	687	374	230	94.0	48.0	28.0	17.4	7.70	3.75	1.87	0.91	0.40	0.13	0.01
0.4	1.10	6 310	1 530	660	356	221	89.0	46.0	26.5	16.6	7.40	3.60	1.80	0.88	0.39	0.13	0.01
0.6	0.84	5 700	1 380	590	322	199	81.0	42.0	24.0	15.0	6.60	3.20	1.60	0.80	0.36	0.12	0.01
0.8	0.42	4 680	1 130	486	264	164	66.0	34.0	19.6	12.2	5.50	2.70	1.34	0.66	0.31	0.11	0.02
1.0	0.24	4 260	1 030	443	240	149	60.0	31.0	17.8	11.1	5.00	2.40	1.20	0.61	0.29	0.11	0.02
1.4	0.10	3 930	950	408	221	137	55.6	28.4	16.4	10.3	4.60	2.25	1.15	0.58	0.28	0.11	0.03
2.0	0.02	3 770	910	391	212	134	53.0	27.4	15.8	9.30	4.40	2.20	1.13	0.58	0.28	0.12	0.04
3.0	0	3 765	913	392	214	132	53.5	27.5	15.9	10.0	4.50	2.24	1.17	0.61	0.31	0.15	0.06
4.0	0	3 775	930	400	215	132	53.8	27.7	16.2	10.0	4.60	2.25	1.20	0.64	0.35	0.16	0.08
5.0	0	3 850	936	400	220	133	55.5	28.5	16.5	10.5	4.75	2.40	1.28	0.69	0.37	0.20	0.10
6.0	0	3 870	940	400	222	133	55.8	28.5	16.6	10.5	4.80	2.42	1.32	0.70	0.40	0.21	0.12
7.0	0	4 000	950	405	230	135	55.9	29.0	17.0	10.9	5.00	2.50	1.38	0.74	0.43	0.23	0.14
8.0	0	4 000	965	410	236	137	56.0	30.0	17.2	11.2	5.10	2.58	1.45	0.78	0.45	0.25	0.16
9.0	0	4 080	985	420	240	140	57.0	30.0	17.4	11.4	5.30	2.62	1.50	0.80	0.50	0.28	0.18
10	0	4 110	1 000	430	245	146	59.7	31.0	18.2	11.5	5.40	2.80	1.57	0.89	0.53	0.32	0.20

4 Physical model experimental results

This chapter will present the results obtained by running experiments using physical model in several scenarios possible to occur in the new pump storage plant configuration. As the study focuses on the evolution of the water surface level in the two surge tanks upstream and downstream the power plant, namely mass oscillations, the results presented will show the oscillations in these shafts during different possible maneuvers in Roskrepp Pump Storage Plant operation. For the beginning, simple turbining operations such as start up, shut down and emergency shut down will be proceeded following with simple pumping operations similar with the ones mentioned for turbining. In the end, complex maneuvers such as combinations of turbining and pumping or resonance will be analyzed. The experiments were performed in 4 different sets of measurements in order to ensure the correctitude of the process. Each set of measurements follows a different order of test scenarios and setups in order to avoid systematic errors. All the four sets will be represented on the same graph among with a mean value with respect to all of them. On the graphs, with red horizontal lines, will be represented the limits of each surge tank. During the experiments, these limits might be exceeded, one of the purposes of this study being to identify the cases where these boundaries are exceeded.

4.1 Turbining simulation experiments

The turbining experiments will be proceeded with the physical model setup as presented in chapter 3.4. The operations of start up and shut down will be simulated using the globe valve installed, while for the emergency shut down operations, the pneumatic-controlled butterfly valve is being used.
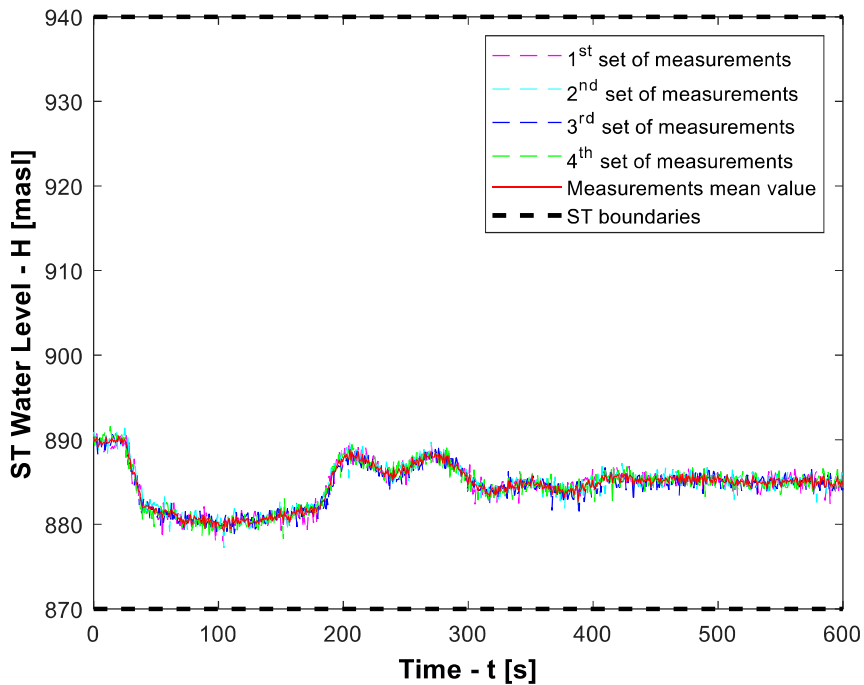
4.1.1 Startup turbining

Data analysis focuses on the surge tanks for each one of them with respect to the worst case that can occur in the operation. For example, in case of turbining start up, the water level in the upstream surge tank will suddenly decrease reaching a global minimum value in the first surge, while for the downstream surge tank, water will increase suddenly reaching a global maximum value in the first surge. Thus, the characteristic levels in the reservoirs have been chosen as following: minimum level in the upper reservoir and maximum level in the lower reservoir. The parameters setup for the start up experiment are presented in Table 4.1.

Table 4.1 Start up turbining setup parameters

	Upper reservoir water level (relative)	*Lower reservoir water level (relative)*	*Upper reservoir water level (absolute)*	*Lower reservoir water level (absolute)*	*Final discharge*
	[m]	[m]	[masl]	[masl]	[m³/s]
Physical model	0.977	0.216	N/A	N/A	0.00145
Prototype	68	15	890	837	60

After running the experiment, the data resulted is presented in Figure 4.1 for the upstream surge tank and in Figure 4.2 for the downstream surge tank, respectively.

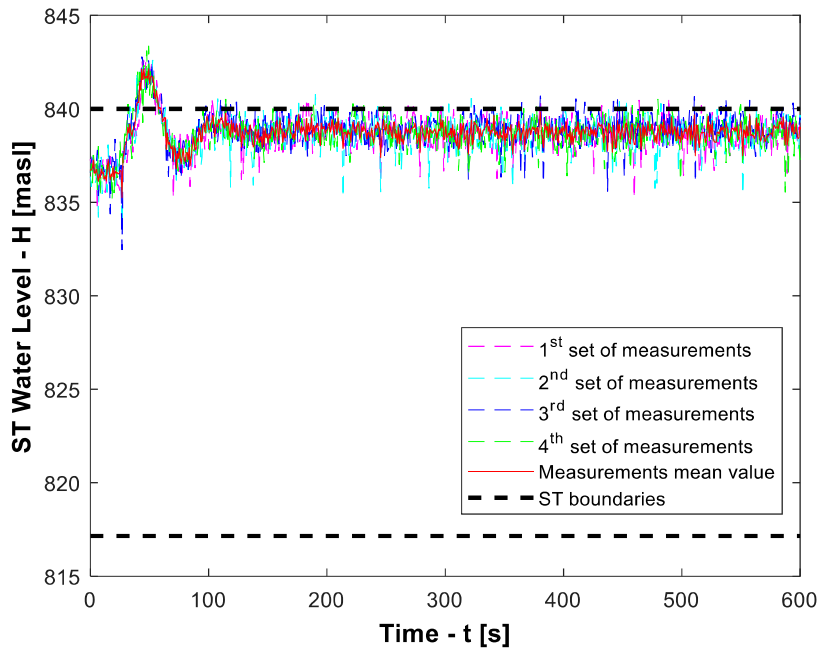*Figure 4.1 Turbining start up - upstream surge tank*

Figure 4.2 Turbining start up - downstream surge tank

4.1.2 Turbining shut down

In what regards shut down from turbining, the worse cases that can occurs in the matter of water levels in the reservoirs are as following: maximum water level in the upper reservoir in order to get a maximum surge in upstream surge tank and minimum water level in lower reservoir in order to get a minimum surge in downstream surge tank. The setup parameters for the shut down turbining experiment are presented in Table 4.2.

Table 4.2 Turbining shut down setup parameters

	Upper reservoir water level (relative)	Lower reservoir water level (relative)	Upper reservoir water level (absolute)	Lower reservoir water level (absolute)	Initial discharge
	[m]	[m]	[masl]	[masl]	[m³/s]
Physical model	1.537	0.043	N/A	N/A	0.00145
Prototype	107	3	929	825	60

The experiment retrieved the data shown in Figure 4.3 for the upstream surge tank, Figure 4.4 for the downstream surge tank, respectively.
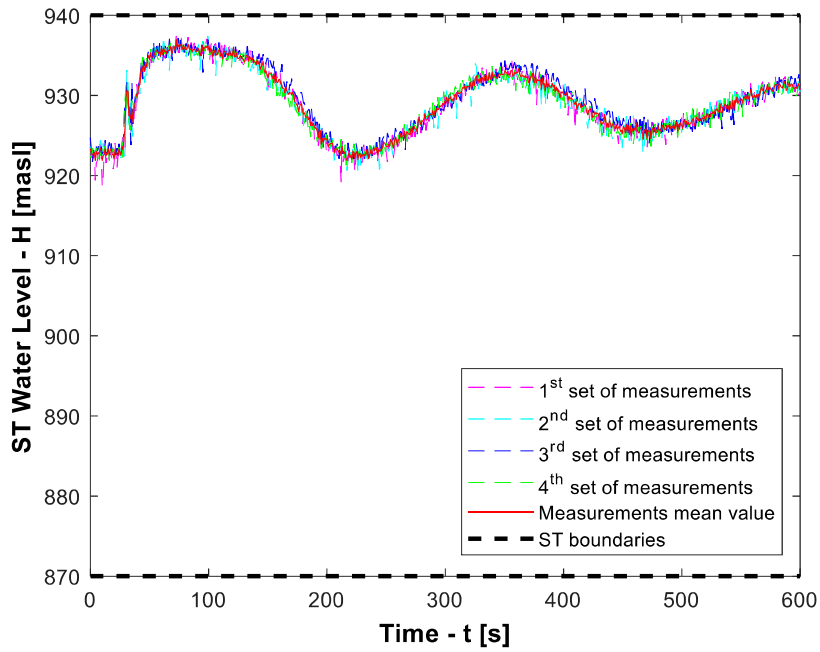
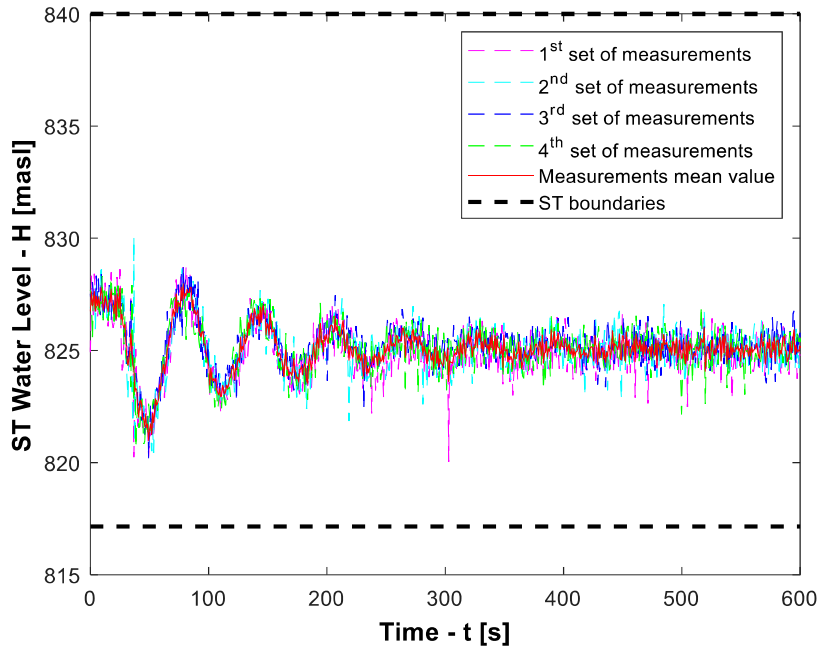*Figure 4.3 Turbining shut down - upstream surge tank*

Figure 4.4 Turbining shut down - downstream surge tank

4.1.3 Emergency shut down

Emergency shut down from turbining will be analyzed similar as normal shut down, namely maximum water level in the upper reservoir and minimum water level in the lower reservoir. The setup for the physical model is as presented in Table 4.3.

Table 4.3 Emergency shut down setup parameters

	Upper reservoir water level (relative)	Lower reservoir water level (relative)	Upper reservoir water level (absolute)	Lower reservoir water level (absolute)	Initial discharge
	[m]	[m]	[masl]	[masl]	[m³/s]
Physical model	1.537	0.043	N/A	N/A	0.00145
Prototype	107	3	929	825	60

The results of the emergency shut down experiment are presented in Figure 4.5 for the upstream surge tank, Figure 4.6 for the downstream surge tank respectively.
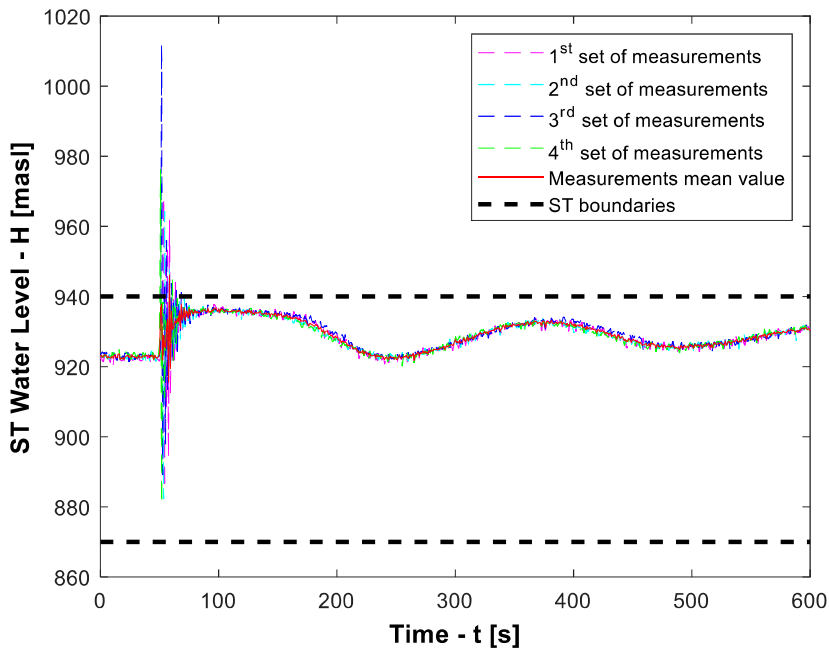

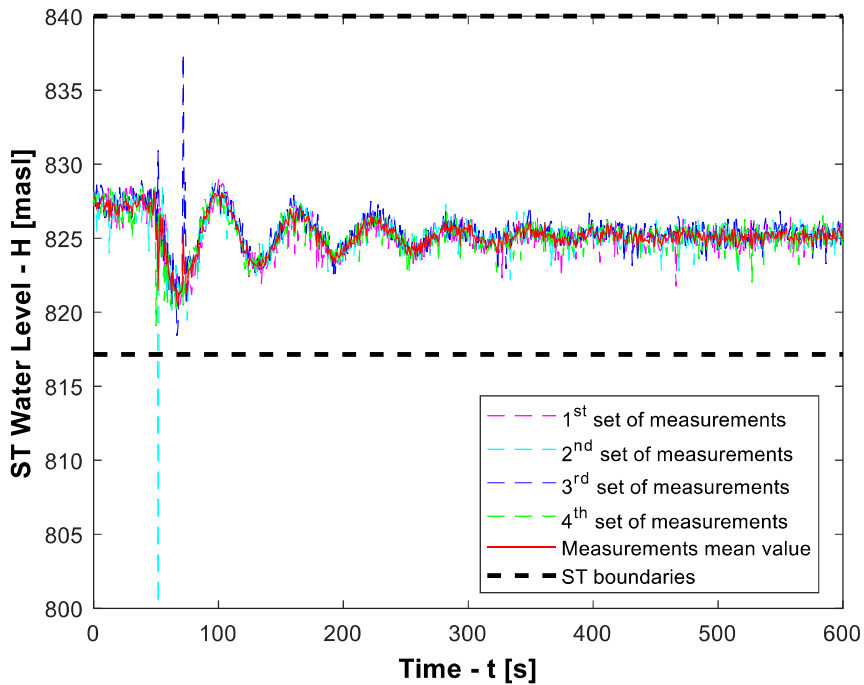*Figure 4.5 Turbining emergency shut down - upstream surge tank*

Figure 4.6 Turbining emergency shut down - downstream surge tank

4.1.4 Resonance experiments

Maneuvers combining alternate start up and shut down of the power plant are the most demanding in what regards surge tanks, thus, similar experiments have been performed in the present study in order to evaluate the behavior of the surge tanks in this situation. On an aleatory basis, the decision of three startups for the power plant, each one followed by an emergency shut down has been made. The setup for this experiment considered both scenarios of maximum and minimum water levels in the reservoirs. The flow for the experiments was the nominal flow in the power plant operating, namely 60 m^3/s.

For the maximum water level in both reservoirs, the results are represented in Figure 4.7 for the upstream surge tank and Figure 4.8 for the downstream surge tank, respectively.
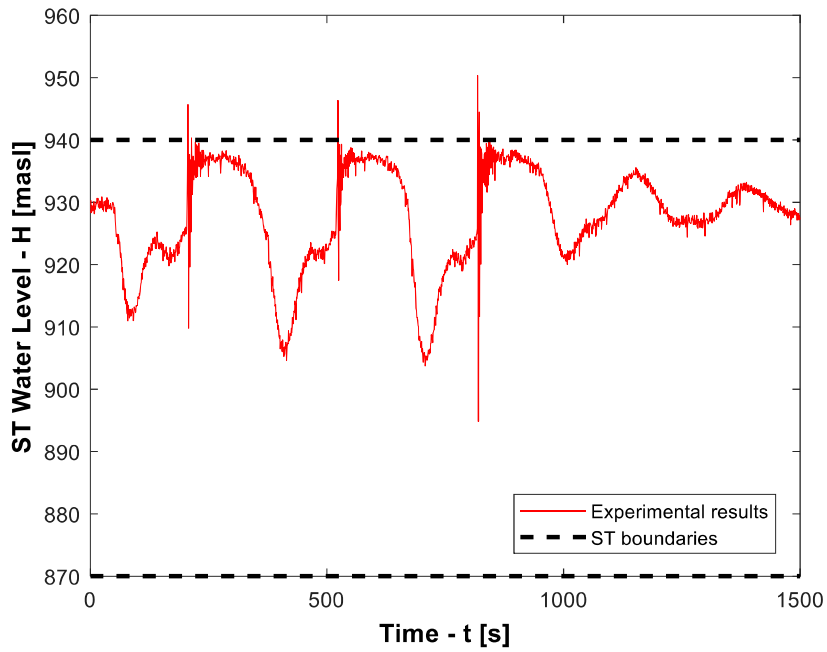
Figure 4.7 Upstream surge tank resonance - maximum water level
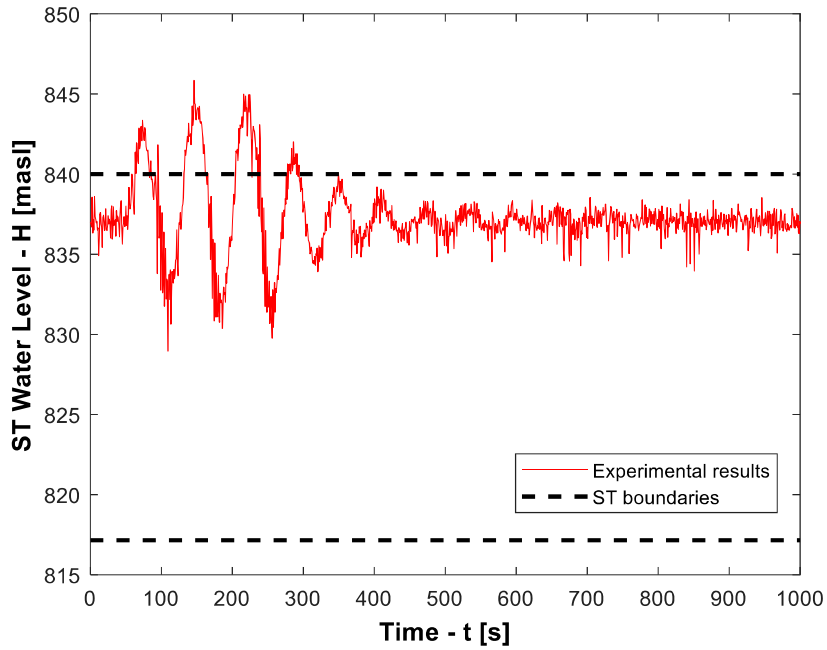

Figure 4.8 Downstream surge tank resonance - maximum water level

For minimum water levels in the reservoirs, the results are presented in Figure 4.9 for the upstream surge tank and Figure 4.10 respectively, for the downstream surge tank.
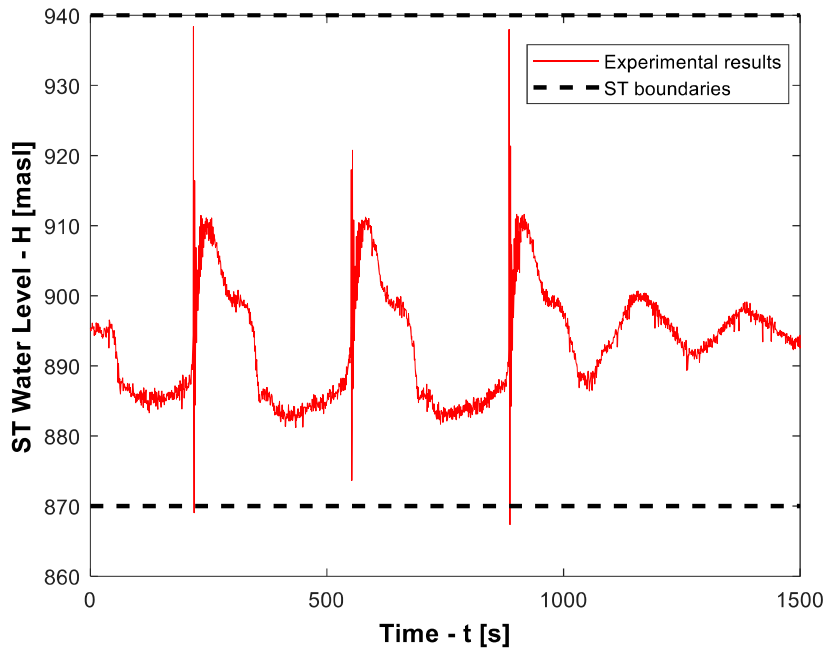
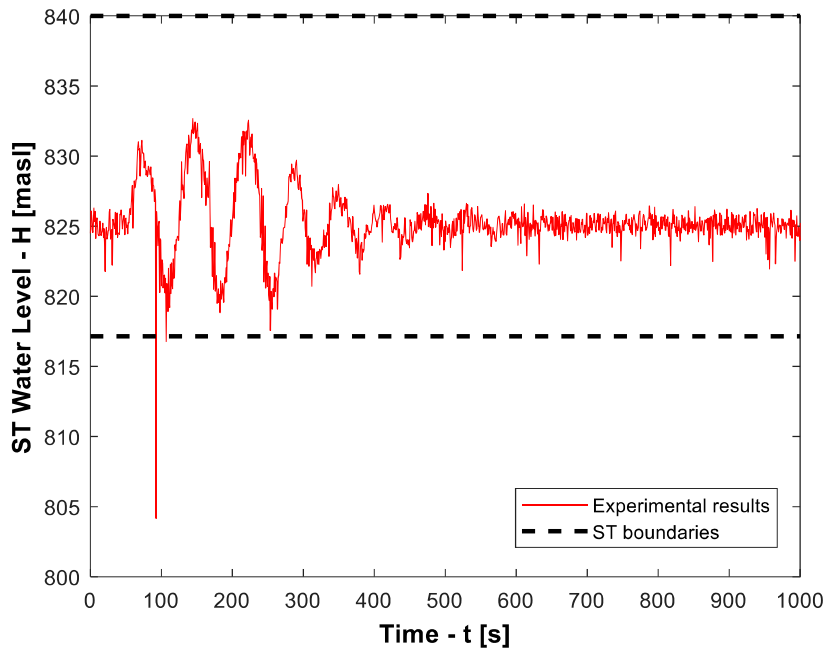*Figure 4.9 Upstream surge tank resonance - minimum water level*

Figure 4.10 Downstream surge tank resonance - minimum water level

4.2 Pumping simulation experiments

Simulation of the pumping process has been done in a maximum flow hypothesis. This supposed a maximum velocity of water in the system in what regards hydraulic head losses of approximately 2 m/s. This corresponds to a value for the discharge in the physical model of 2 l/s which scaled in prototype values results in a value of 80 m³/s.

The configuration of the physical model is the same as for the turbining experiments.

4.2.1 Pumping startup

For the startup pumping maneuver, the purpose was similar to turbining experiments, namely to find the worse situations that can occur in what regards levels in the reservoirs. Thus, the experiment was performed with minimum water level in the lower reservoir to get the global minimum value for the surge in the downstream surge tank. The upper reservoir water level has been set to maximum in order to find the global maximum value for the surge in the upstream surge tank. Setup parameters for the startup pumping experiment are presented in Table 4.4.

Table 4.4 Startup pumping setup parameters

	Upper reservoir water level (relative)	*Lower reservoir water level (relative)*	*Upper reservoir water level (absolute)*	*Lower reservoir water level (absolute)*	*Final pump discharge*
	[m]	[m]	[masl]	[masl]	[m³/s]
Physical model	1.537	0.043	N/A	N/A	0.002
Prototype	107	3	929	825	80

Water level oscillations in the surge tanks for the startup pumping experiment are presented in Figure 4.11 for the upstream surge tank and Figure 4.12 for the downstream surge tank.
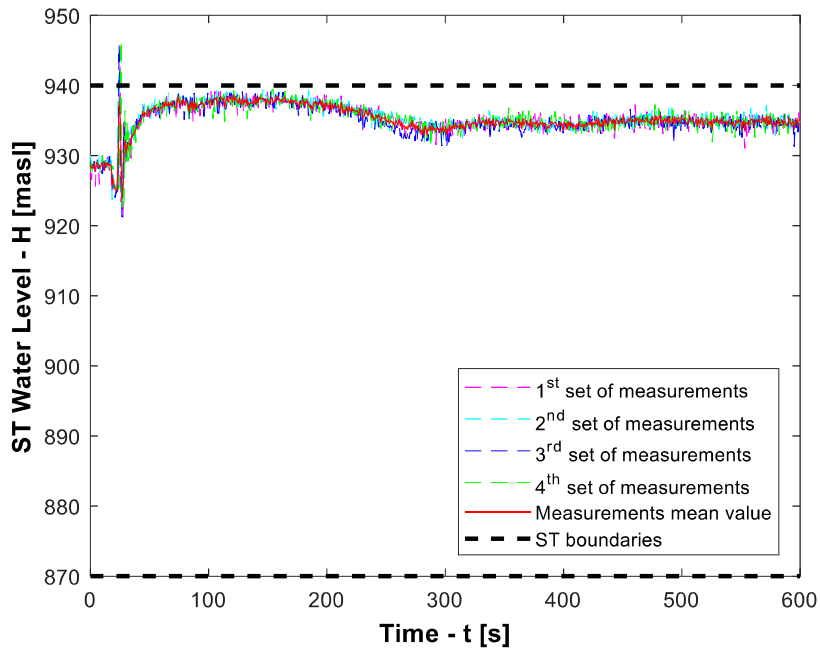
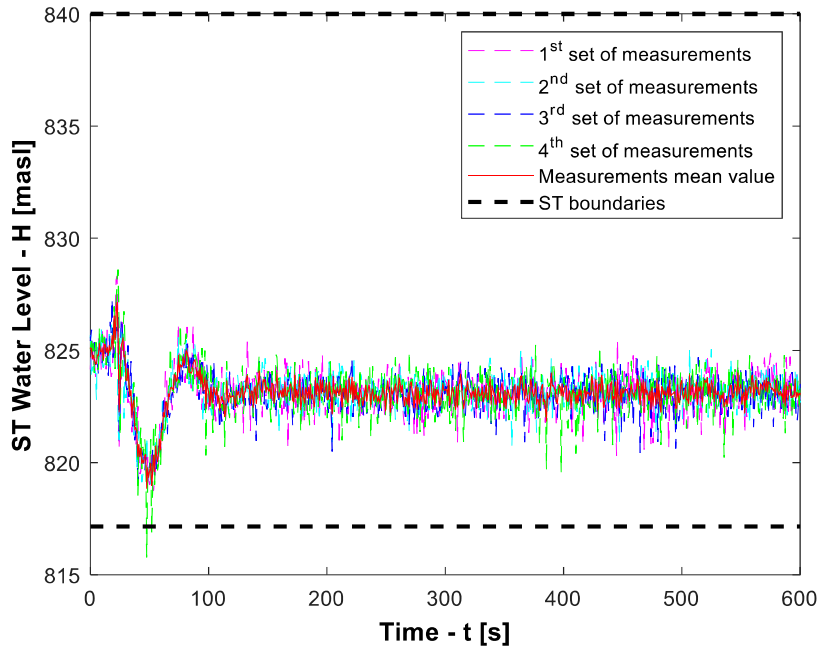*Figure 4.11 Pumping start up - upstream surge tank*

Figure 4.12 Pumping start up - downstream surge tank

4.2.2 Pumping shutdown

Pump shutdown maneuver equivalates with a sudden increase of the water surface in the downstream surge tank and the opposite in the upstream surge tank, namely a sudden decrease of the water level. Therefore, the worst case to be studied in such an operation is maximum water level in lower reservoir, minimum water level in upper reservoir, respectively. The setup parameters for the experiment are presented in Table 4.5.

Table 4.5 Pumping shut down setup parameters

	Upper reservoir water level (relative)	*Lower reservoir water level (relative)*	*Upper reservoir water level (absolute)*	*Lower reservoir water level (absolute)*	*Initial pump discharge*
	[m]	[m]	[masl]	[masl]	[m³/s]
Physical model	0.977	0.216	N/A	N/A	0.002
Prototype	68	15	890	837	80

After running the experiment, the evolution of the water level in the surge tanks are presented in Figure 4.13 for the upstream surge tank, Figure 4.14 for the downstream surge tank, respectively.
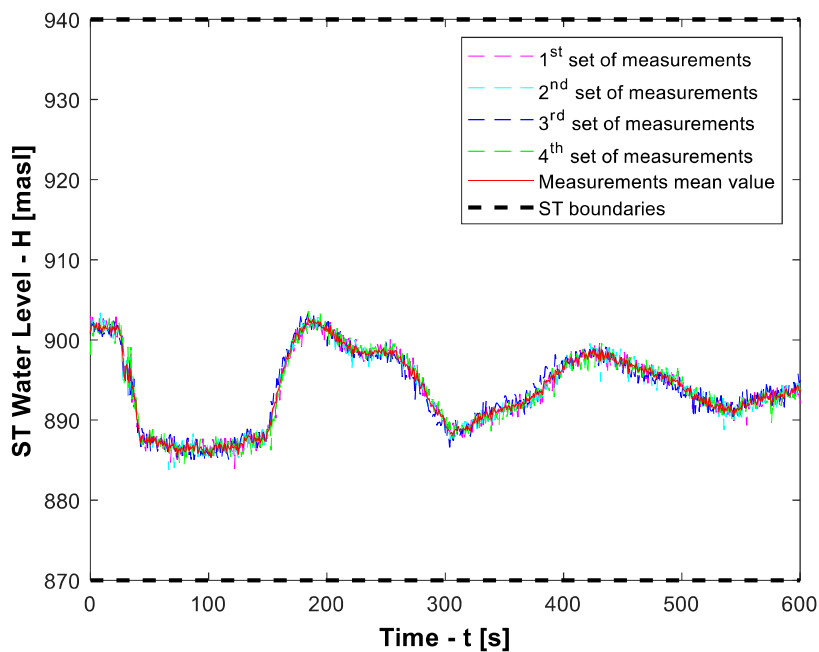

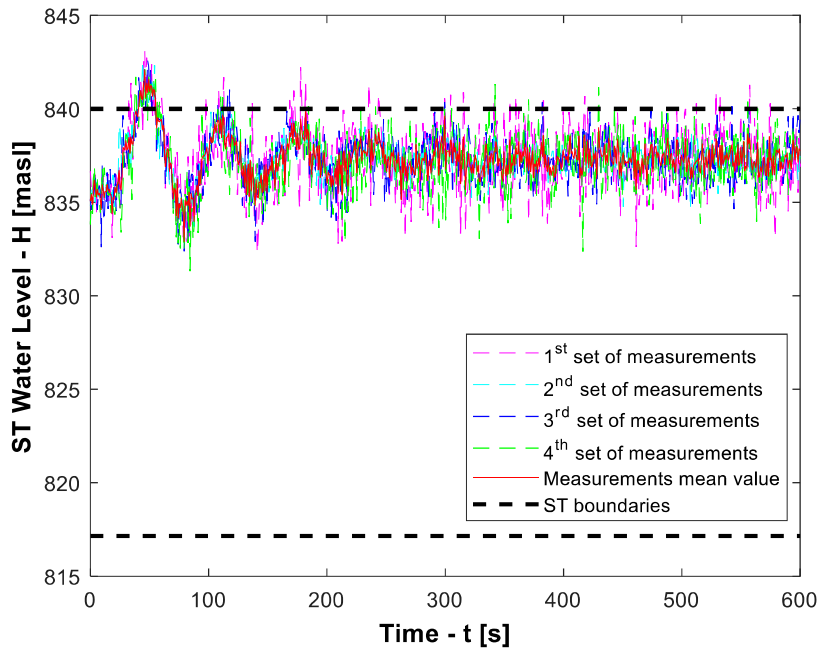*Figure 4.13 Pumping shutdown - upstream surge tank*

Figure 4.14 Pumping shutdown - downstream surge tank

4.3 Combined pumping-turbining simulation experiments

4.3.1 Pump failure with trip to turbining

The first scenario studied for the combination of the two processes of pumping and turbining is the assumption of switching from a pumping regime directly to turbining. This scenario can occur due to various reasons such as either a pump failure without the possibility to close the valves, either it can be required in the operation due to power grid demands. The discharges considered for this experiment are the combination between the values considered for the turbining and pumping treated separately. This means that the pumping process performs at the maximum discharge of 80 m^3/s, while the turbining is being performed at the maximum turbining discharge of 60 m^3/s. Another important aspect to be mentioned here is the fact that the pump failure occurs after enough time for the oscillations in the surge tanks damped completely. Namely, from a steady state of pumping, the regime changes to reach a steady state of turbining.

The evolution of the water levels in the surge tanks will be as following: a sudden decrease in the upstream surge tank when the discharge reverses in the system and a sudden increase in the downstream surge tank, respectively. Therefore, the configuration for this experiment will

consist in minimum level in the upper reservoir and maximum in the lower reservoir. The setup parameters for this experiment are presented in Table 4.6.

Table 4.6 Pumping failure with trip to turbining setup paramters

	Upper reservoir water level (relative)	Lower reservoir water level (relative)	Upper reservoir water level (absolute)	Lower reservoir water level (absolute)	Pumping discharge	Turbining discharge
	[m]	[m]	[masl]	[masl]	[m^3/s]	[m^3/s]
Physical model	0.977	0.216	N/A	N/A	0.002	0.00145
Prototype	68	15	890	837	80	60

The oscillations resulted after running the experiment are presented in Figure 4.15 for the upstream surge tank and Figure 4.16 for the downstream surge tank.
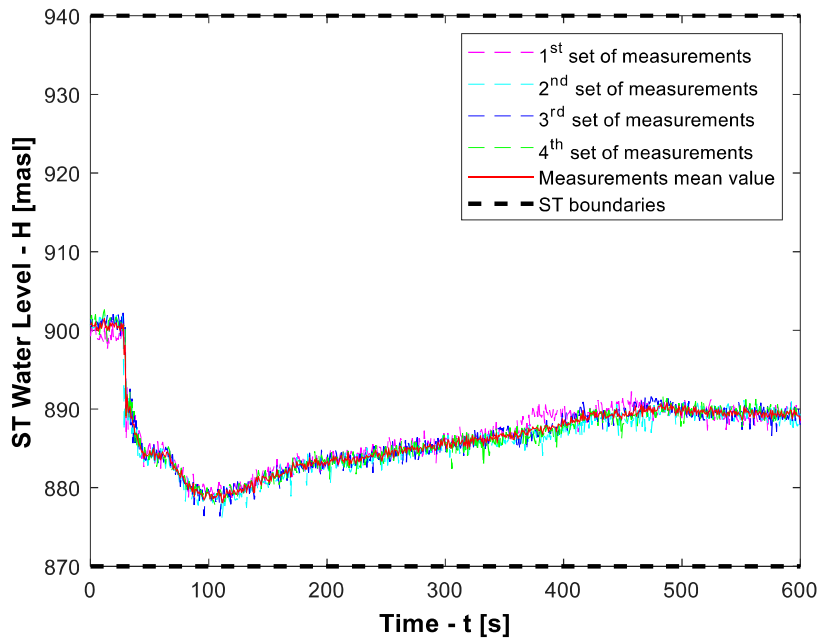

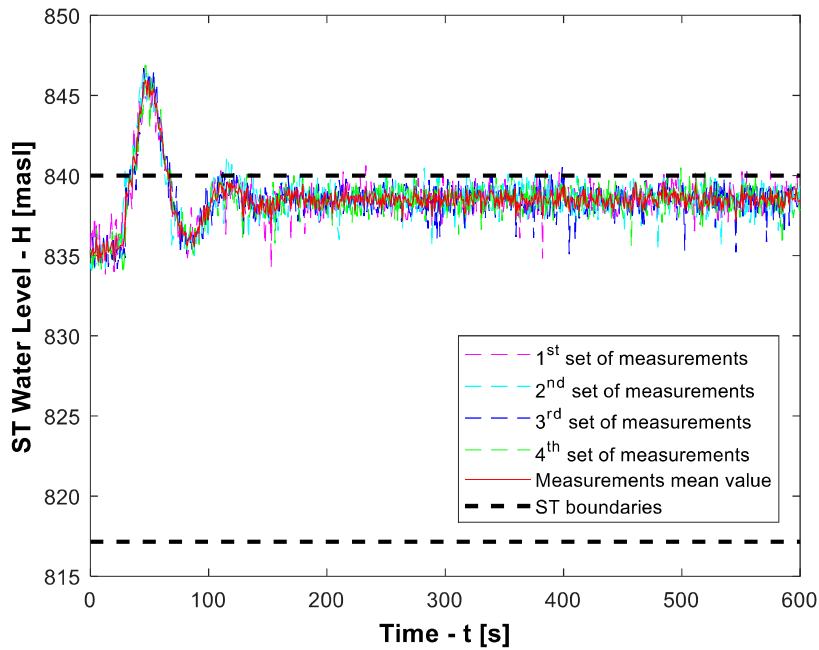*Figure 4.15 Pumping failure with trip to turbining - upstream surge tank*

Figure 4.16 Pumping failure with trip to turbining - downstream surge tank

4.3.2 Pump startup failure with trip to turbining

The previous experiment was considering failure to occur long after the pump started in order for the water level oscillations in the surge tanks to be completely damped at the failure moment. However, that is not always likely to be fulfilled as a quicker pump failure, due to various reasons could occur. In these conditions, the worst moment for a pump failure, in matter of surge tank oscillations is as following:

• for the upstream surge tank, when the level decreases in the first surge, the water surface oscillation reaches a maximum velocity, thus, this is the most unfavorable point for the turbining process to start;

• for the downstream surge tank, when the level increases in the first surge, the water surface oscillation reaches a maximum velocity, thus, this is the most unfavorable point for the turbining process to start.

Both points mentioned above consists basically in a time interval that must be set in between the two processes. These time delays between pumping and turbining were determined experimentally by running another pumping startup experiment, this time with minimum water level in upper reservoir and maximum level in the lower reservoir, respectively. The procedure

of determining the time delay between pump startup and turbining is shown in Figure 4.17 for the upstream surge tank, respectively Figure 4.18 for the downstream surge tank.
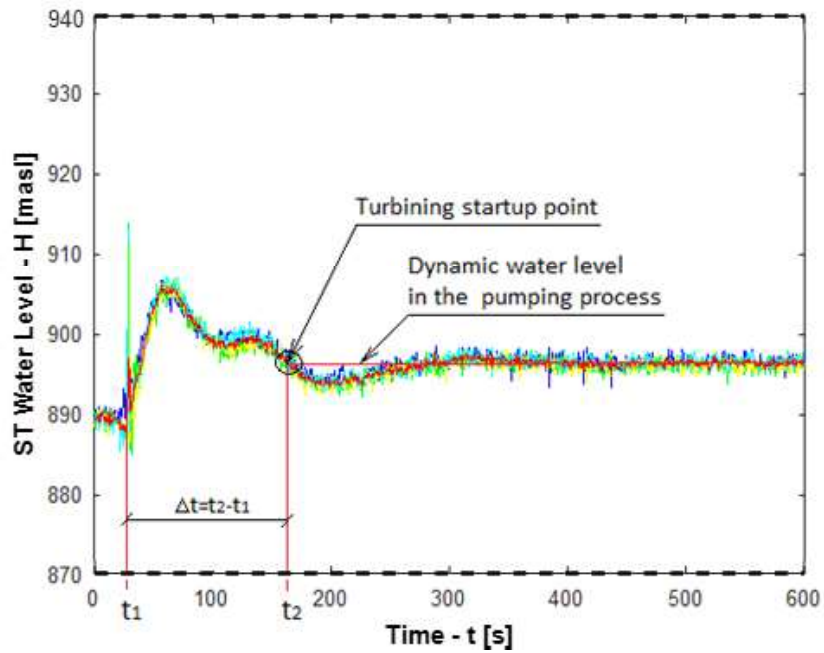

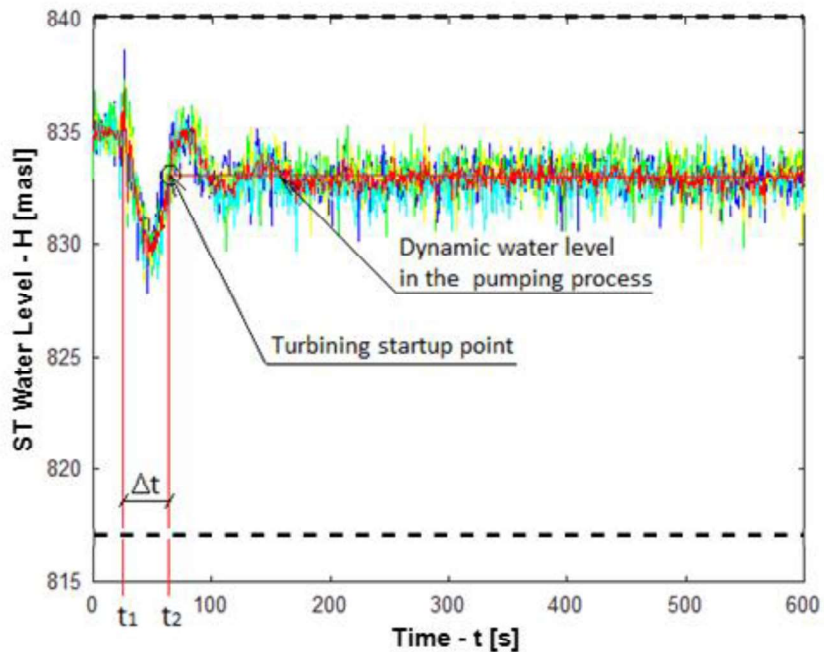*Figure 4.17 Failure time delay determination - upstream surge tank*

Figure 4.18 Failure time delay determination - downstream surge tank

After determining the delays for both upstream and downstream surge tanks, two experiments have been performed with the setup parameters for the pump failure experiment as presented in Table 4.7.

Table 4.7 Pump startup failure with trip to turbining setup parameters

	Upper reservoir water level (relative)	Lower reservoir water level (relative)	Upper reservoir water level (absolute)	Lower reservoir water level (absolute)	Pumping discharge	Turbining discharge
	[m]	[m]	[masl]	[masl]	[m³/s]	[m³/s]
Physical model	0.977	0.216	N/A	N/A	0.002	0.00145
Prototype	68	15	890	837	80	60

The results of the experiment are shown in Figure 4.19 for the upstream surge tank and Figure 4.20 respectively, for the downstream surge tank.
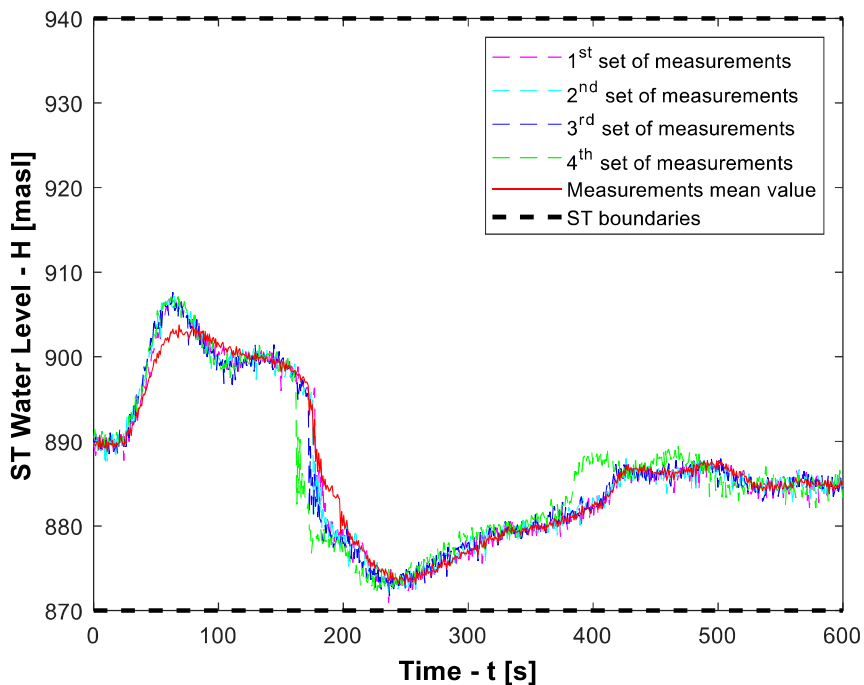

Figure 4.19 Pump startup failure with trip to turbining - upstream surge tank
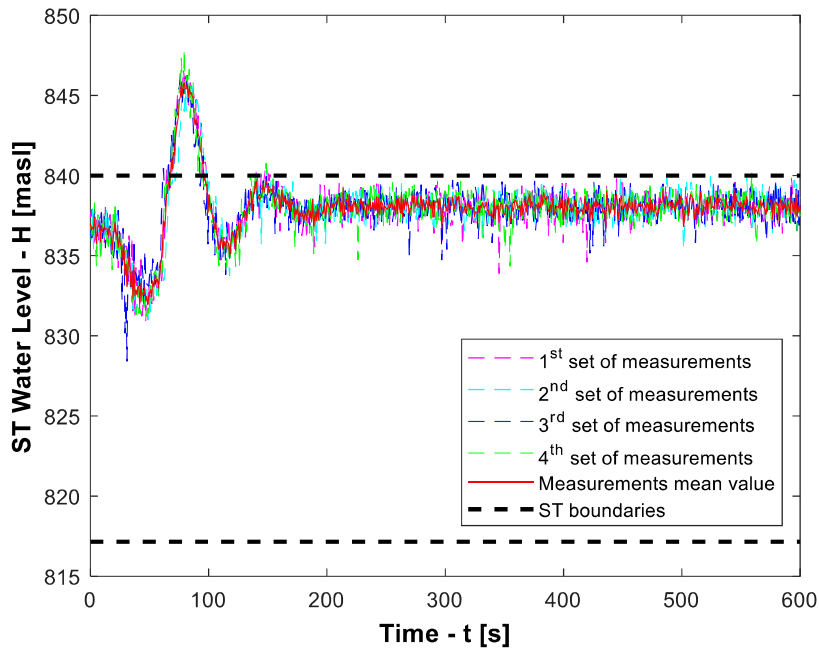
Figure 4.20 Pump startup failure with trip to turbining - downstream surge tank
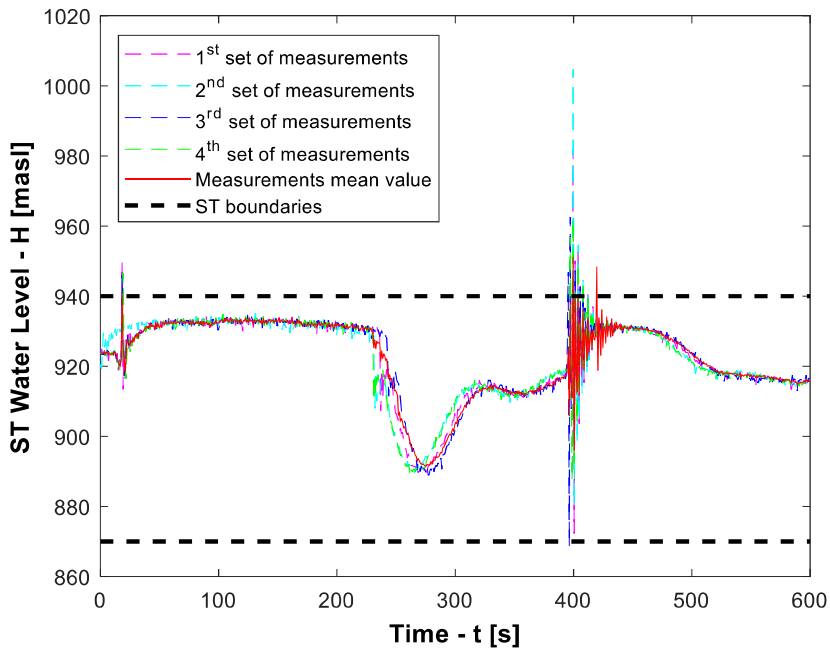
4.3.3 Pump startup failure with emergency shut down

A pump failure can occur in a very unoptimistic moment, thus, the circumstances might require an emergency shut down. However, an emergency shut down can bring some issues in what regards oscillations in the surge tanks. Basically, an emergency shut down after the flow reversed in the system will increase the amplitude of the surge even more comparing with the case presented before, namely pump failure to turbining. The most unfavorable moment to perform the emergency shut down in this experiment is determined similar to the one for the pump failure to turbining presented in Figure 4.17 and Figure 4.18, respectively. Here it was determined the maximum velocity point on the first water level increase after the failure for the upstream surge tank, or the first water level decrease for the downstream surge tank. This way, the purpose was to check if the water level in the upstream surge tank will increase above the tank boundary and decrease under the boundary for the downstream surge tank.

The values for the discharge fulfilled the requirements stated for the other experiments performed, namely 60 m^3/s for turbining and 80 m^3/s for pumping. Table 4.8 presents the setup parameters for the experiment.

Table 4.8 Pump startup failure + emergency shutdown setup parameters

	Upper reservoir water level (relative)	Lower reservoir water level (relative)	Upper reservoir water level (absolute)	Lower reservoir water level (absolute)	Pumping discharge	Turbining discharge
	[m]	[m]	[masl]	[masl]	[m³/s]	[m³/s]
Physical model	1.537	0.043	N/A	N/A	0.002	0.00145
Prototype	107	3	929	825	80	60

The experiment retrieved the results presented in Figure 4.21 for the upstream surge tank and Figure 4.22 for the downstream surge tank.

Figure 4.21 Pump start-up failure + emergency shut down - upstream surge tank
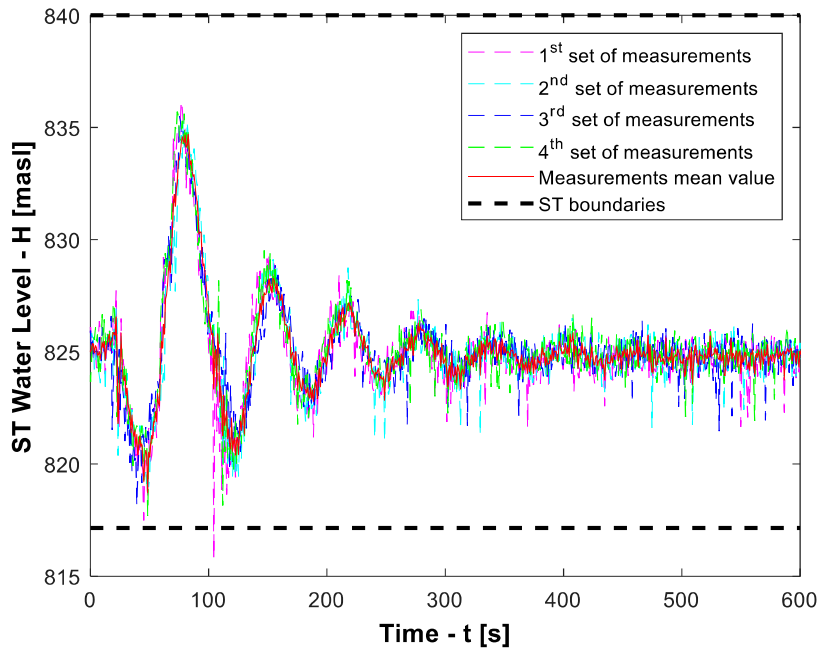
Figure 4.22 Pump start-up failure + emergency shut down - downstream surge tank

4.3.4 Turbining to pumping

An interesting scenario to be studied is the switch from turbining directly to pumping. This can be imagined as having a reversible unit able to switch from turbining straight to pumping resulting this way a very short, almost zero, time between the processes. Table 4.9 presents the setup for the turbining to pumping experiment.

Table 4.9 Turbining to pumping setup parameters

	Upper reservoir water level (relative)	Lower reservoir water level (relative)	Upper reservoir water level (absolute)	Lower reservoir water level (absolute)	Turbining discharge	Pumping discharge
	[m]	[m]	[masl]	[masl]	[m³/s]	[m³/s]
Physical model	1.537	0.043	N/A	N/A	0.00145	0.002
Prototype	107	3	929	825	60	80

The experiment performed retrieved the results presented in Figure 4.23 for the upstream surge tank, respectively Figure 4.24 for the downstream surge tank.

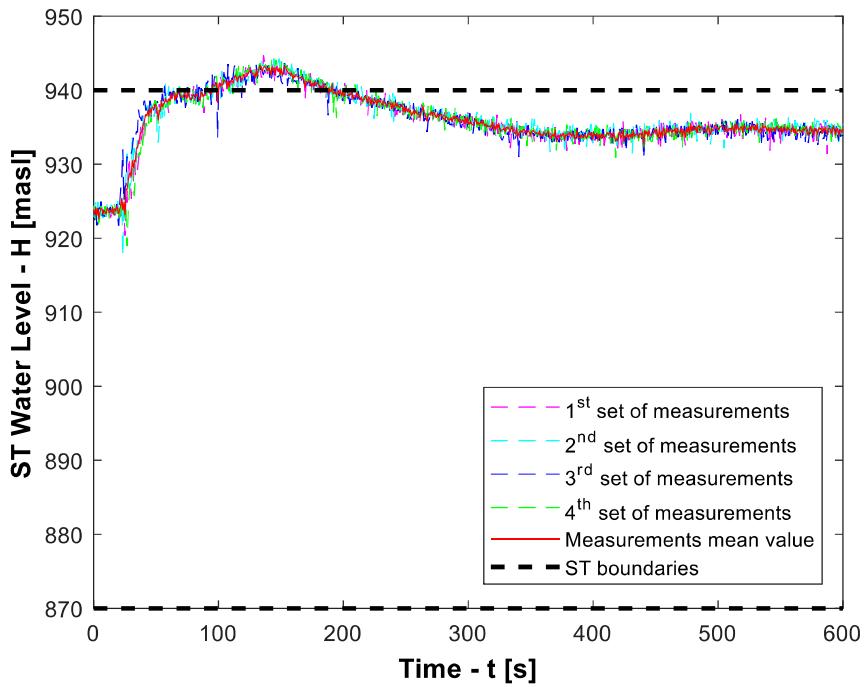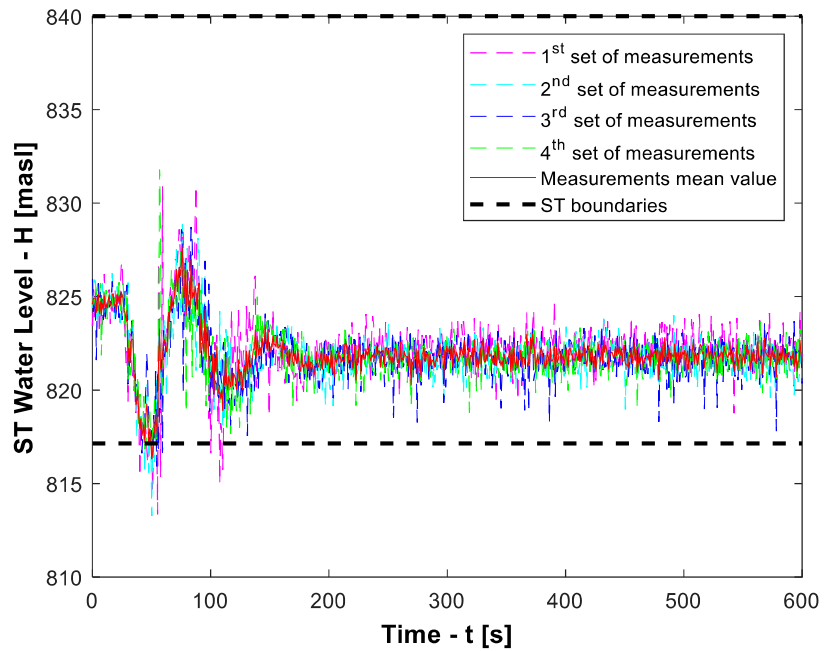*Figure 4.23 Turbining to pumping - upstream surge tank*

Figure 4.24 Turbining to pumping - downstream surge tank

4.3.5 Startup turbining to pumping

Similar to the startup pumping to turbining scenario, this experiment consist of switching between the two processes at the worst moment of time. The procedure followed for determining this worst point for the pump to start, right after a turbining startup, is as presented in chapter 4.3.2. Basically, after the turbining startup, the oscillations in the surge tanks are:

• in the upstream surge tank water level decreases due to the water demanded by the turbining process reaching a minimum value, afterwards it increases. When it reaches a maximum velocity in this increase, the pump contributing in the surge with a high amount of energy and thus, a maximum value of the surge will be reached;

• in the downstream surge tank the water level increases as a consequence of the turbining process startup. After reaching a maximum value, the level thereafter decreases, reaching a maximum velocity. This is the worse point for the pump to start in what regards downstream surge tank because the pump startup will lead to a minimum level for the surge.

The time intervals between turbining and pumping will be determined experimentally from the results obtained in the startup turbining experiment. The procedure followed is same as for the startup pumping to turbining experiment, presented in Figure 4.17, respectively Figure 4.18.

In what regards the reservoir levels, considering the two points stated above, it is clearly that the most unfavorable configuration for this experiment will be a maximum level in the upper reservoir, respectively a minimum level in the lower reservoir. The setup for the startup turbining to pumping experiment are presented in Table 4.10.

Table 4.10 Startup turbining to pumping setup parameters

	Upper reservoir water level (relative)	*Lower reservoir water level (relative)*	*Upper reservoir water level (absolute)*	*Lower reservoir water level (absolute)*	*Turbining discharge*	*Pumping discharge*
	[m]	[m]	[masl]	[masl]	[m³/s]	[m³/s]
Physical model	1.537	0.043	N/A	N/A	0.00145	0.002
Prototype	107	3	929	825	60	80

The results for the experiment are presented in Figure 4.25 for the upstream surge tank, respectively Figure 4.26 for the downstream surge tank.
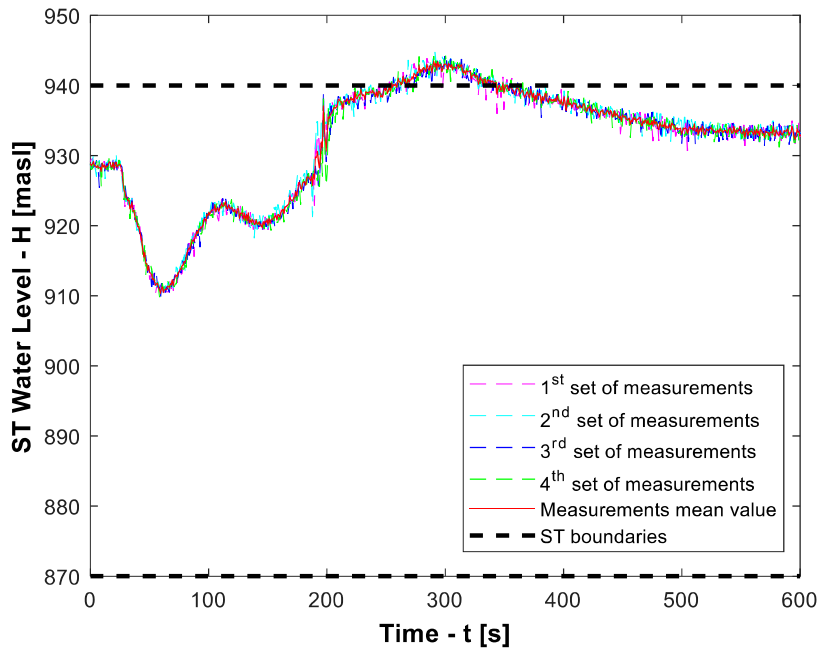
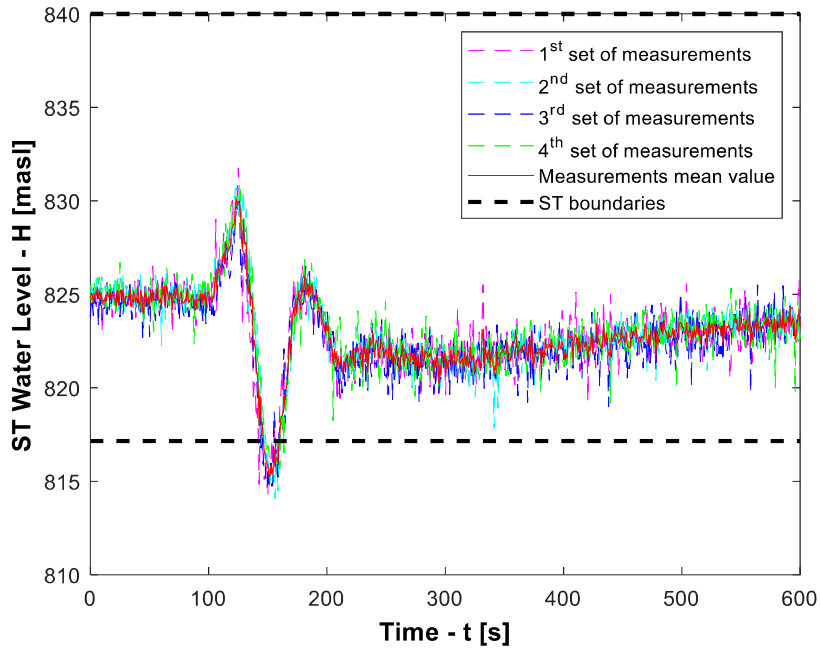*Figure 4.25 Startup turbining to pumping - upstream surge tank*

Figure 4.26 Startup turbining to pumping - downstream surge tank

5 Discussion and improvement solution analysis

In this chapter, the issues resulted from running the experiments will be discussed. Considering the main purpose of this study is mass oscillations, the focus will be on the exceeding of the surge tank boundaries. Generally, this far, the upstream surge tank registered no exceeding during the experiments performed, thus, the exceeding of the downstream surge tank boundaries will be treated.

The approach of the study in what regards the surge tank improvements, first consisted in determining the maximum exceeding of the surge tanks boundaries during the experiments performed. This determination has been done based on the graph obtained, by reading the maximum values that the water surface reaches. Thus, Table 5.1 presents the maximum values that water surface reaches during possible mass oscillations scenarios in the two Roskrepp surge shafts.

Table 5.1 Maximum values of the surges during the experiments

	Highest water level reached during experiments	Lowest water level reached during experiments	Exceeding level above the tank lower boundary	Exceeding level below the tank lower boundary
	[masl]	[masl]	[m]	[m]
Upstream surge tank	945	874	5	0
Downstream surge tank	845	813	5	4.1

The focus of the present study is on the downstream surge tank and the approach considered is to apply the numerical model for each one of the third improvement methods proposed. The scenario considered as being the worst in the one presented in Table 5.1. Therefore, the experiment of startup turbining to pumping will be considered for the study of the lower boundary of the surge tank, while the experiment of pump startup failure with trip to turbining will be considered for the study of the upper boundary of the surge tank.

5.1 Enlargement of the surge tank

5.1.1 Lower boundary - startup turbining to pumping

In the hypothesis of a startup turbining to pumping, the numerical model has been adapted to fulfil the conditions in the experiment considered. To study the influence of the surge tank cross section area on the oscillations amplitude and to find the optimal value for the cross section,

several values for the enlarged area have been considered. The values considered for the enlargement of the surge tank are presented in Table 5.2.

Table 5.2 Cross section areas considered for enlargement – lower boundary

Experiment	Cross section area	Unit
Physical model	110	[m^2]
Numerical model	110	[m^2]
Numerical model A$_1$	200	[m^2]
Numerical model A$_2$	300	[m^2]
Numerical model A$_3$	400	[m^2]

Figure 5.1 presents the evolution of the mass oscillations in the surge tank at the considered cross section areas.

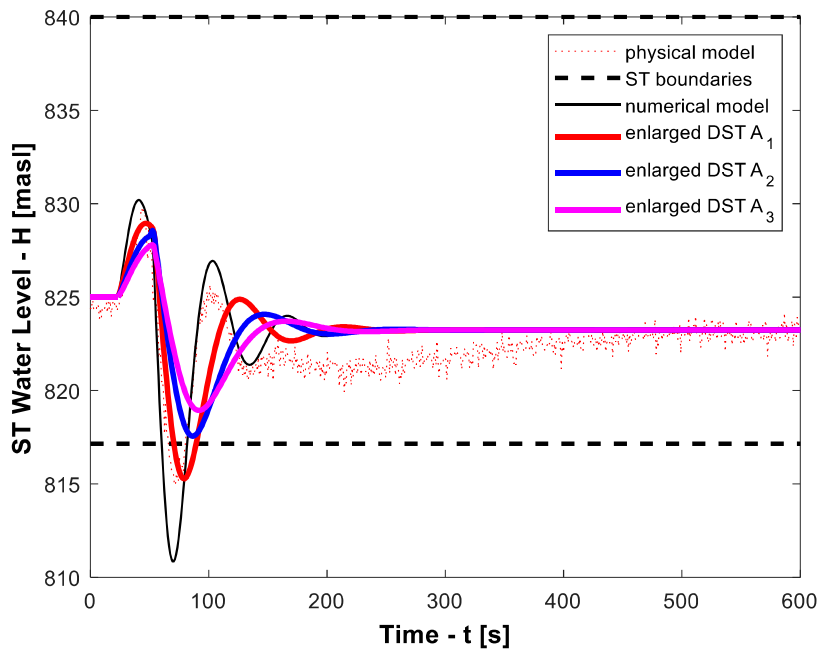*Figure 5.1 Surge tank enlargement - lower boundary*

5.1.2 Upper boundary - pump startup failure with trip to turbining

For the experiment of pump startup failure to turbining, the highest exceed of the upper boundary of the surge tank has been reached. Thus, the numerical model has been adapted for the mentioned experiment and similar as proceeded for the lower boundary, several values for

the new cross section area have been considered. Table 5.3 presents the considered values for the surge tank enlargement.

Table 5.3 Cross section areas considered for enlargement – upper boundary

Experiment	Cross section area	Unit
Physical model	110	[m^2]
Numerical model	110	[m^2]
Numerical model A_1	300	[m^2]
Numerical model A_2	400	[m^2]
Numerical model A_3	500	[m^2]

During simulation, values higher than 500 m^2 for the surge tank have been considered. However, above this value the damping is not growing at all. Thus 500 m^2 is the highest cross section possible for the enlargement. The results for the simulation are presented in Figure 5.2.
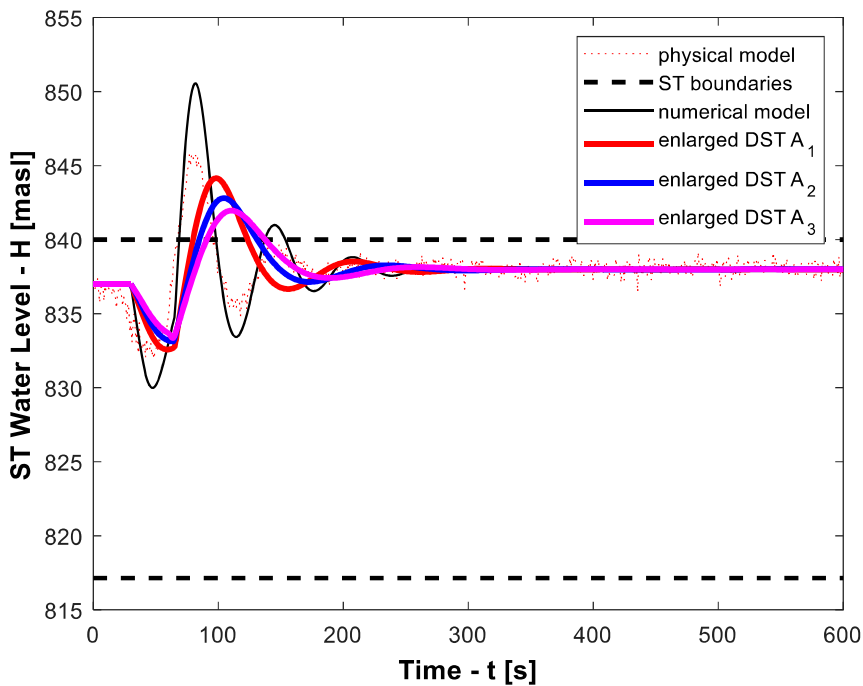

Figure 5.2 Surge tank enlargement - upper boundary

5.1.3 Enlarged surge tank proposed dimensions

Considering the results obtained in the numerical simulation, the solution proposed for the surge tank enlargement is a constant section surge tank of 500 m^2. The surge tank proposed requires physical modelling in order to be verified.

The configuration for the enlarged surge tank has been designed and it is presented in **ANNEXE 1**. The modelling of the surge tank and repeating the experiments are mandatory to ensure the relevance of the proposal. The surge tank shall be made of acrylic plates according to the drawing presented.

5.2 Variable surge tank

The variable surge tank will consider the same experiment for the surge tank boundaries check. The geometry of the chambers is going to be same as the galleries that the upstream surge tank chambers have been built. Therefore, these chambers will consist of tunnels with 6 meters height. The chambers will be placed at the surge tank boundaries as presented in Table 5.4.

Table 5.4 Variable surge tank configuration

	Cross section area [m^2]	Lower boundary [masl]	Upper boundary [masl]
Lower chamber	A_{LC}	817.1	823.1
Shaft	110	823.1	834
Upper chamber	A_{UC}	834	840

5.2.1 Lower boundary - startup turbining to pumping

The variable surge tank will consider the experiment of startup turbining to pumping for the lower boundary check. The geometry of the chamber is going to be same as presented in Table 5.4 and several cross section areas for the lower chamber have been considered. The cross section areas values considered for the lower chamber are presented in Table 5.5.

Table 5.5 Cross section areas considered for lower chamber

Experiment	Cross section area	Unit
Physical model	110	[m^2]
Numerical model	110	[m^2]
Numerical model A_1	300	[m^2]
Numerical model A_2	400	[m^2]

Numerical model A_3	500	[m^2]

The results for the numerical simulation of the variable surge tank in each of the considered value for the lower chamber cross section area are presented in Figure 5.3.
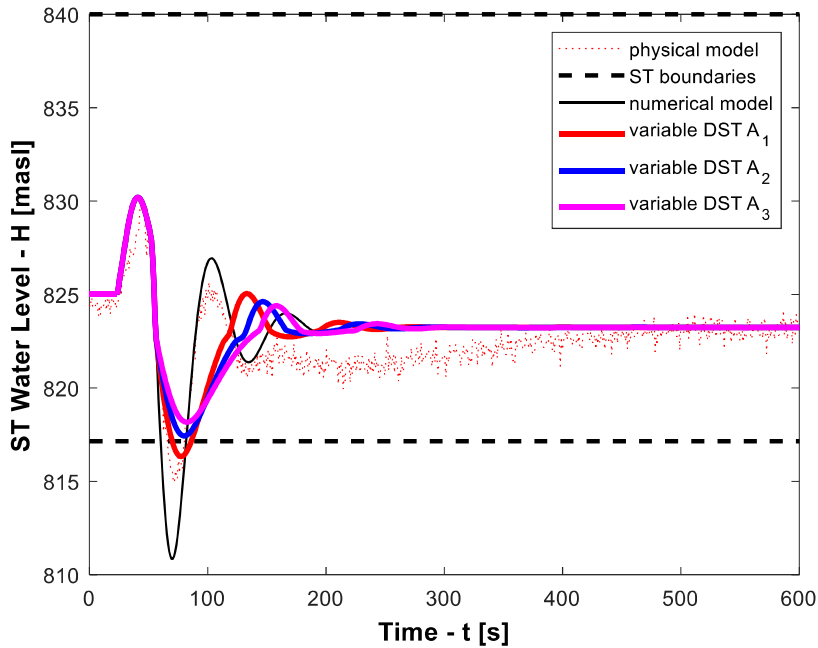

Figure 5.3 Variable surge tank - lower boundary

5.2.2 Upper boundary - pump startup failure with trip to turbining

Numerical simulation for the upper boundary is based on the pump startup failure with trip to turbining experiment. Similar as for the lower boundary simulation, several values for the cross section area of the upper chamber will be studied. The values considered are presented in Table 5.6.

Table 5.6 Cross section areas considered for upper chamber

Experiment	Cross section area	Unit
Physical model	110	[m^2]
Numerical model	110	[m^2]
Numerical model A_1	300	[m^2]
Numerical model A_2	400	[m^2]
Numerical model A_3	500	[m^2]

The result of the numerical simulation is presented in Figure 5.4. The simulation considered higher values for the upper chamber, however, above the value of 500 m^2 chamber cross section, the damping growth becomes unsignificant. Therefore, the optimal cross section area to be considered for the upper chamber of the surge tank is the value A$_3$ from the numerical simulation, namely 500 m^2.
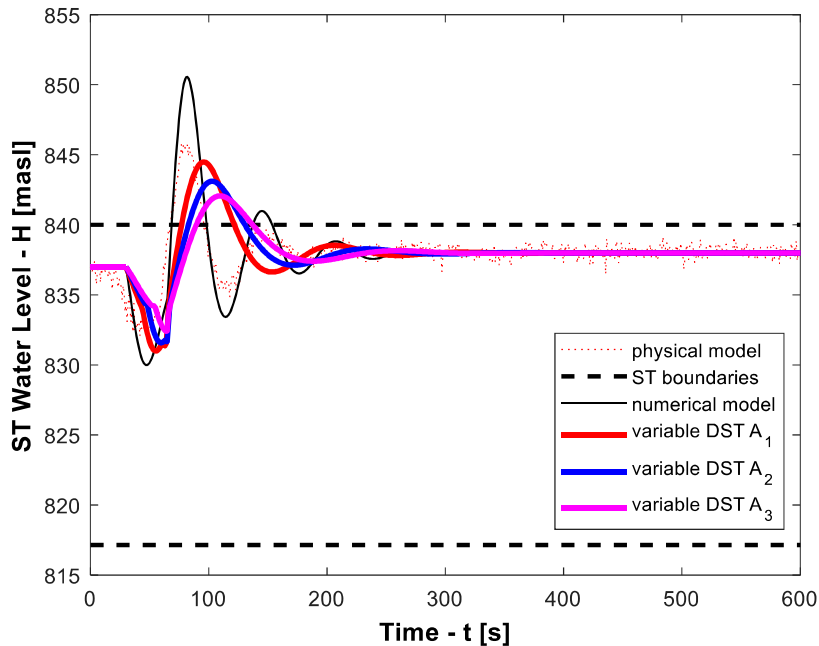

Figure 5.4 Variable surge tank - upper boundary

5.2.3 Variable surge tank proposed dimensions

The configuration proposed for the variable surge tank after the numerical simulation is the 500 m^2 for the upper chamber. For the simplification, the lower chamber has been made similar to the upper one. The variable surge tank has been designed and it is presented in **ANNEXE 2**. This model scale surge tank shall be made of acrylic plates and is required to be modelled and verified by physical experiments. It is expected that the physical modelling to retrieve a higher damping due to the head losses introduced by the chambers.

5.3 Throttled surge tank

Based on the theory presented in chapter 3.6.3, several simple throttles have been considered for the downstream surge tank. A simple thick edge diaphragm with a concentric orifice has been considered the throttle. The variation of the singular head loss introduced by this proposed

throttle was done by changing the orifice diameter inside the diaphragm. The thickness of the diaphragm is considered 1 m for the calculus simplification.

5.3.1 Lower boundary - startup turbining to pumping

The implementation of a throttle has been computed using the numerical model similar to the other proposed improvement methods. Similar to those, several singular head loss coefficient of the throttle have been considered. These are presented in Table 5.7.

Table 5.7 Considered throttle head loss coefficients – lower boundary

Experiment	Head loss coefficient symbol	Head loss coefficient value [-]	Orifice diameter [m]
Throttle 1	ζ_1	50	5.5
Throttle 2	ζ_2	100	4.8
Throttle 3	ζ_3	200	4

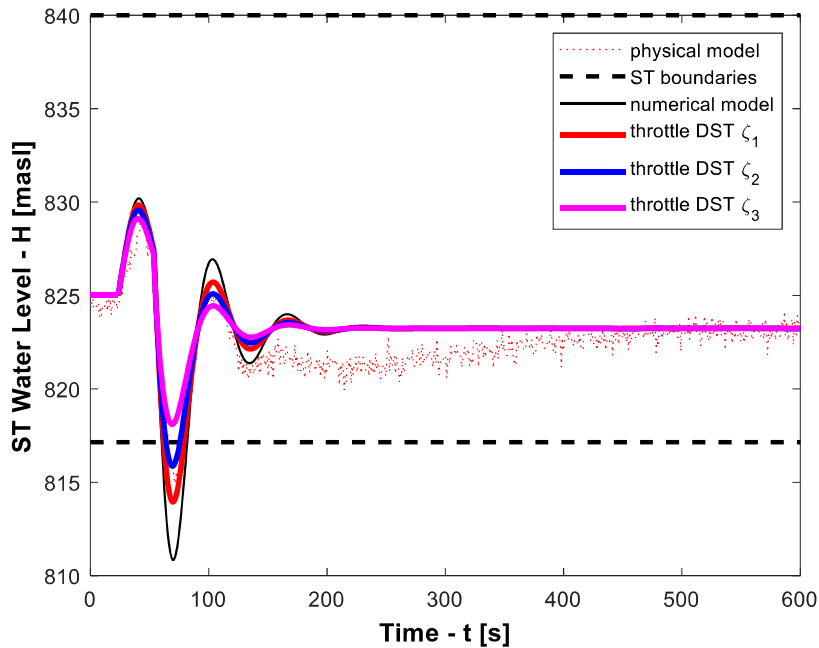The results retrieved by the numerical model are as shown in Figure 5.5.

Figure 5.5 Throttle surge tank – lower boundary

5.3.2   Upper boundary - pump startup failure with trip to turbining

Following the same procedure as for the lower boundary computation, the upper boundary will be studied using the results obtained by running pump startup failure to turbining experiment. Several values for the head loss coefficient introduced by the throttle have been considered. These values for ζ are according to Table 3.13 (Idelchik, 1986) and they are shown in Table 5.8.

Table 5.8 Considered throttle head loss coefficients – upper boundary

Experiment	*Head loss coefficient symbol*	*Head loss coefficient value [-]*	*Orifice diameter [m]*
Throttle 1	ζ_1	150	4.25
Throttle 2	ζ_2	300	3.5
Throttle 3	ζ_3	600	3

The numerical simulation of the throttles shown in Table 5.8 retrieved the results shown in Figure 5.6. Despite the lower boundary, for the upper one to not be exceeded, higher values for ζ are required. As seen in Figure 5.6, for a 3 m diameter throttle, the upper boundary of the surge tank is not exceeded anymore.
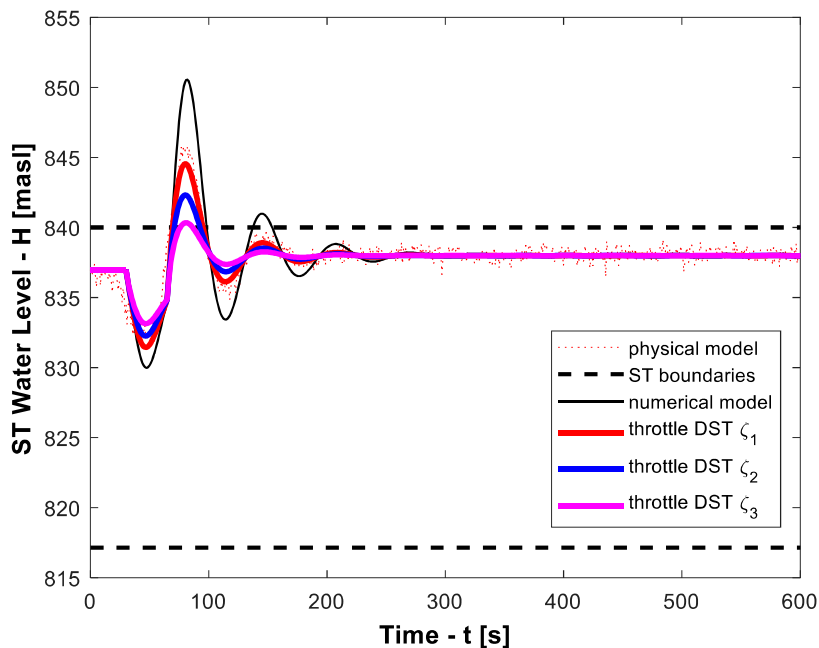

Figure 5.6 Throttle surge tank – upper boundary

5.3.3 Throttle surge tank proposed dimensions

After analyzing the results retrieved by the numerical model, a configuration for the throttle has been proposed. Throttle will consist of a diaphragm with a concentric orifice of 3 m diameter. The diaphragm thickness was considered 1 m, thus the singular headloss introduced by the throttle will have a coefficient of approximately 600. The throttle will be installed in the physical model surge tank as presented in the **ANNEXE 3**. It will be made of acrylic plates and is required to be installed and checked by repeating the experiments. The experimental analysis is required to check if the proposed configuration of the throttle surge tank complies with the pump storage plant configuration.

6 Conclusions and further directions of study

6.1 Conclusions

The physical model calibration and validation were based on the prototype data collected from the Roskrepp Power Plant, thus, they confirm that the results in what regards mass oscillations in the surge tanks for the scenarios studied have a good accuracy. Therefore, the results obtained must be considered in the event of upgrading Roskrepp HPP into a pump storage plant.

The study considered the addition of a reversible pump turbine unit, with respect to the maximum discharge that can be transported economically by the existing tunnel system. The new unit has been considered in the actual turbine place.

The results of the study showed several issues in what regards mass oscillations in the pump storage configuration of the plant:

- for the upstream surge tank, the oscillations exceed its upper boundary only in the event of a sudden switch from turbining to pumping, when the level in the upstream reservoir is at maximum. However, the upstream surge tank behaves perfectly fine for any other scenario. Thus, the study did not focus on the upstream surge tank, as its boundary exceeding can be easily avoided by introducing a few restrictions in the power plant operation;

- for the downstream surge tank, on the other hand, several scenarios with boundaries exceeding have been registered. Therefore, its redesigning and reconstruction is mandatory for the new pump storage configuration to be operative.

In the study, three methods for the improvement have been treated and each of them conducted to a possible solution for the downstream surge tank reconstruction. The solutions proposed were as following:

- the enlargement of the surge tank cross section area was the first solution treated. Knowing that the oscillations amplitude in the surge tank depend proportionally by the cross section area of the surge tank, this method naturally comes as the first option to be considered. However, enlarging the entire surge tank might result in a very costly process mostly due to very high volumes for excavation and time required;

- the variable surge tank solution proposed consists in the addition of two chambers at the boundaries of the actual shaft. This method is basically the enlargement of the surge tank only there where this is required. This way, the volume excavated reduces significantly, thus the costs and the time for the reconstruction are reduced;

- the implementation of a throttle in the actual surge tank was the third method studied as it does not change the configuration of the shaft as much as the other two methods. The throttle considered in the study is basically a diaphragm with an orifice installed at the lower boundary of the shaft. This way, the space required for the reconstruction and the volumes excavated are reduced at minimum.

6.2 Further directions of study

The solutions proposed were based on and checked only using the numerical model due to time constraints. Therefore, since the accuracy of the numerical model was not very high, the first direction of study is physical modelling and verification of the solutions proposed. In the event of exceeding surges even after the surge tank improvement in the physical model, different combinations of the methods can be evaluated. For example, the throttle can be combined with the variable surge tank globally improving, this way, the result.

The next possible direction of study shall focus on the economic analysis of the solutions proposed in this paper at their prototype scale, since the present study focused exclusively on the technical approach of reducing mass oscillations amplitude in the surge tank. The economic analysis is very important in prioritizing the solutions proposed.

Another possible direction of study is the improvement of the upstream surge tank since the present study focused exclusively on the downstream surge tank. The approach of the study for the upstream surge tank proposed the introduction of some restrictions in the power plant operation for eliminating the possibility of its boundary exceeding. However, restrictions in the plant operation might not be the optimal solution, therefore, the improvement of the upstream surge tank is to be studied.

Bibliography

Ancey, C. (2014). *Mécanique des fluides - Une introduction à l'hydraulique pour les ingénieurs civils.* Laboratoire hydraulique environnementale (LHE) - EPFL.

Bulu, A. (n.d.). *HYDROELECTRIC POWER PLANTS*. Retrieved from Lecture Notes: https://web.itu.edu.tr/~bulu/hyroelectic_power_files/lecture_notes_11.pdf

Bureau Of Reclamation, U. D. (1980). *Hydraulic laboratory techniques.* Denver, Colorado: United States Government Printing Office.

Chaudhry, M. (2014). *Applied hydraulic transients.* New York: Van Nostrand Reinhold.

Gomsrud, D. (2015, June). *Design of a Surge Tank Throttle for Tonstad Hydropower Plant*. Retrieved from NTNU Open: https://ntnuopen.ntnu.no/ntnu-xmlui/handle/11250/2350567

Idelchik, I. (1986). *Handbook of Hydraulic Resistance.* Washington: Hemisphere Publ.

Landskaug, R. (2015, July). *Physical Modelling of Surge Tank Throttling*. Retrieved from NTNU Open: https://ntnuopen.ntnu.no/ntnu-xmlui/handle/11250/2350561

Leknes, E. (2016, June). *Comparison of the Svee and Thoma Stability Criteria for Mass Oscillations in Surge Tanks*. Retrieved from NTNU Open: https://ntnuopen.ntnu.no/ntnu-xmlui/handle/11250/2404377

Leroquais, A. (2018, January). *Upgrading of Roskrepp hydropower plant to a pumped storage plant: Necessary reconstruction of the surge tank*. Retrieved from NTNU Open: https://ntnuopen.ntnu.no/ntnu-xmlui/handle/11250/2496223

Nielsen, T. (1990). *Dynamisk dimensjonering av vannkraftverk.* Trondheim: SINTEF, Strømningsmaskiner.

Nistoran Gogoase, D. (2017-2018). Castele de echilibru. *Curs de Hidraulica Tehnica*. Bucuresti: Universitatea Politehnica din Bucuresti, Facultatea de Energetica.

Nistoran, D., Moatar, F., Manoliu, M., & Ionescu, C. (2007). *Hidraulica Tehnica.* Bucuresti: Editura Printech.

Pitorac, L., Vereide, K., & Lia, L. (2020). Upgrading hydropower plants to pump storage plants: a hydraulic scale model of the tunnel system. *8th IAHR International Symposium on Hydraulic Structures ISHS2020.* Santiago: 8th IAHR ISHS 2020.

Popescu, M., Arsenie, D., & Vlase, P. (2003). *Applied Hydraulic Transients For Hydropower Plants and Pumping Stations.* Lisse: A.A. Balkema Publishers.

Richter, W., Zenz, G., & Vereide, K. (2016). Hydraulic design and modelling of large surge tanks. *12th International Conference on Pressure Surges* (pp. 745-759). Dublin: BHR Group Limited.

Stefan, E. (n.d.). *CALCULUL AUTOMAT AL STRUCTURILOR HIDROTEHNICE*. Retrieved from Academia: https://www.academia.edu/36976435/Universitatea_Ovidius_din_Constanta_Facultate a_de_Constructii_IMRA_CALCULUL_AUTOMAT_AL_STRUCTURILOR_HIDR OTEHNICE

Travas, V. (2014). Water mass oscillations in a generic surge chamber. *GRAĐEVINAR, 66 (4)*, 323-334. doi:https://doi.org/10.14256/JCE.989.2013

Vaage, B. (2016, June). *Simulation of hydraulic transients of operation at two hydro power plants.* Retrieved from NTNU Open: https://ntnuopen.ntnu.no/ntnu-xmlui/handle/11250/2402305

Vereide, K., Richter, W., & Lia, L. (2015). *Surge Tank Research in Austria and Norway.* Retrieved from NTNU Open: https://ntnuopen.ntnu.no/ntnu-xmlui/bitstream/handle/11250/2476135/Surge+tank+research+in+Austria+and+Norwa y.pdf?sequence=2

Wylie, E., & Streeter, V. (1978). *Fluid transients.* New York: McGraw-Hill International Book Co.

ANNEXES

Annexe 0 – Numerical model script

```matlab
%ROSKREPP HYDROPOWER PLANT SURGE TANKS OSCILLATIONS

clear all
clc
clf

global g Lht Ltt A Aust Adst Adst_e Athr A_uc A_lc z_uc z_lc ALC AUC
Q0 Qf zUR zLR t0 tm kht ksht ksthr ktt kstt zLC zUC

%General inputs

g=9.81; %[m/s²]            gravitational acceleration

%Tunnel related parameters

M=33; %[-]               Manning's coefficient for unlined tunnel
A=38; %[m²]              tunnel cross section area
Rh=sqrt(4*A/pi)/4;%[m]   hydraulic radius

%Headrace tunnel

Lht=3170; %[m]                  headrace tunnel length
k=L/((M^2)*Rh^(4/3));
kht=Lht/((M^2)*Rh^(4/3)); %[-]  headrace friction loss coefficient
zita_ht=0.05; %[-]              headrace singular loss specific
coefficient
ksht=zita_ht/(2*9.81); %[-]     headrace singular loss coefficient

%Tailrace tunnel

Ltt=320; %[m]                   tailrace tunnel length
ktt=Ltt/((M^2)*Rh^(4/3)); %[-]  tailrace friction loss coefficient
zita_tt=3; %[-]             tailrace singular loss specific coefficient
kstt=zita_tt/(2*9.81);%[-]singular loss coefficient

%Upstream surge tank

Aust=60; %[m²]  upstream surge tank shaft cross section area
ALC=450; %[m²]  upstream surge tank lower chamber cross section area
AUC=667; %[m²]  upstream surge tank upper chamber cross section area
zLC=885; %[m]   lower surge chamber's top elevation
zUC=936; %[m]   upper surge chamber's botoom elevation

%Downstream surge tank

Adst=110; %[m²]  downstream surge tank cross section area

%Enlarged downstream surge tank
Adst_e=500;%[m²] enlarged downstream surge tank cross section area

%Throttled downstream surge tank
Athr=4; %[m²]    throttle cross section area
zita_thr=200;%[-]           throttle singular loss coefficient
```

```matlab
ksthr=zita_thr/(2*9.81);

%Variable downstream surge tank
A_uc=500; %[m^2]              lower surge chamber cross section area;
A_lc=500; %[m^2]              lower surge chamber cross section area;
z_uc=834; %[m^2]             lower surge chamber top elevation
z_lc=823.1;%[m^2]           upper surge chamber botoom elevation

%Reservoirs water levels

zUR=input('Upper reservoir water level zUR=');%[masl] upper
reservoir water level
zLR=input('Lower reservoir water level zLR=');%[masl] lower
reservoir water level

%Discharge

Q0=60; %[m^3/s]              initial  discharge
Qi=-80;%[m^3/s]             intermediar discharge
Qf=0;  %[m^3/s]             final discharge

%Maneuver time

tm=10; %[s]                 maneuvre time

%Numerical analysis time

tfin=1000; %[s]             analisys time

%INITIAL CONDITIONS

t0=10; %[s]                 analysis start time
velocity=Q0/A; %[m/s]       mean velocity in the tunnels

zUST=zUR-(ksht+kht+k)*velocity*abs(velocity); %[m]    UST initial
elevation
zDST=zLR+ktt*velocity*abs(velocity);             %[m]    DST initial
elevation

%Compute UST
x0=[velocity zUST];
tf=[t0 tfin];
[t,x]=ode23('UST',tf,x0);
UST1=x(:,2);

NM_ESD_ust=[t,UST1];

plot(t,UST1,'k','LineWidth',2,'DisplayName','numerical model');grid;
xlabel('t [s]');ylabel('H [m]');
title('UST')
xlim([0 300])
ylim([800 950])

hold on

initial_time=[0 t0];
```

```matlab
x_initial=[UST1(1) UST1(1)];
h(1)=plot(initial_time,x_initial,'k','LineWidth',2);
set( get( get( h(1), 'Annotation'), 'LegendInformation'),
'IconDisplayStyle', 'off' );
legend show

%Compute DST
x1=[velocity zDST];
tf=[t0:1:tfin];
[t,x]=ode23('DST',tf,x1);
DST1=x(:,2);

figure

plot(t,DST1,'k','LineWidth',1,'DisplayName','numerical model');grid;
xlabel('t [s]');ylabel('H [m]');
title('DST')

hold on

%Compute enlarged DST
x1=[velocity zDST];
tf=[t0:1:tfin];
[t,x]=ode23('DST_enlarged',tf,x1);
DST_enlarged=x(:,2);

plot(t,DST_enlarged,'r','LineWidth',2,'DisplayName','enlarged
DST');grid;
xlabel('t [s]');ylabel('H [m]');
title('DST');

%Compute throttled DST
x1=[velocity zDST];
tf=[t0:1:tfin];
[t,x]=ode23('DST_t',tf,x1);
DST_thr=x(:,2);

plot(t,DST_thr,'m','LineWidth',2,'DisplayName','throttled
DST');grid;
xlabel('t [s]');ylabel('H [m]');
title('DST');

%Compute variable DST
x1=[velocity zDST];
tf=[t0:1:tfin];
[t,x]=ode23('DST_chamber',tf,x1);
DST_chamber=x(:,2);

plot(t,DST_chamber,'c','LineWidth',2,'DisplayName','variable
DST');grid;
xlabel('t [s]');ylabel('H [m]');
title('DST');

legend show

%Existing DST function
```

```matlab
function xdt=DST(t,x)
global g Lht Ltt A Aust Adst Adst_e Athr A_uc A_lc z_uc z_lc ALC AUC
Q0 Qf zUR zLR t0 tm kht ksht ksthr ktt kstt zLC zUC


Ac=Adst;

if t<=t0
    Qc=Q0;
elseif t<=t0+tm
    Qc=Q0-(Q0-Qf)*t/(t0+tm);
else
    Qc=Qf;
end

a=g/Ltt;
c=A/Ac;
xdt=zeros(2,1);
xdt(1)=a*(x(2)-zLR-ktt*x(1)*abs(x(1))-kstt*x(1)*abs(x(1)));
xdt(2)=-(c*x(1)-Qc/Ac);
end

%Enlarged DST function

function xdt=DST(t,x)
global g Lht Ltt A Aust Adst Adst_e Athr A_uc A_lc z_uc z_lc ALC AUC
Q0 Qf zUR zLR t0 tm kht ksht ksthr ktt kstt zLC zUC


Ac=Adst_e;

if t<=t0
    Qc=Q0;
elseif t<=t0+tm
    Qc=Q0-(Q0-Qf)*t/(t0+tm);
else
    Qc=Qf;
end

a=g/Ltt;
c=A/Ac;
xdt=zeros(2,1);
xdt(1)=a*(x(2)-zLR-ktt*x(1)*abs(x(1))-kstt*x(1)*abs(x(1)));
xdt(2)=-(c*x(1)-Qc/Ac);
end

%Variable DST function

function xdt=DST_chamber(t,x)
global g Lht Ltt A Aust Adst Adst_e Athr A_uc A_lc z_uc z_lc ALC AUC
Q0 Qf zUR zLR t0 tm kht ksht ksthr ktt kstt zLC zUC


Ac=Adst;
```
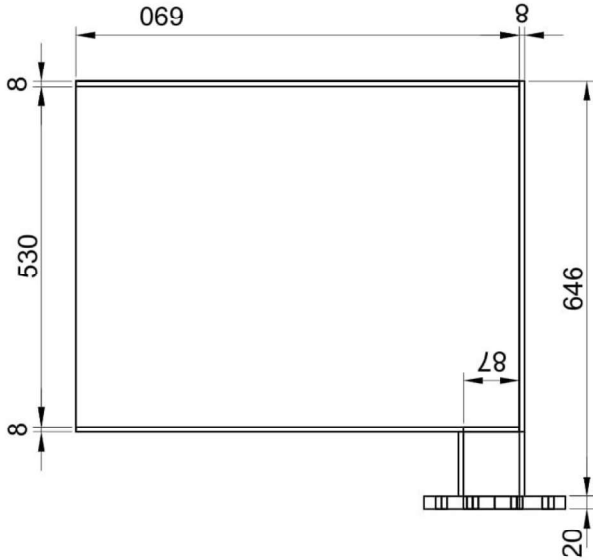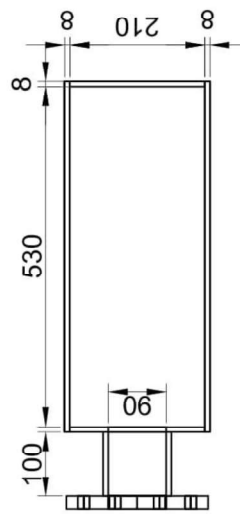
```matlab
if x(2)<=z_lc
    Ac=A_lc;
elseif x(2)<=z_uc
    Ac=Adst;
else
    Ac=A_uc;
end

if t<=t0
    Qc=Q0;
elseif t<=t0+tm
    Qc=Q0-(Q0-Qf)*t/(t0+tm);
else
    Qc=Qf;
end

a=g/Ltt;
c=A/Ac;
xdt=zeros(2,1);
xdt(1)=a*(x(2)-zLR-ktt*x(1)*abs(x(1))-kstt*x(1)*abs(x(1)));
xdt(2)=-(c*x(1)-Qc/Ac);
end

%Throttle DST function

function xdt=DST_t(t,x)
global g Lht Ltt A Aust Adst Adst_e Athr A_uc A_lc z_uc z_lc ALC AUC
Q0 Qf zUR zLR t0 tm kht ksht ksthr ktt kstt zLC zUC

Ac=Adst;

if t<=t0
    Qc=Q0;
elseif t<=t0+tm
    Qc=Q0-(Q0-Qf)*t/(t0+tm);
else
    Qc=Qf;
end

a=g/Ltt;
c=A/Ac;
xdt=zeros(2,1);
    xdt(1)=a*(x(2)-zLR-ktt*x(1)*abs(x(1))-kstt*x(1)*abs(x(1))-
ksthr/(Adst^2)*(x(1)*A-Qc)*abs(x(1)*A-Qc));
    xdt(2)=-(c*x(1)-Qc/Ac);
end
```
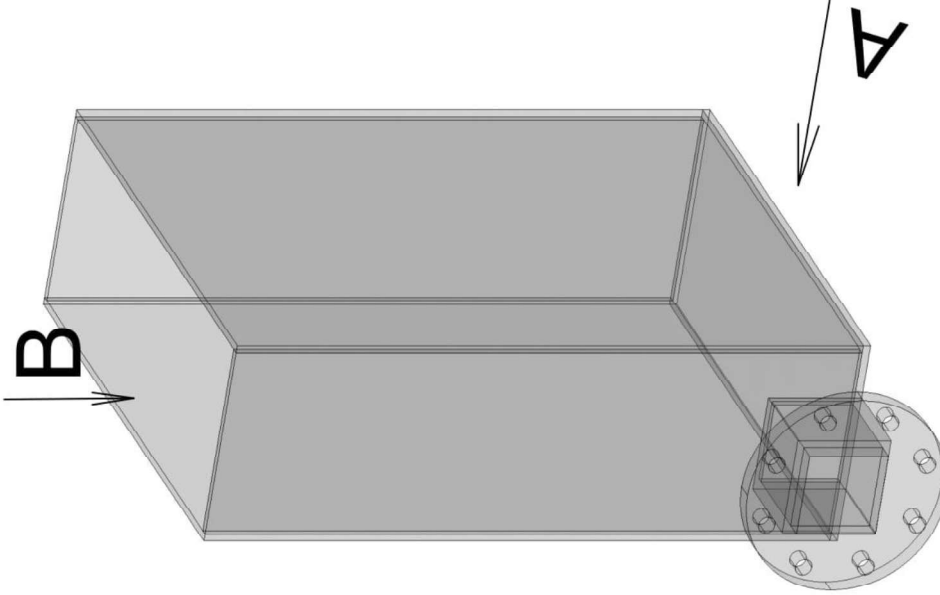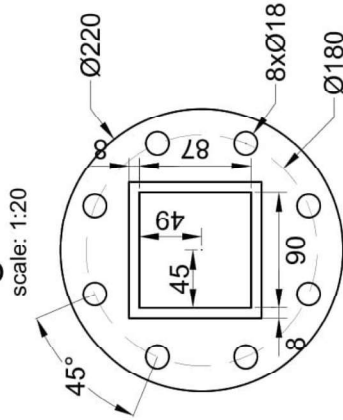
Flange detail
scale: 1:20

Ø220
8×Ø18
Ø180
90
45
49
45°
87
8
8

A view
scale: 1:10

069
8
8
530
646
87

B view
scale: 1:10

8
210
8
8
530
90
100
20

ANNEXE 1

B

A

A view
scale: 1:10

266
8
900
8
241
8

8 87 8 134 8 87 8 84 8 8

B view
scale: 1:10

8 94 8
8
900
8
241
100 8
06 8
20

Flange detail
scale: 1:20

Ø220
8x Ø18
Ø180
87
8
90
45
49
8
45°

Drawn	Alexandru MILCA
Checked	
Approved	

Code:
Contr./Pos.:
Date: 07.2020

Variable DST for Roskrepp physical model

Vassdragslaboratoriet NTNU

A4(210x297=0,062sqm)

ANNEXE 2

Scale:
1:10
1:20

A4

Flange detail
scale: 1:20

Ø220
8xØ18
Ø180
87
49
45
90
8
8
45°

A view
scale: 1:10

580
8
241
8
15
95
8
87
357
20

B view
scale: 1:10

8
94
8
8
241
8
Ø43
100
90
8
20

A4(210x297=0,062sqm)

Throttle DST for Roskrepp physical model

Vassdragslaboratoriet NTNU
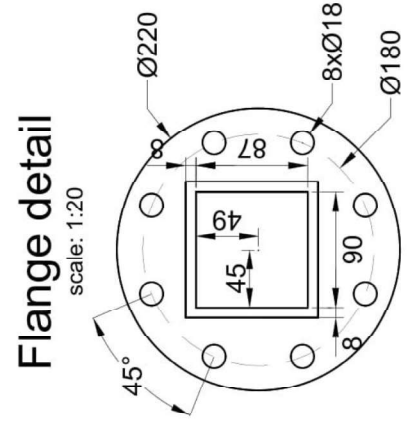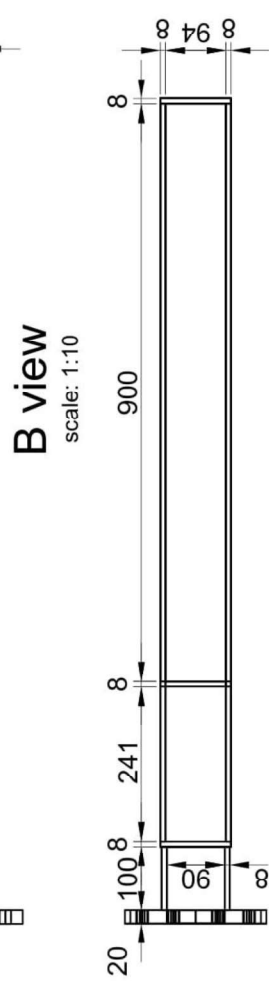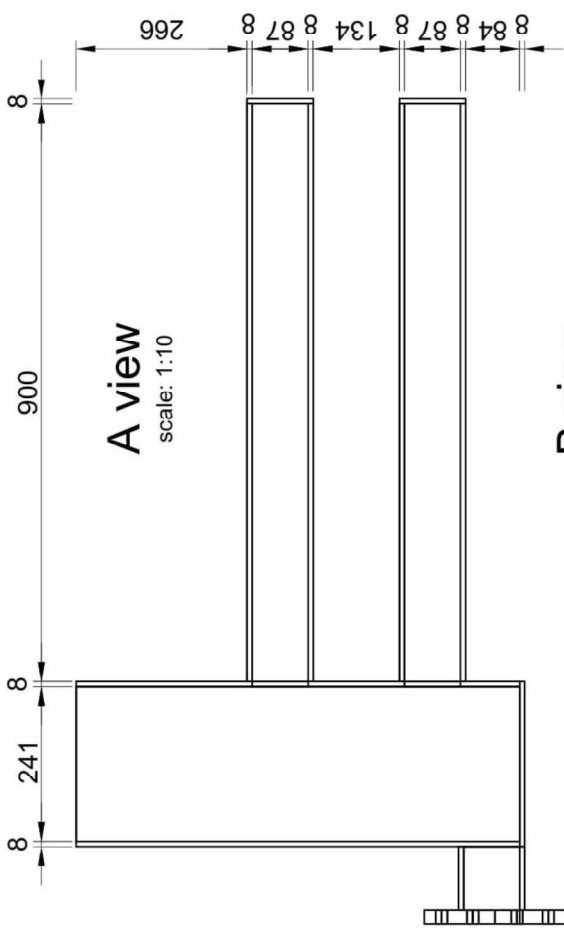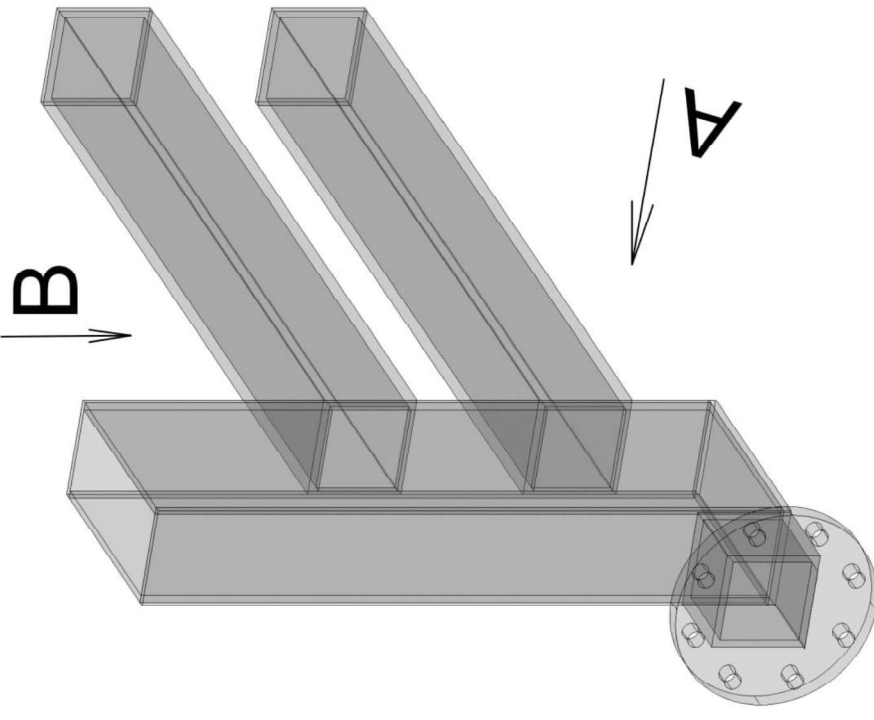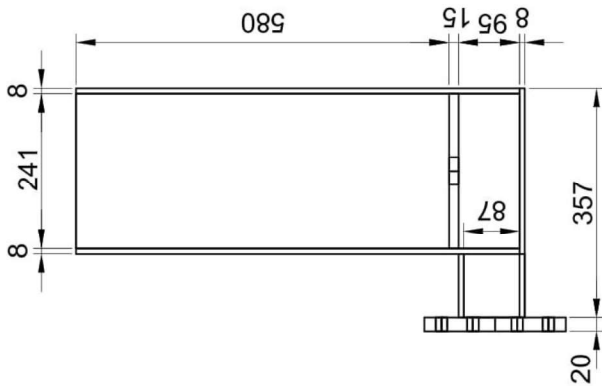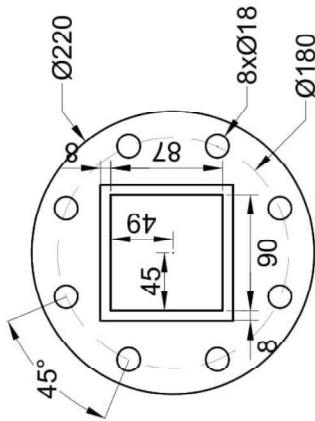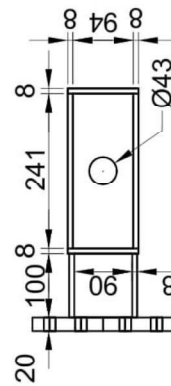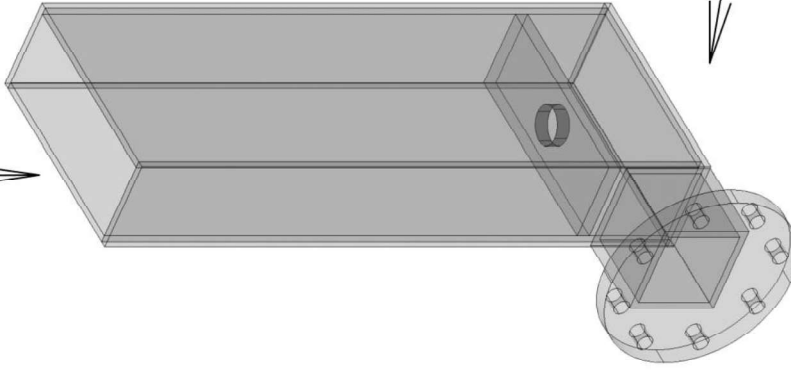
Drawn	Alexandru MILCA	Code:
Checked		Contr./Pos.:
Approved		Date: 07.2020

ANNEXE 3

Scale:
1:10
1:20

A4